UNIVERSITA' DEGLI STUDI DI MILANO

Dipartimento di Scienze Farmacologiche e Biomolecolari

Graduate School in Pharmacological Sciences
Ciclo XXVI

Shrm4, a protein involved in X-LID, drives $GABA_B$ receptors into dendrites through its association with the dynein/dynactin complex

Settore disciplinare BIO /14

Docente guida: Dott.ssa Maria Passafaro
Coordinatore del corso: Prof. Alberto Panerai

Tesi di dottorato di ricerca di:
Zapata Jonathan

Matr. n. R09364

Anno Accademico 2012-2013

CONTENT

ABSTRACT

Mutations in the *KIAA1202* gene coding for the Shrm4 protein have been involved in intellectual disabilities (ID). However, its expression and role in the brain is still unknown. Our data revealed that Shrm4 is present in both cortical and hippocampal primary cultured neurons and localizes at the pre- and post-synapse. ShRNA-mediated Shrm4 knock-down leads to a dramatic reduction in spine density and length. Furthermore, we detected a significant decrease in the expression level of synaptic markers compared to scrambled control. Using different biochemical and imaging approaches, we showed that the N-terminal PDZ domain of Shrm4 interacts directly with the C-terminal tail of $GABA_B$ receptor subunit isoforms 1 ($GABA_{B1}$) (both $GABA_{B1a}$ and $GABA_{B1b}$ subunits). We observed for the first time that Shrm4 regulates $GABA_B$Rs transport in dendrites by modulating its association with the microtubule-dependent dynein/dynactin motor complex. According to our hypothesis, *in vivo* and *in vitro* Shrm4 knockdown reduces $GABA_B$ receptor-mediated K+ currents induced by baclofen application. These results supported the presence of a trimeric complex, necessary for the correct targeting of $GABA_B$ receptors to dendrites and for its physiological role in brain transmission. These observations raised evidences that symptoms observed in Shrm4 deficient human patients such as epilectic seizures could arise from reduced level of functional $GABA_B$ receptors.

ABBREVIATIONS

ID: Intellectual disability

XLID: X-linked intellectual disability

shRNA: short hairpin RNA

PDZ: PSD-95/Disc-large/ZO-1

GABA: γ-Aminobutyric acid

IQ: intelligent quotient

EVH1: WH1, RanBP1-WASP, or enabled/VASP homology 1 domain

$GABA_BRs$: $GABA_A$ receptors

$GABA_ARs$: $GABA_B$ receptors

VGCCs: voltage-gated Ca^{2+} channels

GIRKs: G protein-activated inwardly rectifying potassium channels

GPCRs: G protein coupled receptors

$GABA_{B1a}$: $GABA_B$ receptors subunit isoform 1a

$GABA_{B1b}$: $GABA_B$ receptors subunit isoform 1b

$GABA_{B1}$: $GABA_B$ receptors subunits 1

KCTD: K^+ channel tetramerization domain-containing

SNARE: soluble N-ethylmaleimide-sensitive (NSF) factor attachment protein (SNAP) receptor

cAMP: cyclic Adenosine Monophosphate

LTP: Long Term Potentiation

IPSPs: inhibitory postsynaptic potentials

Ba^{2+}: Barium (ii)

NMDAR: N-methyl-D-aspartate receptor

AMPAR: α-amino-3-hydroxy-5-methyl-4-isoxazolepropionic acid receptor

PKA: Protein Kinase A

ER: Endoplamic Reticulum

ERGIC: ER to Golgi Intermediate Compartment

GFP: Green Fluorescence Protein

RFP: Red Fluorescence Protein

ASDs: Autism spectrum disorders

N-KIFs: N-terminal motor domain KIFs

M-KIFs: middle motor domain KIFs

C-KIFs: C-terminal motor domain KIFs

HAP1: huntingtin-associated protein 1

CRMP-2: Collapsin-response mediator protein-2

Pi: inorganic phosphate

p50: dynamitin

CC1: first coiled-coil domain of $p150^{Glued}$

BDNF: Brain-derived neurotrophic factor

ORF: Open reading frame

GST: Glutathione *S*-transferase

HEK293 cells: Human Embryonic Kidney 293 cells

MAP2: Microtubule-associated protein 2

PSD95: postsynaptic density protein 95

1. INTRODUCTION

1.1 X-linked intellectual disability (XLID)

Intellectual disability (ID) is a developemental brain disorder characterized by an intelligent quotient (IQ) below 70. The severity of ID is not measurable, however it is generally evaluated through the variation in the IQ. ID is defined as mild when the IQ is comprised between 55 and 70, moderate between 35 and 55 and severe when lower than 20 according to the *Diagnostic and Statistical Manual of Mental Disorder, Fourth Edition*. ID can originate from environmental causes and/or genetic abnormalities, and its incidence in children is around 1% to 2% (Ellison et al., 2013; Leornard et al., 2002; Piton et al., 2013; Bassani et al., 2013). X-linked Intellectual disability (XLID) grouped various disorders arising from mutations in X-chromosome genes. They are involved in 5% to 10% of all the intellectual disabilities in males and affects 1% to 3% of the population (Bassani et al., 2013).

XLID is subdivided in two groups: syndromic forms, in which ID is only one of a large set of symptoms such as microcephaly and facial dysmorphisms; and non-syndromic forms, in which ID is the principal manifestation of the pathology. Different approaches have been established to identify genes and associated mutations, however the validation of a gene newly associated with XLID requires functional and/or genetic analyses (Piton et al., 2013). It has been recently published a list of 106 genes proposed to be associated with XLID (Figure 1). The XLID genes mostly encode for proteins that are highly expressed in the brain, particularly in the hippocampus, region that is important for learning processes and memory formation (Boda et al., 2002; Bassani et al., 2013).

Mutations in XLID genes frequently involved loss of function, affecting neuronal functions by impairing both inhibitory and excitatory pathways. One of the principal hallmark of XLID is the alteration of dendritic spines (Purpura, 1974; Bassani et al., 2013) (Figure 2). Dendritic spines are tiny protrusions on dendrites processes where the majority of excitatory synapses are localized. They are highly dynamic structures and their stabilization and morphology are modulated by synaptic activity. Impaired dendritic spines lead to abnormal synaptic function, which interferes with the balance between excitatory and inhibitory circuits necessary for the central nervous system to respond correctly to external and internal stimuli.

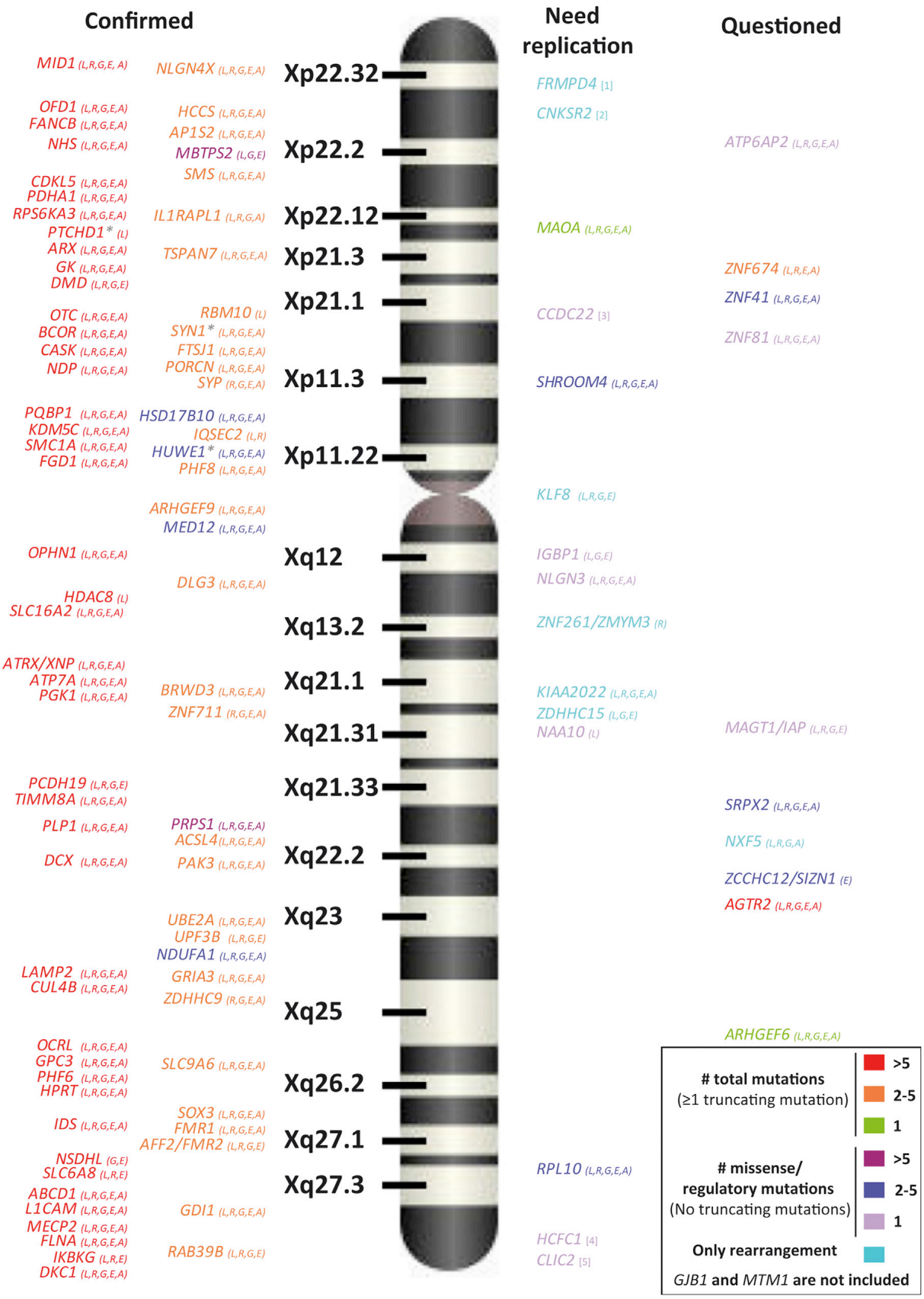

Figure 1: Representation along the X chromosome of the 106 genes in which mutations have been reported in XLID and classification according to both the type and number of mutations reported in OMIM (Figure from Piton et al., 2013 with permission).

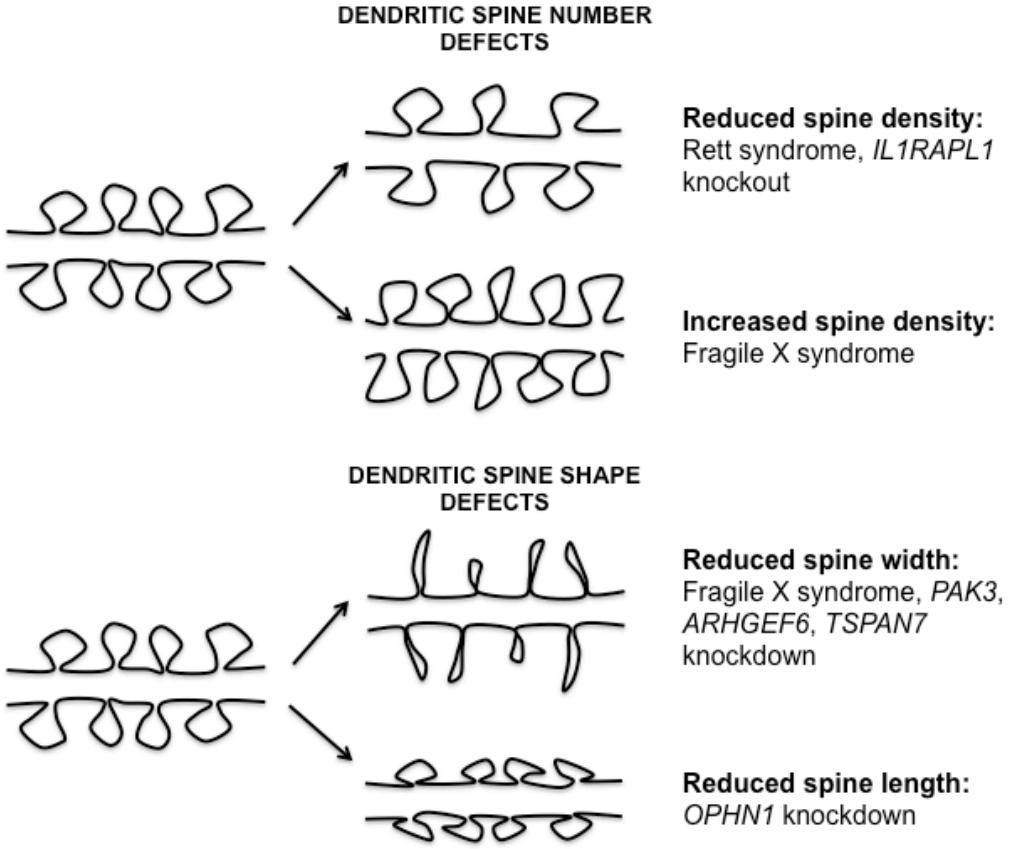

Figure 2: Dendritic spine defects associated with X-linked intellectual disability (XLID). Dendritic spine defects include spine number and spine shape abnormalities. Reduced spine density is observed in Rett syndrome and following IL1RAPL1 knockout. Fragile X syndrome (FXS) is characterized by both spine density increase and spine width reduction. Also PAK3, ARHGEF6, and TSPAN7 loss of function is associated with immature, narrow spines. OPHN1 knockdown impairs spine length (Figure from Bassani et al., 2013).

The vast majority of the XLID genes now identified are involved in synaptic plasticity and the formation and maturation of dendritic spines. Indeed, XLID genes are implicated both in spine morphology (through the regulation of actin cytoskeleton remodelling) and spines function. In addition, the proteins encoded by XLID genes could also provide the correct localization and activity of surface receptors and intracellular signalling molecules (Humeau et al., 2009; Bassani et al., 2013).

The aim of our study was to analyse the subcellular localization and function of Shrm4 in the brain, protein in which mutations have been involved in XLID (Hagens et al., 2006).

1.2 Shrm4 and the Shroom family of proteins

1.2.1 The Shroom family of proteins

The Shroom (Shrm) family of proteins is a small group of actin binding proteins involved in cytoskeletal organization and cell shape. Four Shrm proteins have been described in vertebrates formerly called Apx (Staub et al., 1992), Apxl (Schiaffino et al., 1995), Shroom (Hildebrand and Soriano, 1999) and KIAA1202 (Hagens et al., 2006; Yoder et al., 2007) and more recently named Shrm1, Shrm2, Shrm3 and Shrm4, respectively (Hagens et al., 2006) (Figure 3).

GenBank Accession Number	Previous name	New name
CAA78718	*X. laevis* Apx	xShroom1
NP_597713	*H. sapiens* APXL2	hShroom1
CAA58534	*H. sapiens* APXL	hShroom2
ABD19518	*M. musculus* Apxl	mShroom2
AAF13269	*M. musculus* ShroomL	mShroom3a
AAF13270	*M. musculus* ShroomS	mShroom3b
NP_065910	*H. sapiens* Shroom	hShroom3
ABD59319	*X. laevis* Shroom-like	xShroom3
NP_065768	*H. sapiens* KIAA1202	hShroom4a
AAK95579	*H. sapiens* SHAP-A	hShroom4b
DQ435686	*M. musculus* KIAA1202	mShroom4
ABA81834	*D. melanogaster* Shroom	dmShroom
EAA12598	*A. gambiae* Shroom	agShroom
XP_392427	*A. mellifera* Shroom	amShroom
XP_783573	*S. purpuratus* Shroom	spShroom

Figure 3: New nomenclature for Shroom-related proteins (Table from Hagens et al., 2006).

The Shroom family has been assembled based on the conservation of specific structures: an N-terminal PDZ domain, a central domain called ASD1 domain (formely Apx/Shrm Domain 1) and a C-terminal ASD2 domain. Only Shrm4 differs from the other member of the Shroom family and lacks the ASD1 motif. It has been observed that Shrm2 and Shrm3 required the conserved ASD1 motif for their targeting to actin (Hildebrand and Soriano, 1999; Haigo et al., 2003; Hildebrand, 2005; Dietz et al., 2006) while their PDZ domains have been involved in other functions. Indeed, the PDZ domain is required for the proper function of Shrm3 while it is involved in the subcellular targeting of Shrm2 (Haigo et al., 2003; Hildebrand, 2005; Dietz et al., 2006). A recent study has demonstrated that the structure of the ASD2 motif of Shrm3 is composed by an arrangement of three coiled-coil segment

required for the interaction with the Rho-associated coiled-coil kinase (Rock) (Mohan et al., 2012).

Proteins from the Shroom family have been involved in distinct cellular functions as cytoskeletal organization, adaptors, cell shape and have been detected in a various range of polarized cell types and tissues (Hildebrand et al., 1999; Fairbank et al., 2006; Nishimura and Takeichi, 2008; Taylor et al., 2008; Lee et al., 2009; Plageman et al., 2010).

1.2.2 Shrm4 structure and association with XLID

1.2.2.1 Shrm4 structure

Characterization and cloning of *Mus musculus* Shrm4 (mShrm4) revealed an open reading frame of 4425 bp encoding a predicted protein of 1475 aminoacids. mShrm4 contains an N-terminal PDZ domain and a C-terminal ASD2 motif (Yoder et al., 2007). As the *Homo sapiens* Shrm4 (hShrm4) (Figure 4), mShrm4 contains putative binding sites for EVH1 (poly-proline rich domain-FPPPP) and PDZ (SNF) domains (Gertler et al., 1996; Songyang et al., 1997; Yoder et al., 2007). Moreover, a stretch of glutamines and glutamic acids residues that precedes the ASD2 motif is conserved in hShrm4 but not in other Shroom proteins (Yoder et al., 2007). Using real-time PCR (RT-PCR), it has been observed that mShrm4 transcripts are expressed ubiquitously in adult and embryonic mouse tissues and in all brain regions (Hagens et al., 2006) (Figure 5).

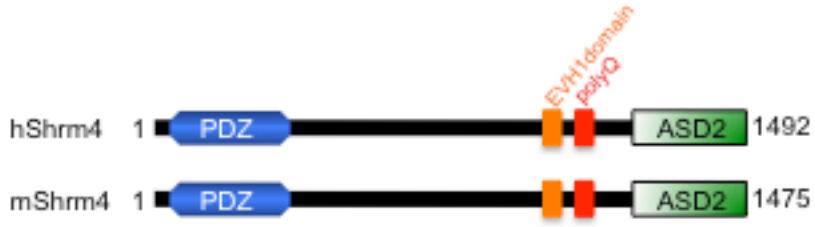

Figure 4: hShrm4 and mShrm4 structures. Shrm4 contains an N-terminal PDZ domain and a C-terminal ASD2 motif. A poly-proline rich domain (EVH1 domain; orange) and polyQ (glutamines and glutamic acids residues; red) precede the ASD2 motif.

Additionally, western blot analyses using purified polyclonal antibodies anti-Shrm4 have shown that the protein is expressed in all adult and whole E12,5 embryo mouse tissues (Figure 6). Interestingly, endogenous mShrm4 colocalizes with F-actin in non-

neuronal cells and binds directly to F-actin as shown by actin co-sedimentation assay experiments (Yoder et al., 2007).

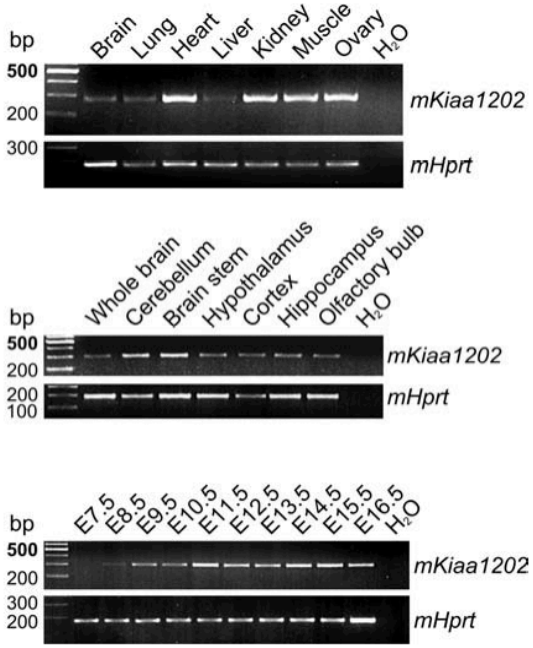

Figure 5: RT-PCR assays show a ubiquitous expression of mKiaa1202 in adult mouse tissues (top panel) and in all brain regions analysed (middle panel). The bottom panel shows mKiaa1202 expression during mouse development. mHprt was used as an internal control (Figure from Hagens et al., 2006).

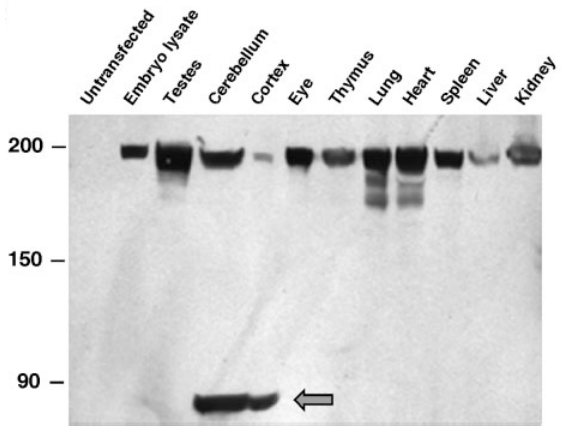

Figure 6: Western blot analysis of lysates from a whole e12.5 mouse embryo and the indicated adult tissues. Equal amounts of protein lysate were resolved by SDS-PAGE, transferred to nitrocellulose, and probed with affinity purified rabbit anti-mouse Shrm4 antibody (UPT114). Lysate from untransfected cells serves as a negative control (Figure from Yoder et al., 2007).

1.2.2.2 Shrm4 is involved in XLID

Disruptions of the KIAA1202 gene coding for Shrm4 have been associated with XLID. Indeed, two balanced (X; autosome) translocations found in unrelated female

patients with moderate ID have been shown to disrupt the KIAA1202 gene. Importantly, severe seizures were observed in one patient (Hagens et al., 2006). These findings supported the implication of Shrm4 in brain disorders and analysis of Shrm4 localization and function in the brain is needed to better define this pathology.

1.3 Metabotropic $GABA_B$ receptors

The following section will provide a brief explanation of the structure and function of metabotropic $GABA_B$ receptors as, in our study, we identified this receptor as a new Shrm4 direct interactor.

γ-Aminobutyric acid (GABA) is the major inhibitory neurotransmitter in the central nervous system and plays a key role in the modulation of neuronal activity. GABA mediates its effect via distinct types of receptors: the ionotropic $GABA_A$ ($GABA_ARs$) and metabotropic $GABA_B$ receptors ($GABA_BRs$). Unlike $GABA_ARs$ that produce fast inhibitory (< 10 ms) synaptic conductances, $GABA_BRs$ address second messenger systems through the coupling and activation of guanine nucleotide-binding proteins (G proteins) that modulate calcium (Ca^{2+}) and potassium (K^+) channels and subsequently elicit presynaptic and slow postsynaptic inhibition (sub-seconds to minutes). $GABA_BRs$ activate $G_{i/o}$-type G proteins, that inhibit Adenylate cyclase and cAMP production through the $G\alpha_{i/o}$ subunit while the released Gβγ inhibits voltage-gated Ca^{2+} channels (VGCCs) or opens dendritic G protein-activated inwardly rectifying potassium channels (GIRKs) (Benarroch, 2012; Gassmann and Bettler, 2012).

1.3.1 Structure of $GABA_B$ receptors

1.3.1.1 Principal $GABA_BR$ subunits

$GABA_BR$ subunits are G protein-coupled receptors (GPCRs). They are constituted of 7 transmembrane helices and contain a large extracellular loop that forms the ligand binding site. $GABA_BRs$ are physiologically obligatory heterodimers and are formed by two principal subunits: $GABA_{B1}$ and $GABA_{B2}$ (Bettler et al., 2004; Emson, 2007; Benarroch, 2012; Gassmann and Bettler, 2012) (Figure 7). The $GABA_{B1}$ subunit contains the ligand-binding site while the $GABA_{B2}$ subunit is coupled to G proteins.

The $GABA_{B1}$ subunit has two isoforms: $GABA_{B1a}$ and $GABA_{B1b}$; which differ by the presence of a tandem pair of sushi domains in the N-terminal extracellular region of $GABA_{B1a}$. Sushi domains have been involved in the axonal targeting (Biermann et al., 2010; Valdés et al., 2012) and cell surface stabilization of $GABA_B$Rs (Hannan et al., 2012).

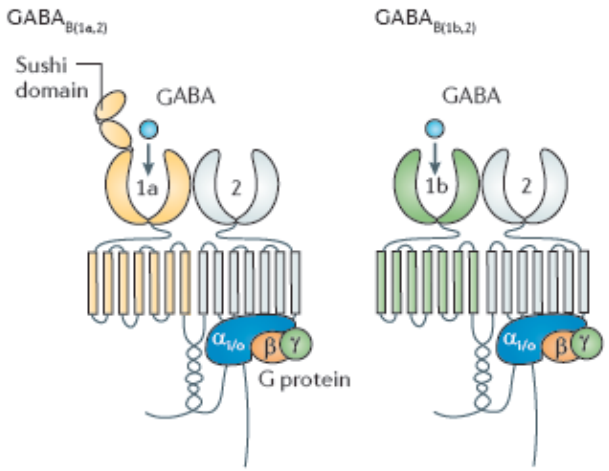

Figure 6: $GABA_B$ receptor subunit composition. The principal subunits of $GABA_B$ receptors ($GABA_B$Rs)-$GABA_{B1a}$, $GABA_{B1b}$ and $GABA_{B2}$-have the prototypical seven transmembrane domains of G protein-coupled receptors and form two distinct core units: $GABA_B$ (1a, 2) and $GABA_B$(1b, 2) (Marshall et al., 1999). $GABA_{B1a}$ and $GABA_{B1b}$ are subunit isoforms that differ by the presence of two amino-terminal sushi domains in $GABA_{B1a}$. Whereas these subunits contain the GABA binding site, $GABA_{B2}$ subunits couple to the G protein (Rondard et al., 2011) (Figure from Gassmann and Bettler, 2012 with permission).

Heteromerization and trafficking of $GABA_B$Rs are dependent on the coiled-coil interaction between the C-termini of the $GABA_{B1}$ subunit isoforms ($GABA_{B1}$) and $GABA_{B2}$. Indeed, it has been well described that $GABA_{B1}$ contains an endoplamic reticulum (ER) retention motif [RXR(R)] in the coiled-coil region of the C-terminal tail. Through this interaction, the $GABA_{B2}$ masks the retention signal present in $GABA_{B1}$ thus leading to the surface expression of functional $GABA_B$Rs (Couve et al., 1998; Margeta-Mitrovic et al., 2000). In addition, it has been demonstrated that $GABA_{B1}$/$GABA_{B2}$ interaction, through the $GABA_{B1}$ C-terminus is essential for the correct trafficking of $GABA_B$Rs to the cell surface but not for receptor signalling (Pagano et al., 2001; Calver et al., 2001).

1.3.1.2 Auxiliary $GABA_BR$ subunits

Using unbiased proteomics approaches, it has been identified four cytosolic proteins of the K^+ channel tetramerization domain-containing (KCTD) family as constituents of $GABA_BR$ complex which have the capacity to modify $GABA_BR$ responses (Bartoi et al., 2010; Schwenk et al., 2010) (Figure 7). Interestingly, KCTD8, KCTD12, KCTD12b and KCTD16 bind to the C-terminal domain of $GABA_{B2}$ subunits. It has been observed that KCTD subunits determine the pharmacology and kinetics of $GABA_BR$-mediated responses (Schwenk et al., 2010).

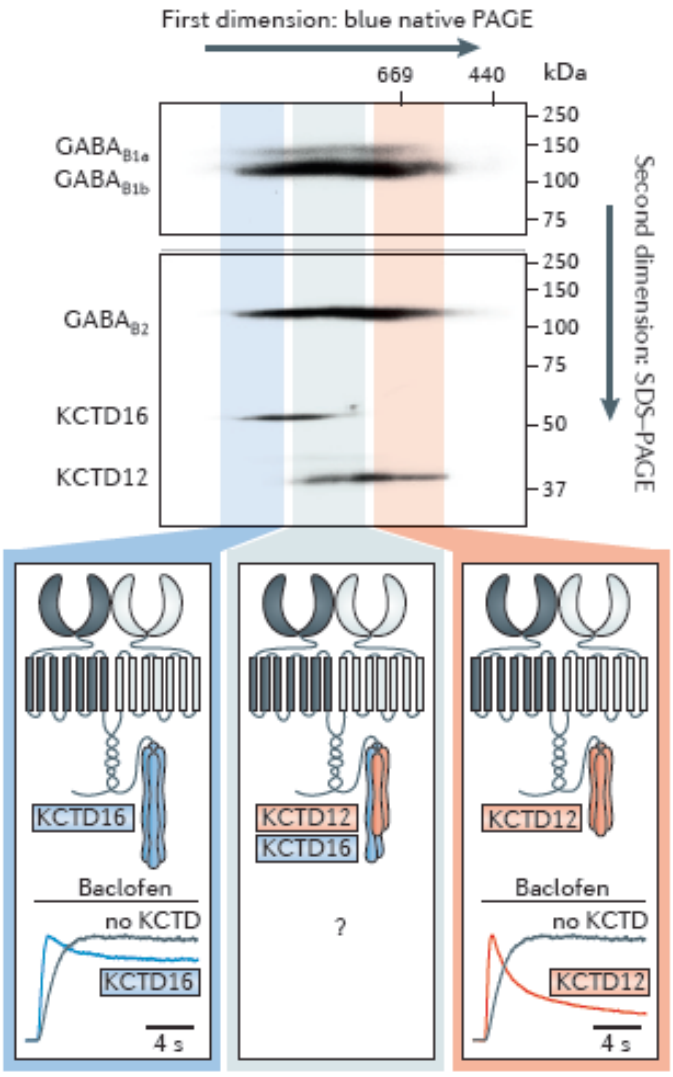

Figure 7: $GABA_B$ receptor auxiliary subunits. Biochemical experiments demonstrated the association of principal with auxiliary $GABA_BR$ subunits. The panel shows solubilized native $GABA_BR$ complexes from rat brain that were size-fractionated on non-denaturing blue native PAGE and SDS–PAGE. Receptor subunits were detected with specific antibodies. KCTD16 was associated with high molecular weight receptor complexes, whereas KCTD12 was associated with low molecular weight complexes (molecular weights are indicated in kDa) (Figure from Gassmann and Bettler, 2012 with permission).

1.3.2 Presynaptic modulation by $GABA_BRs$

Presynaptic $GABA_BRs$ are present in both inhibitory and excitatory terminals. They function as autoreceptors to control GABA release at GABAergic terminals while they function as heteroreceptors at glutamatergic terminals and control glutamate release. Indeed, presynaptic $GABA_BRs$ activation inhibits VGCCs via the release of Gβγ that reduce Ca^{2+} influx at the synaptic terminal and consequently inhibits neurotransmitters release (Figure 8) (Bettler et al., 2004; Bowery et al., 2002; Couve et al., 2000; Gassmann and Bettler, 2012).

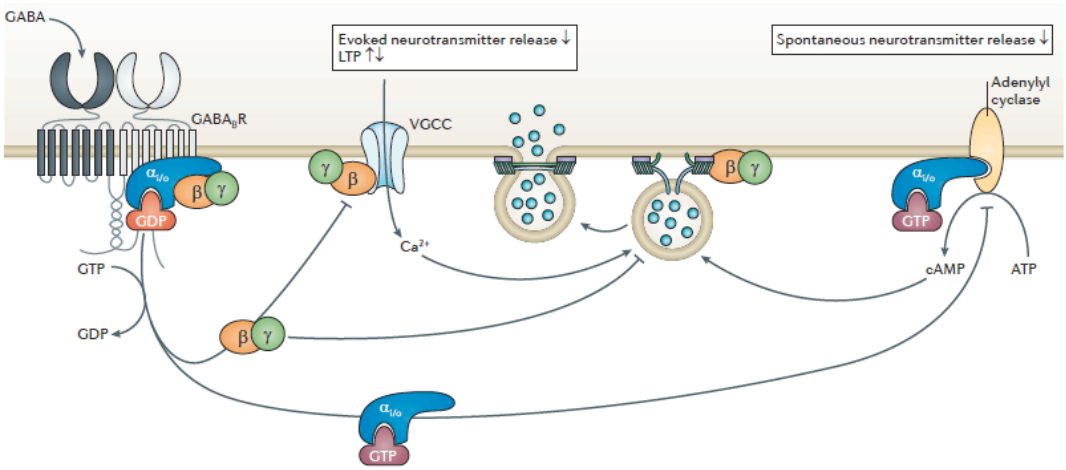

Figure 8: Presynaptic modulation by $GABA_BRs$. In presynaptic compartments, $GABA_B$ receptors ($GABA_BRs$) activate Gαi/o type G proteins that negatively couple to adenylyl cyclase to decrease the level of cyclic adenosine monophosphate (cAMP) in the cell. Downregulation of cAMP at the axon terminal prevents vesicle fusion and spontaneous neurotransmitter release (Rost et al., 2011; Sakaba et al., 2003). Released Gβγ inhibits voltage-gated Ca2+ channels (VGCCs) and hence inhibits evoked Ca2+-dependent neurotransmitter release. In addition, Gβγ directly binds to the SNARE (soluble N-ethylmaleimide-sensitive factor attachment protein receptor) complex required for vesicle fusion, thereby limiting neurotransmitter release downstream of Ca2+ entry (Wells et al., 2012). The effects of Gβγ on VGCCs and the release apparatus may be additive or synergistic (Yoon et al., 2007). $GABA_BR$-mediated inhibition of neurotransmitter release regulates long-term potentiation (LTP) processes (Davies et al., 1991) (Figure from Gassmann and Bettler, 2012 with permission).

Moreover, Gβγ subunit released after $GABA_BRs$ activation directly interacts with the C-terminal tail of SNAP25, a (soluble N-ethylmaleimide-sensitive factor attachment protein (SNAP) receptor) SNARE protein subsequently limiting vesicle fusion (Wells et al., 2012; Yoon et al., 2007) (Figure 8). Finally, it has also been demonstrated that $GABA_BRs$ activation retards spontaneous neurotransmitters vesicles release by inducing a decrease in cAMP concentration (Chalifoux et al., 2011).

More importantly, it has been observed that the genetic ablation of the $GABA_{B1a}$ subunit isoform at glutamatergic terminals ($GABA_B$ heteroreceptors) induced a loss of

LTP at CA3-CA1 synapses in the hippocampus (Vigot et al., 2006). These effects can be explained by a desinhibition of glutamate release that results in the saturation of synaptic potentiation (Gassmann and Bettler, 2012). In addition, induction of LTP has been previously shown to depend on $GABA_B$ autoreceptors at GABAergic terminals (Davies et al., 991). Consistently, *Gabbr1*$^{-/-}$ mice, which have a complete absence of $GABA_B$ autoreceptors, also fail to induce LTP (Vigot et al., 2006). These results suggest that without control of GABA release, an increase in phasic or tonic activity mediated by extrasynaptic $GABA_A$ could contribute to the loss of LTP.

1.3.3 Postsynaptic modulation by $GABA_BRs$

$GABA_BRs$ control postsynaptic excitability by releasing Gβγ that activate inwardly rectifying K^+ channels (Kir3 channels; also called GIRK channels) (Gähwiler and Brown, 1985; Lüscher et al., 1997; Sodickson and Bean, 1996) (Figure 9). GIRK channels activation generates slow inhibitory postsynaptic potentials (IPSPs) (Dutar and Nicoll, 1988; Newberry and Nicoll, 1984; Tamás et al., 2003). Consistent with these observations, $GABA_BR$-induced slow IPSP can be inhibited by the Kir3 channel blocker Ba^{2+} (Jarolimek et al., 1994; Pitler et al., 1994; Thompson et al., 1994). Moreover, $GABA_BRs$ through the GIRK activation are involved in the suppression of backpropagating antidromic spikes in hippocampal CA1 that induced a decrease in membrane depolarization and in Ca^{2+} influx (Leung et al., 2006).

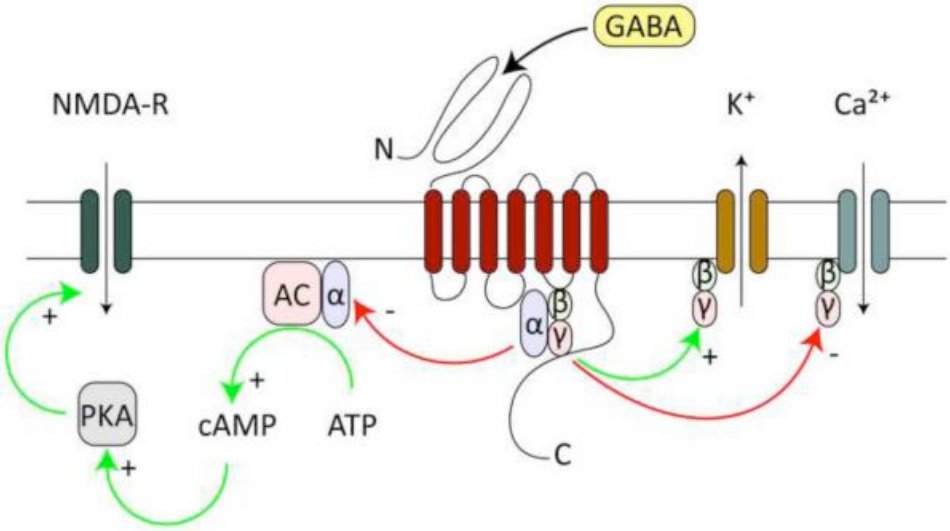

Figure 9: Post-synaptic intracellular $GABA_BR$ signaling. GABA binding to $GABA_BR$ heterodimers releases Gβγ subunits that locally diffuse to open K^+ channels and close Ca^{2+} channels. In addition, released Gαi/Gαo subunits inhibit adenylyl cyclase (AC), which constitutively produces cAMP to activate PKA, with potentially many downstream targets including NMDA-Rs (Figure from Chalifoux et al., 2010).

Interestingly, recent studies have demonstrated that $GABA_BRs$ directly inhibit NMDA receptors Ca^{2+} influx. This effect is mediated by $G\alpha_{i/o}$ subunits that inhibit the adenylate cyclase to decrease cAMP levels and suppress PKA activity that in normal condition enhances Ca^{2+} influx (Chalifoux et al., 2010) (Figure 9).

1.3.4 Axonal and somatodendritic trafficking of $GABA_B$ receptors

By a Golgi apparatus-dependent mechanism, most $GABA_{B1}$ subunit isoform enter the somatodendritic compartment (Figure 10). However, a fraction of $GABA_{B1a}$ is selected in pre-Golgi compartments (ER and ERGIC) and targeted to axon. It has been found that kinesin-1 contributes to the axonal localization of $GABA_{B1a}$ (Valdés et al., 2012). Interestingly, $GABA_{B1a}$ contains a tandem of sushi domains in its extracellular region that could provide interaction with binding partners containing axonal sorting signals (Roos et al., 2000).

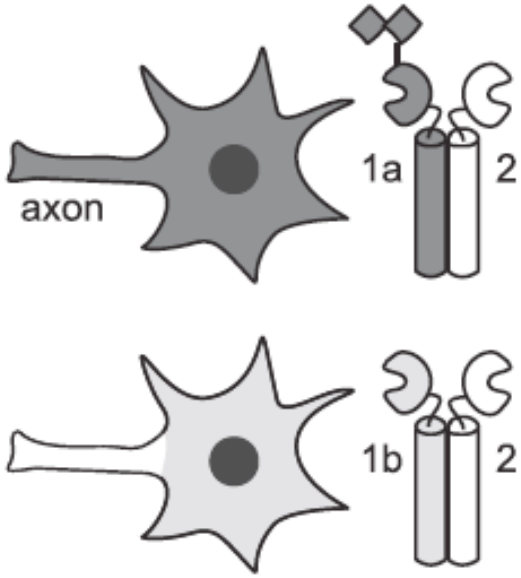

Figure 10: Schematic depiction of endogenous $GABA_B$ (1a,2) and $GABA_B$ (1b,2) receptor distribution in hippocampal neurons. Squares indicate the two in tandem arranged SDs at the N terminus of $GABA_{B1a}$ (Figure from Biermann et al., 2010 with permission).

The distribution of $GABA_{B1a}$ and $GABA_{B1b}$ differs also within the somatodendritic compartment. Indeed, using organotypic slices, it has been observed that $GABA_{B1a}$-GFP is mostly excluded from spines while $GABA_{B1b}$-GFP is mostly expressed in dendritic spines (Vigot et al., 2006), a synaptic location where $GABA_BRs$ are found with GIRK channels (Kulik et al., 2006).

However, it remains unknown how and by which mechanism $GABA_B$ receptors are transported toward dendrites. Because both $GABA_{B1a}$ and $GABA_{B1b}$ are found together in the somatodendritic compartment, targeting signals could reside in their identical C-terminus and be recognized by adaptor molecules and/or motor proteins.

1.3.5 Implication of $GABA_B$Rs in neurological disorders

1.3.5.1 Epilepsy

Epilepsy is a neurological disorder associated with transient, hypersynchronous neuronal discharges and characterized by spontaneous and recurrent epileptic sizures. Many disease-causing genes for epilepsy and epileptic encephalopathy have been identified and various genes implicated in the etilogy of epilepsy have been involved in neuronal functions such as synaptogenesis, pruning, neuronal migration, neurotransmitter synthesis and release, and functions of membrane receptors and transporters (Deng et al., 2013; Zupanc et al., 2009; Galanopoulou et al., 2009).

$GABA_B$Rs have been frequently associated with epilepsy. Indeed, seizures have been reported in a *Girk2* null mutant mouse lacking the GIRK2 channel as well as in the *weaver* mice that has a mutated GIRK2 channel. These channels are postsynaptically activated by $GABA_B$Rs and a loss in $GABA_B$R-activated GIRK current appears coincident with seizures (Slesinger et al., 1997).

Consistently, adult $GABA_{B1}^{-/-}$ mice showed hyperactivity and displayed several episodes of spontaneous clonic seizures that could be explained by a loss of control over neuronal excitability (Schuler et al., 2001). Finally, it has been reported a rapid loss of $GABA_B$R-mediated respons in a mouse model of temporal lobe epilepsy after single unilateral injection of kainic acid into the dorsal hippocampus (Straessle et al., 2003).

1.3.5.2 Anxiety

Anxiety is a psychiatric disorder with high morbidity and comorbidity (Pilc and Nowak, 2005). Deficiency in GABAergic transmission has been widely implicated in the physiopathology of anxiety. Indeed, the family of benzodiazepines, that are $GABA_A$ receptor modulators, are frequently used as anxiolytic drugs (Rowlett et al., 2005). Interstingly, it has been observed that $GABA_B$Rs are abundant in the lymbic

system, structure that controls the emotional behaviour (Cryan and Kaupmann, 2005), and mice deficient for $GABA_BRs$ show anxiety in several behavioral tests (Mombereau et al., 2005; Kumar et al., 2013).

Taken as a whole, these studies raise the possiblity of an implication of $GABA_BRs$ in anxiety-related behaviors. However, additional studies are required to clearly define the mechanism by which $GABA_BRs$ could influence anxiety.

1.3.5.3 Autism spectrum disorders

Autism spectrum disorders (ASDs) are developmental disorders that are commonly defined by the appearance of specific symptoms such as communication deficits, irritability and repetitive behaviors (Hampson et al., 2011; Nightingale, 2012; Kumar et al., 2013). Emerging evidence demonstrated abnormalities in the GABAergic system in ASDs, which likely contribute to developmental disorders (Oblak et al., 2010). Indeed, a significant decrease in $GABA_{B1}$ and $GABA_{B2}$ subunits has been reported in the cerebellum, superior frontal and parietal cortical areas of patients with autism compared to matched controls (Fatemi et al., 2009).

In addition, autistic patients show alteration in $GABA_BRs$ amount in the anterior and posterior cingulate cortex, structures important for the socio-emotional and cognitive processing as well as in the fusiform gyrus, important for identification of faces and facial expressions (Oblak et al., 2010).

More recently, $GABA_BRs$ have also been used as clinical target for treatment of ASD and constitutive NMDAR-hypofunction (Gandal et al., 2012). Stimulation of $GABA_BRs$ with baclofen, a $GABA_BR$ agonist, has shown promising beneficial effects.

1.4 Microtubule-based motor proteins

The following section will provide a brief explanation of the two principal microtubule-based motor protein kinesin and dynein in neurons as in our study we identified the dynein/Dynactin as motor complex that specifically drives $GABA_B$ receptors toward dendrites.

Neurons are highly polarized structures that receive and transmit information along dendrites and axons. In the axon and dendrites, microtubules and neurofilaments are

the major longitudinal cytoskeletal filaments while in synaptic regions; actin filaments form the major cytoskeletal architecture (Hirokawa et al., 2010; Kapitein et al., 2010). To establish and maintain this architecture, neurons use active transport driven by microtubules-based motor proteins to transport cargo proteins in dendrites and axons (Kapitein et al., 2010). Kinesins and dyneins are the two principal motor proteins that move along microtubules while Myosins steer cargo along actin filaments. Kinesins drive cargo transport by moving along microtubules to their plus end (the fast growing end), while dyneins to their minus end.

Microtubule orientations established the correct cargo transport and vary with the localization in dendrites or axons. Indeed, in mature neurons, axonal microtubules have uniform orientations with all plus ends pointing outward. By contrast, microtubules in mature proximal dendrites have mixed orientations (Kapitein et al., 2010).

1.4.1 The kinesin superfamily

The kinesin protein superfamily (called KIFs) is composed by three groups of proteins that differ for the position of the motor domain: N-terminal motor domain KIFs (N-KIFs), middle motor domain KIFs (M-KIFs), and C-terminal motor domain KIFs (C-KIFs). In mammals, the number of *Kif* genes is around 45. Most N-KIFs move toward microtubules plus end while C-KIFs move toward the minus end. N-KIFs and C-KIFs are composed of a motor domain, a stalk domain and a tail region (Figure 11). The motor domain binds to microtubules and moves by ATP hydrolysis while the tail region is important for binding to cargo (Hirokawa et al., 2010; Hirokawa and Noda, 2008).

1.4.1.1 kinesins and axonal transport

There are two types of transport in the axon: a fast transport of membranous organelles and a slow transport of cytosolic proteins and cytoskeletal proteins. Concerning the fast transport (50-400 mm/day), various cargo vesicles such as synaptic vesicle precursors (KIF1A and KIF1Bβ), presynaptic membrane (KIF5), mitochondria (KIF1Bα/KIF5), and plasma membrane precursors (KIF3) are transported by kinesins (Figure 11).

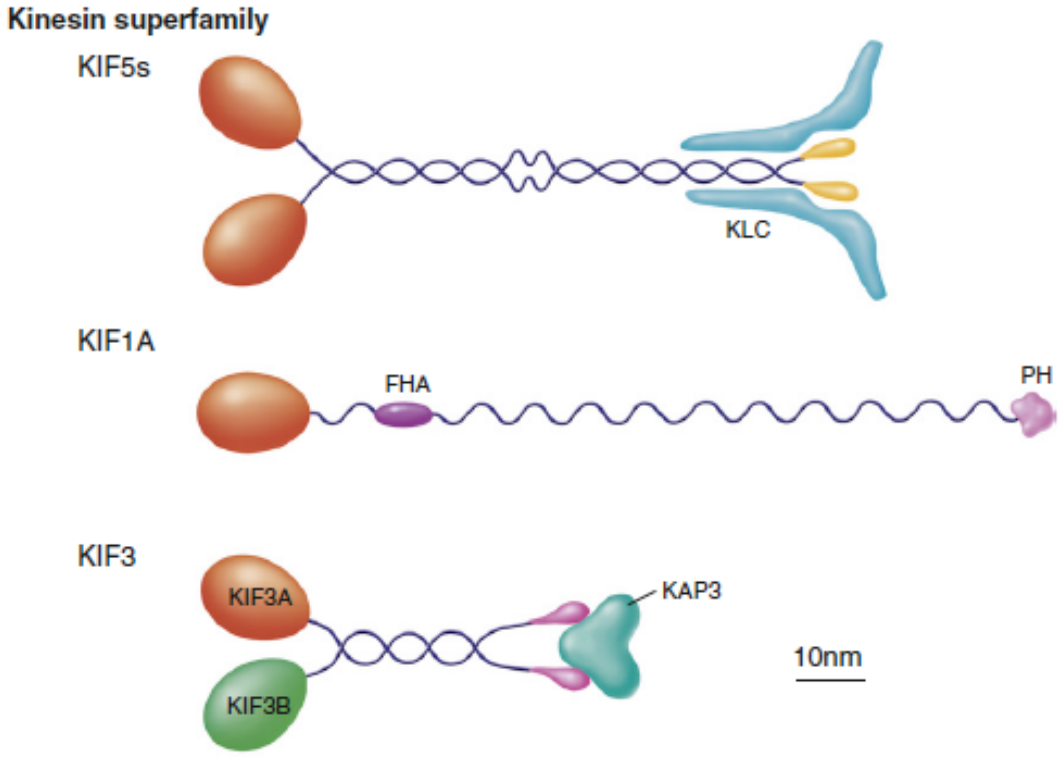

Figure 11: Structure of kinesins. kinesin superfamily proteins. kinesin 1 consists of two KIF5s and two KLCs. KIF1A is a unique monomeric motor. KIF3A, KIF3B, and KAP3 form a tetramer (Figure from Hirokawa et al., 2010 with permission)

In the other hand, the slow transport (less than 8 mm/day) involves the transport of cytoplamic proteins such as tubulin and microtubules in the growing axon. Indeed, it has been shown that the Collapsin-response mediator protein-2 (CRMP-2) regulates tubulin transport by linking tubulin to KIF5 (Kimura et al., 2005).

1.4.1.2 kinesins and dendritic transport

In dendrites, NMDAR vesicles (KIF17) (Setou et al., 2000; Yuen et al., 2005), AMPAR vesicles (KIF5) (Setou et al., 2002), and $GABA_AR$ vesicles (KIF5) (Twelvetrees et al., 2010) are transported by kinesins. These selective transports are mostly mediated by distinct adaptors proteins such as the huntingtin-associated protein 1 (HAP1) that links $GABA_A$ receptors to KIF5 (Twelvetrees et al., 2010).

1.4.2 The dynein superfamily

1.4.2.1 Structure and composition of the cytoplasmic dynein

The cytoplasmic dynein is a complex of proteins (~ 1,5 MDa) that contains: two heavy chains (~ 520 KDa) with ATPase activity that generate movement along microtubules filament and belong to the AAA+ superfamily (Neuwald et al,, 1999), two intermediate chains (~ 74 KDa) and light chains (~ 10-14 KDa) (Karki and Holzbaur, 1999; Pfister et al., 2005; Hirokawa et al., 2010; Roberts et al., 2013) (Figure 11).

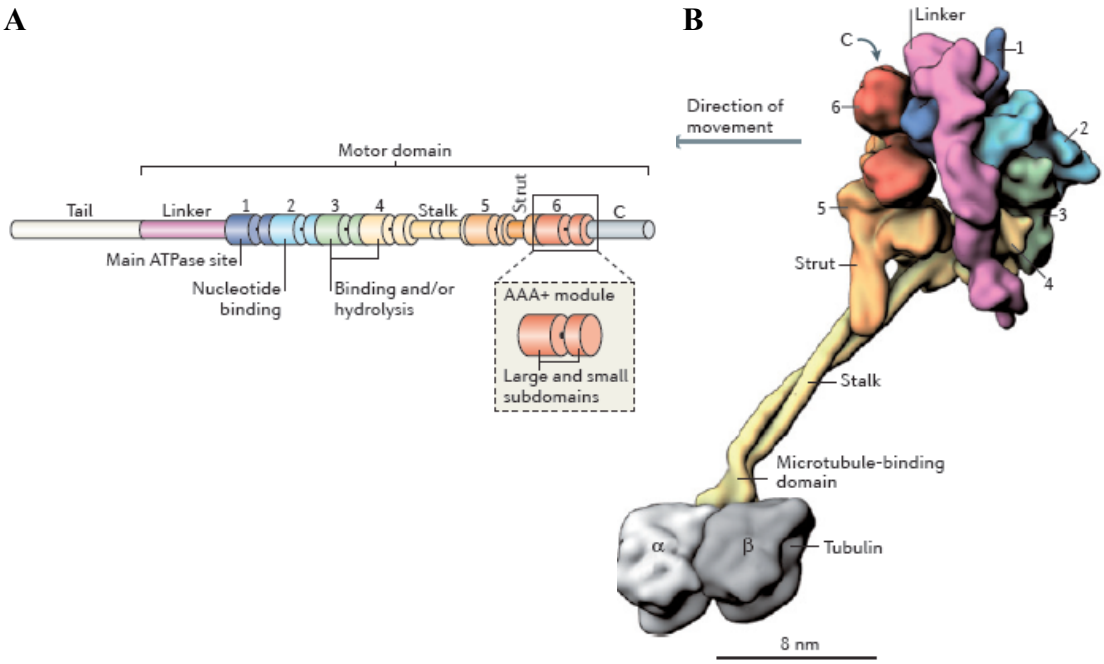

Figure 12: Structure of cytoplamic dynein. (A) Linear representation of domains within the dynein heavy chain. The amino-terminal tail domain is involved in dynein oligomerization, cargo-binding and regulation, but is not part of the minimal motor domain capable of producing movement *in vitro*. The motor domain comprises the linker domain, six AAA+ modules (1–6), the coiled-coil stalk and strut, and the carboxy-terminal region. (B) A 3D model of the cytoplasmic dynein motor domain bound to the microtubule. This model is based on a 2.8 Å crystal structure of the *D. discoideum* dynein motor domain lacking the microtubule-binding domain93 (Protein Data Bank ID: 3VKG), joined to a cryo-electron microscopy-derived model of the mouse microtubule-binding domain bound to an α-tubulin–β-tubulin dimer112 (Protein Data Bank ID: 3J1T). Subdomains are shown in surface representation, with the two long α-helices in the stalk rendered separately to emphasize their coiled-coil arrangement. The six AAA+ modules are numerically labelled (Figure from Roberts et al., 2013).

The tail of cytoplasmic dynein (Figure 12A) is necessary for the binding with the associated subunits which in turn mediate the direct interaction through adaptor to the cargoes. Cytoplasmic dynein is involved in a great variety of cellular functions. In the yeast *Saccharomyces cerevisiae*, dynein positiones the nucleus during cell division

(Moore et al., 2009) while in filamentous fungi, dynein is involved in vesicular transport (Egan et al., 2012). In addition, cytoplasmic dynein steers organelles such as endosomes which regulates dendritic membrane supply (Driskell et al., 2007) as well as vesicles from the endoplamic reticulum (ER) to the Golgi apparatus (Presley et al., 1997) towards microtubules minus ends.

1.4.2.2 Mechanochemical cycle of the dynein motor domain

The cytoplasmic dynein is a mechanoenzyme that moves along microtubules to their minus end by ATP hydrolysis. In this cycle, ATP induces a dissociation of the motor domain with microtubules. After detaching from them, a change in the structure of the motor domain generates force (also called powerstroke) and leads to the rebinding of the motor domain to a new site on microtubules and induces a release of ADP + inorganic phosphate (Pi) (Roberts et al., 2013).

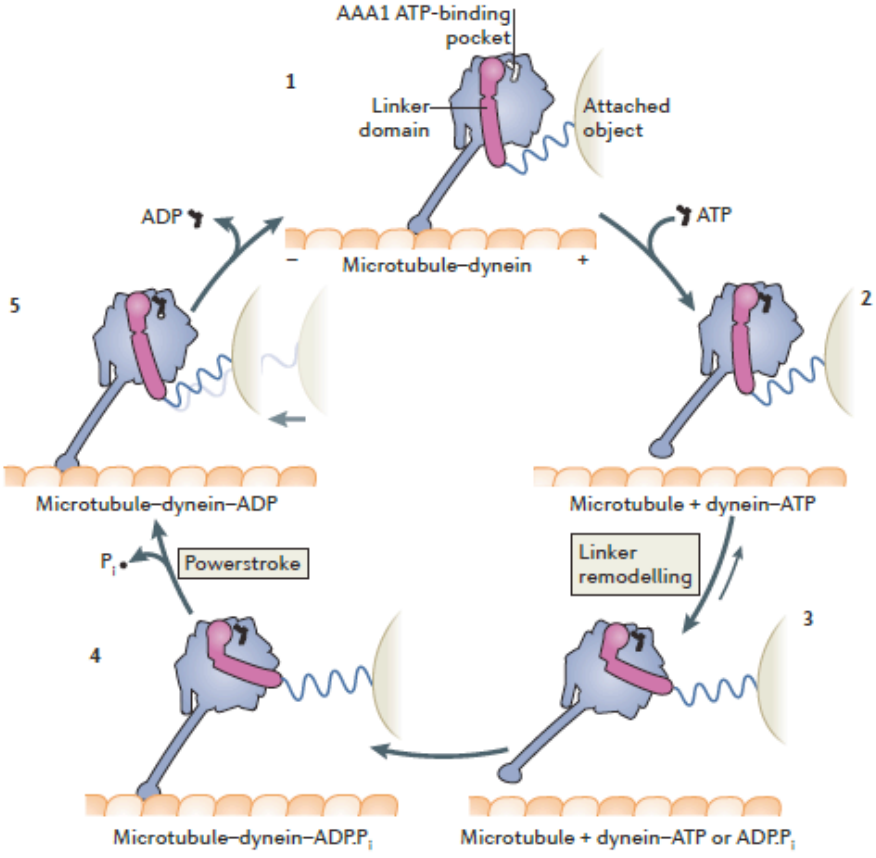

Figure 13: Model of the mechanochemical cycle of a cytoplasmic dynein motor domain (Figure from Roberts et al., 2013).

1.4.2.3 Dynactin: a dynein adaptor complex

Dynein is associated with the dynactin complex that is composed by p150^{Glued}, p62, dynamitin (p50), actin-related protein (Arp) 1, CAPZα and CAPZβ, p27 and p24 (Figure 14). The dynactin complex regulates dynein localization, activity and the binding capacity of dynein for its cargo (Hirokawa et al., 2010; Schroer, 2004). Indeed, it has been demonstrated that intermediate chains of cytoplamic dynein directly bind to the dynactin complex through the interaction with p150^{Glued}, interaction that regulates cargo binding to the tail domain of dynein (Vaughan et al., 1995).

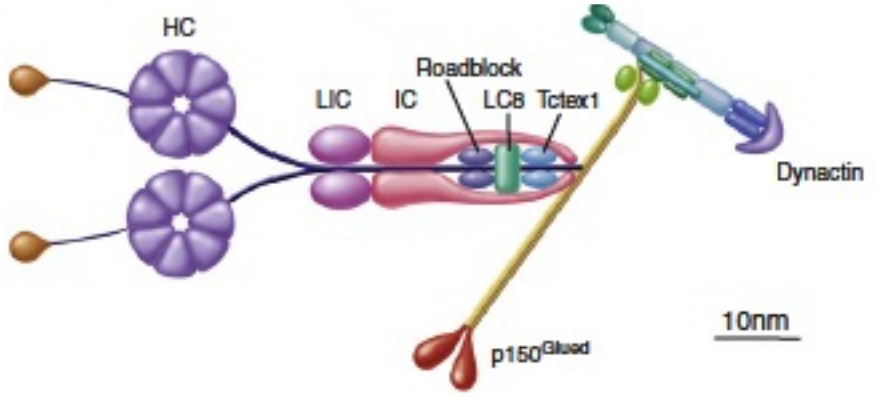

Figure 14: Structure of the dynein/dynactin complex. Cytoplasmic dyneins consist of heavy chains, light intermediate chains, intermediate chains, and light chains. To transport cargos, cytoplasmic dynein binds to the dynactin complex (Figure from Hirokawa et al., 2010 with permission).

In addition, overexpression of both p50/dynamitin and the first coiled-coil domain of p150^{Glued} (CC1) results in a strong inhibition of dynein activity and reduces the flux of dense core vesicles in both directions in the axon and dendrites of cultured hippocampal neurons. These findings support a pivotal role of these two proteins in regulating organelle movement at the level of motor-cargo binding (Burkhardt et al., 1997; Kwinter et al., 2009).

1.4.2.4 Axonal and dendritic transport by the dynein/dynactin complex

In neurons, cytoplasmic dynein drives various cargo proteins. Brain-derived neurotrophic factor (BDNF) vesicles (Gauthier et al., 2004; Colin et al., 2008), the piccolo/bassoon complex (Fejtova et al., 2009) and mitochondria (Van Spronsen et al., 2013) are transported by dynein in the axon while in dendrites, cargos include glycine receptor vesicles (Maas et al., 2009), Rab5 and Rab7 endosomes (Satoh et al., 2008; Johansson et al., 2007) and more recently AMPA receptors (Kapitein et al.,

2010).

In dendrites, where microtubule orientations are mixed, dynein-driven cargo transport moves bidirectionaly indicating that dynein does not selectively recognize a subset of uniformly oriented microtubules. These bidirectional transports maintain a constant density of available cargo into dendrites (Kapitein et al., 2010).

Furthermore and to conclude, dynein has been also involved in the subcellular localization of Golgi outposts in dendrites. Indeed, expression of dynein mutant induces mislocalization of Golgi outposts in axons and impaired dendrites branching in neurons (Zheng et al., 2008). In contrast, Golgi outposts have not been found in axon (Horton and Ehlers, 2003). These findings raised the importance of dynein transport in maintaining transport polarity but also in the correct development of neurons.

2. AIM OF THE WORK

Intellectual disability (ID) is a developemental brain disorder that originate from environmental causes and/or genetic abnormalities. Its incidence in children is around 1% to 2% (Ellison et al., 2013; Leornard et al., 2002; Piton et al., 2013; Bassani et al., 2013). X-linked Intellectual disability (XLID) is involved in 5% to 10% of all the intellectual disabilities in males and affects 1% to 3% of the population (Bassani et al., 2013). Mutations in XLID genes frequently involved loss of function, affecting neuronal activity by impairing both inhibitory and excitatory transmission. The *KIAA1202* gene (Xp11.2) encodes for Shrm4, a protein that belongs to the Shroom familly and disruptions of this gene have been associated with XLID (Hagens et al., 2006).

Interestingly, previous studies have reported high expression of Shrm4 in various brain regions. However, its subcellular localization and function in neurons remain unknown. Therefore, the purpose of this study was to investigate the biological function of Shrm4 in the brain.

The first part of the project was aimed at Shrm4 localization in the rat brain. We explored Shrm4 expression level in different adult rat brain regions and analysed the subcellular localization of endogenous Shrm4 in cultured cortical and hippocampal neurons.

The target of the second part aimed to investigate the effect of Shrm4 loss in cultured hippocampal neurons. We used a small hairpin RNA (shRNA) strategy that induces Shrm4 knockdown and more importantly mimic the Shrm4 loss of function present in patient with XLID.

In a third part of the project, we looked for Shrm4 interactors by using a yeast two-hybrid screening combined with biochemical experiments that validated interactions. Shrm4 contains an N-terminal PDZ domain, important for protein-protein interaction that was consequently used to screen a human adult brain library.

Surprisingly, we found that Shrm4 interacts with the C-terminal tail of the metabotropic $GABA_B$ receptors and that this interaction is important for receptors trafficking in neurons.

Given that $GABA_B$ receptors have been involved in various neurological disorders, we took advantage of viral vectors delivery to carry out an *in vivo* model of Shrm4 knockdown that we characterized in the last part of our study.

Our results identify Shrm4 as a new key molecule for $GABA_B$ receptors targeting in neurons and raised evidences that an impaired receptors transport could lead to cognitive disorders.

3. MATERIALS AND METHODS

3.1 cDNA Constructs, shRNAs

The Homo sapiens KIAA1202 open reading frame 1 (ORF 1) was subcloned in pcDNA4/V5-HisB (Invitrogen) using HindIII/KpnI restriction enzymes to obtain Shrm4-V5 and in pEGFP-C1 (Clontech) using EcoRI/SalI restriction enzymes to obtain GFP-Shrm4 (gift from Vera Kalscheuer). Flag-tagged $GABA_{B2}$, Myc-tagged $GABA_{B1a}$-full length, $GABA_{B1a}$-Δ859-961, $GABA_{B1a}$-Δ922-961; $GABA_{B1a}$-Δ870-961 in pRK5 were used to define the minimal sequence of interaction with Shrm4 (Couve et al., 1998; Hannan et al., 2011) (Gift from Saad Hanaan). GW1-GFP was used as control. GW1-GFP-p150-cc1 and bactin-HA-p50 was kindly donated by Casper Hoogenraad. To analyse the distribution of both $GABA_{B1a}$ and $GABA_{B1b}$ subunit isoforms, pCl-myc-$GABA_{B1a}$ and pCl-myc-$GABA_{B1b}$ constructs were used (Pagano et al., 2001) (gift from Martin Gassmann). The pCl-HA-$GABA_{B2}$ construct was used for the co-immunoprecipitation with Shrm4 (Pagano et al., 2001) (gift from Martin Gassmann). GalNAcT2-mcherry used to localize the Golgi apparatus was kindly donated by R.Pepperkok (EMBL, Heidelberg, Germany) (Girod et al., 1999). The $GABA_{B1a}$-mRFP construct was used for FRAP experiments (Ramirez et al., 2009) (kindly donated by Andrés Couve).

The 21 base pair target sequence that was used to design Shrm4 small hairpin RNA (shRNA#3) is the following: '*GCTCACGGTGTCGAAGATTGA'* (nucleotides: 22-45) and scrambled sequence: '*GATTCTAGCCGGACGGTGTAA'*. ShRNA and scrambled sequences were subcloned in pLVTHM-GFP (*in vitro*) and pAAV-U6-ZsGreenGFP (*in vivo*) (Vectors from Penn Vector Core) create shRNA and scrambled.

For GST pull-down assay, the PDZ domain of Shrm4 (amino acids: 1-91) was subcloned in pGEX-4T-1 to create GST-PDZ.

For two-hybrid test, DNA fragments corresponding to different Shrm4 truncations: 1-1492 (full length), aa 91-1492 (ΔPDZ), aa 1-91 (PDZ) and aa 1213-1492 (ΔASD2) were subcloned in pGBKT7 and used as bait. Potential prey were full-length Shrm4 (1-1492), PDZ domain (1-91), and ΔASD2 (1213-1492).

3.2 Immunofluorescence, surface staining and antibodies

Cultured Hippocampal, cortical neurons or HEK293 cells were fixed in 4% paraformaldeyde- 4% sucrose for 10 minutes at room temperature and incubated with **rabbit anti**: -Shrm4 (1:200, gift from Jeffrey Hildebrand), -Synapsin 1 (1:200, SYnaptic SYstems), -$GABA_A\alpha1$ (1:400, Millipore), -Giantin (1:200, gift from Prof Renz M), -V5 (1:500, Invitrogen), with **mouse anti**: -Ankyrin (1:400, Millipore), -MAP2 (1:1000, SIGMA), -PSD95 (1:400, NeuroMab), -GluA2 (1:200, NeuroMab), -Bassoon (1:100, Assay designs), -$GABA_B$ Receptor 1 (1:200, Abcam), -V5 (1:500, Invitrogen), -myc (1:1000, MBL) or with **Guinea Pig anti**: Brevican (1:500, BD transduction laboratories) in GDB1X solution (2X: gelatin 2%, Triton X100 10%, 0.2 M Na_2HPO_4 pH 7.4, 4 M NaCl) for 2 hours at room temperature.

For surface staining, live DIV18-20 hippocampal neurons were incubated for 10 min at 37°C with $GABA_B$Rs antibody. After washing (PBS supplement with 1mM $MgCl_2$, and 0,1 mM $CaCl_2$), neurons were fixed for 10 minutes at room temperature in 4% paraformaldehyde/ 4% sucrose without permeabilization.

Cells were then washed and incubated with Alexa 488 (1:400, Invitrogen), Alexa 555 (1:400, Invitrogen) or Cy5 (1:200, Jackson Laboratories) secondary antibodies diluted in GDB1X solution for 1 hour at room temperature.

For intracellular staining, a second protocol of staining was used in permeabilization condition (as described above).

3.3 Image acquisition, quantification and statistical analysis

Confocal images were obtained using a Nikon 60x objective with sequential acquisition setting at 1024x1280 pixels resolution. Each image was a 'z' series projection of approximately 7 to 12 images taken at 0.75 µm depth intervals.

Transfected neurons were chosen randomly for quantification from two to ten coverslips from three to five independent experiments.

Morphometric and fluorescence intensity measurements were performed using MetaMorph images analysis software (Universal Imaging, West Chester, PA) and ImageJ. Statistical comparisons were performed with appropriate statistical test. Data are expressed as mean ± SEM.

3.4 GST pull-down, immunoprecipitation

GST fusion proteins were prepared in *E.coli* strain BL21 and purified according to standard procedures. HEK293 cells and cultured neurons were lysed with a standard lysis buffer (PBS, 1% Triton X-100, 1mM EDTA, protease inhibitor cocktail, pH 7.4). The lysates were incubated with 30μg GST fusion protein immobilized on glutathione-Sepharose 4B beads (GE Healthcare) for 3 hours at 4°C, wash 3-5 times in lysis buffer and resuspended in 25μl 3X SDS sample buffer. GST alone was used as control. Samples were separated by SDS-PAGE followed by Western blotting with appropriate antibodies. For immunoprecipitation experiments, HEK293 cells, cultured neurons and rat brains homogenates (homogenization buffer: 50mM TRIS-HCl, 200 mM NaCl, 1 mM EDTA, 1%NP40, 1% Triton X-100, pH 7.4, protease inhibitor cocktail) were centrifuged at 10.000 g for 30 min at 4°C and supernatants were incubated with appropriate antibodies at 4°C for 2 hours. Protein A-agarose beads (Santa Cruz Biotechnology, US) were then incubated with homogenates at 4°C for 2 hours. The beads were washed three times with lysis buffer, resuspended in 3X sample buffer and separed by SDS-PAGE. The following antibodies and dilutions were used for immunoprecipitation: **rabbit anti:** -Shrm4 (1 :100, gift from Jeffrey Hildebrand), -GFP (1:1000, MBL International Corporation), -HA (1 :1000, Invitrogen) or **mouse anti:** - $GABA_B$ Receptor 1 (1:2000, Abcam), -V5 (1:400, Invitrogen), -DIC (1 :1000, Abcam). The secondary antibodies were horseradish peroxidase-conjugated anti-rabbit or anti-mouse (both from 1:2000 GE healthcare) (RT, 1 hour in 5% milk). Immunoreactive bands were visualized by enhanced chemiluminescence (GE Healthcare).

3.5 SDS-PAGE, western blot analysis

Cellular lysis and brain homogenization were performed as previously indicated. Proteins were separated in 10% SDS-PAGE and electroblotted onto nitrocellulose membranes in buffer containing 0.025 M Tris-HCl, 0.192 M glycine, 20% methanol, pH 8.3 at 240 mA for 120 min. Immunoblotting reactions were performed by incubating with the primary antibodies (RT, 2-3h in 5% milk): -**rabbit anti**: -Shrm4 (1:200, gift from Jeffrey Hildebrand), -GFP (1:2000, MBL), -$GABA_A\alpha 1$ (1:1000, Millipore), -GAPDH (1:2000, Santa Cruz), -HA (1:1000, Invitrogen) or **mouse anti**: -

αtubulin (1:10000, SIGMA), -$GABA_B$ Receptor 1 (1:2000, Abcam), -βactin (1:4000, SIGMA), -V5 (1:1000, Invitrogen), -myc (1:2000, MBL), -DIC (1 :1000, Abcam).
Horseradish peroxidase-conjugated anti-rabbit or anti-mouse antibodies (1:2000 GE Healtcare) were used as secondary antibodies (RT, 1h in 5% milk).
Immunoreactive bands were visualized by enhanced chemiluminescence (ECL, PerkinElmer).

3.6 Cell cultures, transfection and lentiviral infection

Human Embryonic Kidney 293 cells (HEK293) at 50-70% confluence (24h after plating onto 6-well plates or onto glass coverslips in 12-well plates) were transiently transfected with cDNA expression constructs (0,5-1 mg DNA/well in optiMEM) using lipofectamine 2000 (Invitrogen) for 1 hour in 5% CO_2 at 37°C. The transfected cells were washed twice with PBS and grown for 48 hours in Dulbecco's modified Eagle medium plus 10% fetal bovine serum and 1% penicillin/Streptomycin, before fixation for immunocytochemistry or lysis for coimmunoprecipitation and GST pull-down. The 293FT cell line for generating lentivirus was grown in 1% G418, an aminoglycoside antibiotic. Primary hippocampal neurons were prepared from rat brains (Brewer et al., 1993) and plated on coverslips coated with poly-D-lysine (0,25mg/ml) at 75.000/well for immunochemistry and 300.000/well for GST pull-down, coimmunoprecipitation and lentivirus infection. Cultured neurons were transfected using Lipofectamine 2000. Immature neurons were transfected or infected at DIV7-11 and fixed or lysed at DIV16-20. The cells were infected with Shrm4-shRNAor scrambled as described by **Lois et al., 2002.**

3.7 Direct stochastic optical reconstruction microscopy (dSTORM)

dStorm was performed on an optical setup based on an Olympus IX-81 (Olympus Imaging, Center Valley, PA, USA) inverted microscope equipped with a 100x 1.49NA objective, a Photometrics Evolve 512 EM-CCD sensor (Photometrics, Tucson, AZ, USA) and 405nm 100mW, 488 nm 50mW and 561 nm 30 mW solid state lasers (405 nm and 488nm: Coherent Cube (Coherent Inc., Santa Clara, CA, USA) , 561 nm: Qioptiq iFlex Mustang (QiOptiq, Luxemburg)). A 1.5x magnifier in

the detection path provided a pixel size in the sample plane of 95nm. The sample was mounted on the stage and the medium was substituted prior to acquisition with a mix of glucose oxidase (560µg/ml), caltalase (400µg/ml) and Cysteamine HCl (10mM) in TN buffer with 10% glucose w/v at pH 8 to induce blinking of the fluorophores (Dempsey et al, 2011). 100nm gold nanoparticles (visible in both channels) were added to correct for stage/sample drift. Cultured hippocampal neurons were stained for endogenous Shrm4 and co-stained for MAP2. Secondary antibodies Alexa 568 and Atto 488 were imaged sequentially (starting from the red channels) using the following filter sets from Semrock (Roechester, NY, USA) Alexa 568: dichroic FF562-Di03-25x36, emitter FF01-617/73-25, Atto 488 LF488-B-OMF filter set. 30000 images were collected for each channel with 50 to 100ms exposure times and an increasing ramp of 405nm laser intensity with powers between 0 and 0.8mW was used to reactivate the molecules in long-lived dark states. The super-resolution images were reconstructed using the localization microscopy plugin in µ-Manager (Edelstein et al., 2010), discarding all the molecules localized with accuracy above 70nm and rendering all detected molecules as normalized gaussians with width corresponding to the localization accuracy.

3.8 Transmission electron Microscopy

Cultured rat cortical neurons at DIV14 were fixed with 4% paraformaldehyde in PBS for 30 minutes, post-fixed in the same fixative overnight at 4°C, washed three times with PBS and incubated with 50 mM Glycine in PBS for 10 minutes.

Cells monolayer were incubated for 1 hour in blocking buffer (5% Normal Goat Serum, 0.1% Saponin in PBS) and then with primary antibody diluted in blocking buffer for 2 hours at room temperature. Cells monolayer were then incubated with secondary antibody with 1.4 nm gold-conjugated (Life technologies™, NANOGOLD conjugate of Fab' fragment of goat anti—rabbit IgG, N-24916) for 1h, washed in blocking buffer and fixed with 1% glutaraldehyde in PBS. After washing cells monolayer with 50 mM Glycine in PBS and with 1% BSA and 0,05% Tween in PBS, we proceeded with gold enhancement according to the GoldEnhance™ EM kit (Nanoprobes, 2113).

Neurons were subsequently postfixed with 0.2% osmium tetroxide in 0.1 M PO_4 buffer, en bloc stained with 0.25% uranyl acetate, dehydrated, embedded in Epoxy

resin (Epon 812; Electron Microscopy Science, Hatfield, PA) and baked for 48 hours at 60°C. Thin sections were obtained with an ultramicrotome (Reichert Ultracut E; Leica Microsystem, Vienna, Austria) and examined with a Philips CM10 transmission electron microscope.

Image and Statistical Analysis

The electron microscopy micrographs were analysed with a test for randomness (Mayhew et al., 2001) to estimate the gold particles distribution in cortical neurons incubated with Shrm4 or without (Control) the specific primary antibody against Shrm4. To evaluate the intracellular distribution of Shrm4 we identified in the images 5 different compartments: synaptic boutons, post-synaptic terminal, thin dendrites, other non-determined structures and empty space.

3.9 Time-Lapse Imaging

Live time-lapse imaging was performed in an environmentally controlled chamber with 5% CO_2 at 37°C, using an Axiovert 200M (Zeiss) confocal system equipped with spinning-disk (Perkin Elmer). The 100x objective, 488 nm laser line were used for acquisition. Cultured hippocampal neurons (DIV18-20) were imaged every 5 min for a total period of 40 min. Z-space slices (0,75 μm) were captured and flattened by maximum intensity projection. Image analysis was performed with the volocity High-performance Image system.

3.10 Yeast Two-Hybrid Screening

For two-hybrid experiments, a fragment corresponding to the Shrm4 N-terminal PDZ domain (aa 1-91) was cloned in frame with the GAL4 DNA-binding domain (pGBKT7 vector), and used as bait to screen a human adult brain cDNA library (Clonetech, Mate and Plate Library). Positives clones (3+) grew on plates containing X-α-GAL and Aureobasidin A (QDO/X/A plates) and expressed all four integrated reporter genes: HIS3, ADE2, AUR1C and MEL1 under the control of three distinct Gal4-responsive promoters. cDNA plamids from positive clones were recovered via DH5a *Escherichia coli* (*E.coli)* transformation and plated on ampicilline plates and sequenced.

3.11 Biotinylation assay

Plasma membrane proteins were biotinylated using membrane-impermeant sulfo-NHS-SS-biotin (0,3 mg/ml, Pierce) for 5 minutes at 37°C. Labeled neurons were washed with TBS supplemented with 0,1 mM $CaCl_2$, 1mM $MgCl_2$ and 50 mM glycine. After 3 washes with TBS supplemented with 0,1 mM $CaCl_2$ and 1mM $MgCl_2$ on ice, cells were lysed in extraction buffer (50 mM Tris-HCl, pH 7.4, 1 mM EDTA, 150 mM NaCl, 1% SDS, and protease inhibitors). Lysates were boiled for 5 minutes and immunoprecipitated with streptavidin-conjugated magnetic beads (Dynabeads, Invitrogen).

3.12 Cannula implantation, Adeno-associated virus (AAV) injections

Cannula implantation and drugs infusions into CA1 were identical to *Rex et al., 2010*. Rats were housed under 12:12 light/dark cycles, with food and water *ad libidum*. Expression of Zoanthus sp. Green Fluorescence Protein (ZsGreen GFP) was used as reporter gene in order to detect correct injection coordinates and volumes.
5-7 weeks male Sprague Dawley rats were anesthetized with Zoletil and Xylazine and secured in Kopf stereotaxic. AAV5-shRNA and AAV5-scrambled (AAV5 production from Penn Vector Core, University of Pennsylvania) were injected direcly into CA1 (AP: -3,8 mm relative to Bregma; L: +2 mm; DV: -2 mm from skull; Paxinos and Watson, 1985). Injection volumes were calculated depending on the experiment. Animals were allowed from 2 weeks to 1 month before experimentation.

3.13 GIRK currents - Whole-cell patch clamp electrophysiology

Membrane potassium currents activated by baclofen (10 and 100 μM) were recorded from individual transfected neurons using whole-cell patch clamp recording as indicated previously (Hannan et al., 2012). Patch pipettes (resistances: 3 – 5 MΩ) were filled with the following electrolyte (mM): 120 KCl, 2 MgCl2, 11 EGTA, 30 KOH, 10 HEPES, 1 CaCl2, 1 GTP, 2 ATP, 14 creatine phosphate, pH 7.0. The GIRK cells were constantly superfused with a salt solution containing (mM): 140 NaCl, 4.7

KCl, 1.2 MgCl2, 2.5 CaCl2, 11 glucose, and 5 HEPES, pH 7.4. To ensure larger GABAB receptor-activated K+ currents, the KCl concentration of the external salt solution was increased to 25 mM coupled with a reduction in the NaCl concentration to 120 mM, prior to the application of baclofen. This shifted EK from -90 to -47 mV. The peak amplitude baclofen-activated K+ currents were now inward at a holding potential of -70 mV. Membrane currents were recorded from neurons at DIV14 after transfection at DIV7 and filtered at 5 kHz (-3dB, 6th pole Bessel, 36 dB/octave) before storage onto a Dell Pentium III computer for analysis with Clampex 8. Changes >10% in the membrane input conductance or series resistance resulted in the recording being discarded.

3.14 Whole-cell miniature inhibitory post-synaptic currents (mIPSCs) patch clamp recordings

Whole-cell miniature inhibitory post-synaptic currents (mIPSCs) patch clamp recordings were performed at room temperature from 14 DIV primary hippocampal neurons transfected with Shrm4-shRNA or scrambled at DIV7-8 and perfused with external solution containing (in mM): 130 NaCl, 2.5 KCl, 2.2 CaCl2, 1.5 MgCl2, 10 D-glucose, 10 HEPES-NaOH (pH 7.4). Blockers of sodium channels (500 μM lidocaine) and NMDA, AMPA/Kainate receptors (Kynurenic acid 3 mM) were routinely added in the extracellular solution for recordings. The composition of the intracellular solution was (mM): 140 mM CsCl, 2 mM MgCl2, 1 mM CaCl2, 10 mM EGTA, 10 mM HEPES-CsOH, 2 mM ATP (disodium salt) (pH 7.3). Recordings were performed with an Multiclamp 700B amplifier (Axon CNS molecular devices, USA). Pipette resistance was 2-3 MΩ and series resistance was always below 20 MΩ. mIPSCs were recorded at a holding potential of -70 mV over a period of 2-5 min, filtered at 2 kHz and digitized at 20 kHz using Clampex 10.1 software. Analysis were performed offline with Clampfit 10.1 software using a threshold crossing principle; detection level was set at 5 pA, and raw data were visually inspected to eliminate false events; cells with noisy or unstable baselines were discarded.

mIPSCs population averages were obtained by aligning the events at the mid-point of the rising phase. The weighted decay time constant (Dt) of currents were calculated as described (Cingolani et al., 2008).

3.15 Hippocampal slices and electrophysiology

Adult (body mass, 250-300 g) male Sprague Dawley CD rats were used for the experiments. Rats, injected unilaterally with AAV5-scrambled (left hemisphere) and AAV5-shRNA (right hemisphere) were anesthetized in a chamber saturated with chloroform and then decapitated. The brain was rapidly removed and placed in an ice-cold cutting solution containing 220 mM sucrose, 2 mM KCl, 1.3 mM NaH2PO4, 12 mM MgSO4, 0.2 mM CaCl2, 10 mM glucose, 2.6 mM NaHCO3 (pH 7.3, equilibrated with 95% O2 and 5% CO2), and 3 mM kynurenic acid for patch-clamp recordings or ice-cold artificial CSF (aCSF) containing (in mM) 125 NaCl, 2.5 KCl, 1.25 NaH2PO4, 1 mM MgCl2, 2 mM CaCl2, 25 mM glucose, and 26 mM NaHCO3 (pH 7.3, equilibrated with 95% O2 and 5% CO2) for field excitatory post synaptic potentials (fEPSPs) recordings.

Coronal hippocampal slices (thickness, 300-400 μm) were prepared with a vibratome VT1000 S (Leica) and then incubated first for 40 min at 36°C or at room temperature in aCSF for patch-clamp or fEPSPs recordings respectively. Slices were transferred to a recording chamber perfused with aCSF at a rate of ~2 ml/min at 32°C of temperature.

Whole-cell patch-clamp and fEPSPs recordings were performed with an Multiclamp 700B amplifier (Axon CNS molecular devices, USA) and using an infrared-differential interference contrast microscope. Microelectrodes (borosilicate capillaries with a filament and an outer diameter of 1.5 μm; Sutter Instruments) were prepared with a four-step horizontal puller (Sutter Instruments) and had a resistance of 3–5 MΩ.

Whole cell $GABA_BR$-mediated currents where recorded from hippocampal CA1 pyramidal neurons at holding potential of -80 mV by perfusion of baclofen 100 μM to evoke $GABA_BR$ currents and kynurenic acid (3mM) to block glutamatergic transmission. At the end of every recording, we perfused rat brain slices with the $GABA_BR$ antagonist CGP55845 (5 μM) to control currents specificity. The pipettes were filled with an intracellular solution K-gluconate based, containing (mM): 126 K-gluconate, 4 NaCl, 1 EGTA, 1 MgSO4, 0.5 CaCl2, 3 ATP (magnesium salt), 0.1 GTP (sodium salt), 10 glucose, 10 HEPES-KOH (pH 7.3).

fEPSPs were evoked by stimulation of the Schaffer-collateral pathway of the CA1 region of the hippocampus using aCSF-filled monopolar glass electrodes. fEPSPs

were elicited at a frequency of 0.05 Hz and recorded from the dendritic field of the CA1 pyramidal neurons using aCSF-filled monopolar glass electrodes. fEPSPs were acquired at 20 kHz and filtered at 5 kHz. Stimulus strength was adjusted to give 50% maximal response. Long-term potentiation was elicited by high frequency stimulation (HFS), 100 stimuli at 250 Hz.
Recordings were acquired using Clampex 10.1 software and the analisys of the slope were made offline with Clampfit 10.1 software.

3.16 Behavioral procedures

3.16.1 Elevated Plus Maze

Elevated plus maze paradigm was used to study anxiety related behavior. The test was carried out as previously described (Braida *et al.*, 2008). The apparatus consisted of two opposite open arms (50 cmx10 cm) and two enclosed arms (50 cmx10 cmx40 cm) that extended from a common central platform (10 cmx10 cm) based on a design validated by Lister (1987). The apparatus was constructed from white wood, elevated to a height of 50 cm above floor level and placed in the center of a small quiet room under dim light (about 30 lux). Testing was conducted during the early light phase (9.30–13.30 am) of the light cycle. After 20 min adaptation to the novel surroundings, rats were placed individually onto the center of the apparatus facing an open arm. The number of open- and closed-arm entries and the time spent in open arms were recorded for 5 min.

3.16.2 Spontaneous motor activity

Spontaneous motor activity was evaluated as previously described (Braida and Sala, 2000) in an automated activity cage (43×43×32 cm) (Ugo Basile, Varese, Italy), placed in a sound-attenuating room. The cage was fitted with two parallel horizontal infrared beams located 2 cm from the floor. Cumulative horizontal beam breaks were counted for 30 min.

3.16.3 Pentylenetetrazole (PTZ)-Induced Seizures

Animals (n=5 for each condition) were treated with pentylenetetrazole (45 mg/kg, i.p.) (PTZ, Sigma Aldrich, St. Louis, MO 63178, USA). Seizure activity was monitored for 30 min and seizure severity was rated by the Racine scale (Racine, 1972): 0, no change ; I, myoclonic jerks; II, minimum seizures, with convulsive wave through the body; III, fully developed minimal seizures, clonus of the head muscles and forelimbs, righting reflex present; IV, major seizures (generalized without the tonic phase); V, generalized tonic-clonic seizures. The numbers of seizures, the latency (in seconds) to the first one, the total time spent in seizures and lethality were also evaluated.

3.16.4 Statistical analyses

The results were expressed as mean ± SEM or percentage. The data with normally distributed weights were analysed using Student t-test. Data related to lethality and percentage of animals displaying seizures was analysed using Fisher's exact probability test. Statistically analysis was done using Prism 5 software (GraphPad, San Diego, CA). The accepted level of significance was $p < 0.05$.

3.17 Live cell internalisation assay

Internalisation of $GABA_B$ receptors in live hippocampal neurons was studied as described previously (Hannan et. al, 2012). Briefly, this involved transfection of hippocampal neurons at DIV7 with cDNAs encoding for R1a containing a bungarotoxin (BTX) binding site (R1aBBS), R2 and Shrm4-siRNA or scrambled-siRNA. At DIV 14-21, neurons were pre-incubated in 1 mM d-tubocurarine (Sigma) for 5 min at room temperature followed by incubation in 4 ug/ml BTX coupled to Alexa-fluor 555 (BTX-AF555; Life technologies) for 10 min at room temperature to label cell surface $GABA_B$ receptors. Cells were washed to remove excess BTX-AF555 and superfused with Krebs, in an imaging chamber at 30-32°C. Images were acquired using a Zeiss LSM 510 upright microscope and an Achroplan x40 water DIC objective (NA 0.8). At the first time point (t=0), a rapid z-scan was used to find the optimal z-section and this was imaged as a mean of 4 scans in 8 bits using the 543 nm

Helium-Neon laser and a long-pass 560 nm filter for BTX-AF555 and a 488 nm Argon laser and a 505-530 nm band-pass filter for eGFP. For subsequent time points all the settings including detector gain, amplifier offset, optical slice thickness and laser intensity were kept identical to t=0 and minor changes in drift were corrected by adjusting the position on the z-axis by comparison against the eGFP fluorescence at t=0.

Images were analysed using ImageJ (Ver 1.41o) as described previously (Hannan et al., 2013). The mean fluorescence was determined for 3 regions of interest (ROI), selected for each cell - surface membrane, intracellular compartment, and total cell fluorescence. Background fluorescence was set by imaging a region of the cover-slip devoid of cells. This was subtracted from the ROI fluorescence yielding a mean background-corrected fluorescence. The mean background-corrected fluorescence per unit area (μm2) at each time point was then normalised to the mean background-corrected fluorescence per μm2 at t = 0. These values were then fitted with an monoexponential decay function using Origin (ver 6).

3.18 FRAP (Fluorescent Recovery After Photobleaching) analysis

For live-cell imaging, co-transfected neurons were shifted to an incubator with both controlled temperature and CO_2 mounted on Zeiss LSM510 Meta confocal microscope in the presence of Imaging Medium. Shrm4-shRNA or scrambled expressing neurons were acquired with the 458 nm line of the Argon laser, while 543 nm laser line was used for $GABA_{B1}$-mRFP imaging.

For FRAP experiments of $GABA_{B1}$-mRFP positive dendrites, one prebleached image was acquired, and then a region of interest (ROI) on dendrites was drawn and bleached by scanning 30 times with both 405 nm and 458 nm lasers at 100% power. Recovery of the fluorescence signal was recorded for 10 min. All images were analyzed with ImageJ software. In FRAP experiments, the fluorescence recovery of the bleached ROI was measured over time and normalized to the total fluorescence of the bleached neuron, which was always checked to be constant over time. In all the experiments background signal (determined in an area outside the cells) was subtracted from the fluorescent intensities of the ROIs. Finally, data were averaged and the results shown as graph with GraphPad Prism software.

4. RESULTS

4.1 Shrm4 distributes along microtubules and at synapses

We first investigated the expression of Shrm4 in rat brain by western blot. Shrm4 is detectable in both embryonic and adult rat brain where it is highly expressed in the neocortex and hippocampus (Figure 15A), regions on which we focused our attention. Immunocytochemistry (ICC) on mature hippocampal cultured neurons (Days in Vitro, DIV18) shows that Shrm4 distributes along dendrites and axon, as demonstrated by the colocalization with both the dendritic marker MAP2 and the axonal marker Ankyrin (Figure 15B).

We further investigated the subcellular localization of Shrm4 by direct stochastic optical reconstruction microscopy (dSTORM) on DIV20 hippocampal neurons and we observed that Shrm4 puncta distributes along MAP2-positive filaments suggesting an association with microtubules (Figure 15C).

Moreover by performing ultrastructural immunolocalization of Shrm4 in DIV20 rat cortical neurons, we observed that Shrm4 has a preferential distribution in dendrites and at synapses (Table 1). In fact, while in control unstained neurons, gold particles show random distribution in the five subcompartments analysed, in anti-Shrm4 stained neurons, gold particles are significantly enriched in dendrites (relative labelling index, RLI = 2,23; *p < 0,0001) and at presynapses (synaptic boutons) (RLI = 5,64; *p < 0,0001), with a trend of accumulation at postsynapses (Figure 15D).

Taken together, these results suggest that Shrm4 is abundant in hippocampal and cortical neurons where it localizes at synapses and along microtubules.

4.2 Shrm4 regulates the morphology and molecular structure of dendritic spines

To explore the function of Shrm4 in neurons, we designed three different shRNAs that specifically target both the rat and human Shrm4 transcripts.

To test the efficacy of these shRNAs, we analysed Shrm4 protein level in HEK293 cells transfected with the human Shrm4-HA cDNA together with three different shRNA sequences. ShRNA#3 efficiently reduced Shrm4 expression (Figure 16A). We used the shRNA#3 and its scrambled sequence as control for the following Shrm4 silencing experiments. Similarly, we

observed a significant reduction in Shrm4 protein level in cultured hippocampal neurons, following lentiviral-mediated expression of shRNA#3 (Figure 16B).

As Shrm4 is present in synapses as we previously demonstrated, we sought to examine the effect of Shrm4 silencing on synapse structure and molecular composition.

First, dendritic spine morphology and turnover were evaluated in rat hippocampal neurons. Neurons were transfected with Shrm4 shRNA or scrambled as control before synaptogenesis (DIV8), and fixed mature (DIV18-20) for ICC and in vivo imaging (followed by morphometric analysis). In Shrm4 knockdown neurons, we observed a dramatic decrease in the number of dendritic spines (shRNA 22±1,8 versus scrambled 38±2,1; t test **p < 0,01) and a reduction of spines length (shRNA 0,7±0,028 μm versus scrambled 1,1±0,025 μm; t test **p < 0,01), while spine head width was unchanged compared to control neurons (shRNA 0,51±0,09 μm versus scrambled 0,69±0,05 μm) (Figure 17A). Shrm4 knockdown also induced a significant increase in the number of stubby spines versus scrambled (Mushroom: shRNA 38±2,8 versus scrambled 39,3±2,6; Stubby: shRNA 27±3,4 versus scrambled 7±0,3 t test **p < 0,01; Thin: shRNA 35±2,6 versus scrambled 53,7±1,3) (Figure 17B). Dendritic spine turnover was evaluated by timelapse imaging over 40 minutes. In this time span, we observed a significant increase in the number of removed spines in knockdown while the number of ex-novo spines was unchanged with respect to control neurons (number of removed spines: shRNA 8,34±1,24 versus scrambled 6,25±0,98; t test *p < 0,05; Ex-novo spines: shRNA 5,34±1,02 versus scrambled 5,81±1,34). These data suggest an impairment of dendritic spine stability following Shrm4 silencing that could account for the reduction of spine density (Figure 17C).

Next, to complete the morphological analysis of spines, we investigated the expression of synaptic markers: the scaffolding postsynaptic protein PSD95, the AMPA receptor subunit GLUA2, the presynaptic proteins BASSOON and SYNAPSIN. ICC followed by fluorescence analysis showed a reduction in both the number of puncta and mean fluorescence intensity for all the four synaptic markers considered (Mean number of puncta of ShRNA expressing neurons normalized on scrambled neurons: PSD95 = 0,73±0,04; t test **p < 0,01; BASSOON = 0,78±0,02; t test **p < 0,01; GluA2 = 0,60±0,04; t test **p < 0,01; SYNAPSIN = 0,76±0,03; t test **p < 0,01; mean fluorescence intensity of ShRNA expressing neurons normalized on scrambled neurons: PSD95 = 0,53±0,15; t test **p < 0,01; BASSOON = 0,58±0,15; t test **p < 0,01; GluA2 = 0,66±0,08; t test *p < 0,05; SYNAPSIN = 0,51±0,09; t test *p < 0,05) (Figure 17D).

The decrease in synaptic markers correlates with the reduced number of spines and their stability impairment. Finally, to check whether these dendritic spine defects impact the number of established synapses, we evaluated the extent of colocalization between SYNAPSIN and PSD95 puncta and observed a dramatic decrease in the percentage of SYNAPSIN/PSD95 colocalization in knockdown condition versus scrambled (shRNA 8,73±0,53 versus scrambled 19,89±0,48, t test ***p < 0,001) (Figure 17E).
These results taken together indicate that Shrm4 in hippocampal neurons is necessary for the correct morphological and molecular structure of dendritic spines and synaptic contacts.

4.3 Shrm4 binds $GABA_B$ receptor in neurons

To gain insights into the molecular function of Shrm4 in neurons, we looked for Shrm4 interacting partners. We performed a Yeast Two-hybrid Screening using the N-terminal PDZ domain of Shrm4 (aa 1-91; Figure 18A) as a bait to screen a human adult brain cDNA library. Above all the cDNA clones isolated, six of them coded for the C-terminal tail of $GABA_B$ receptor subunit 1 ($GABA_{B1}$). This stretch of 100 amino acids is shared by the two splice variants of this subunit: 1a ($GABA_{B1a}$) and 1b ($GABA_{B1b}$). In fact, both splice variants are coded by the GABBR1 gene and only differ in their amino-terminal extracellular region where $GABA_{B1a}$ contains two sushi domains (Bettler et al., 2004; Gassmann et al., 2012) (Figure 18A).
The region of interaction between Shrm4 and $GABA_{B1}$ subunit was further characterized by yeast two hybrid tests. First we reconfirmed that the PDZ domain of Shrm4 is necessary and sufficient for binding the C-terminal tail of the $GABA_{B1}$ receptor. Indeed, Shrm4 mutants bind $GABA_{B1}$ receptor only in those where the PDZ domain is present (Shrm4 full-length 1-1492: +++; ΔPDZ 91-1492: negative; Shrm4 PDZ domain 1-91: +++; ΔASD2 1-1213: +++) (Figure 18B).
Next, we looked for the minimal region of the C-terminal tail of $GABA_{B1}$ that interacts with Shrm4 by coimmunoprecipitation (CoIP) in HEK293 cells. We cotransfected Shrm4-GFP cDNA with $GABA_{B1a}$ constructs bearing different amino acids deletion in their C-terminal (Figure 19A; Deletion1: Δ859-961; Deletion2: Δ922-961; Deletion3: Δ870-961). Based on CoIP experiments (using both immunoprecipitation of Shrm4-GFP and $GABA_B$ receptors), we found that the sequence of the C-terminal tail of $GABA_{B1}$ that is necessary for the interaction with the PDZ domain of Shrm4 is comprised between amino acids 859 and 870 (Figure 18C).

To reconfirm the interaction, HEK293 cells were transfected with Shrm4-V5, $GABA_{B1}$-myc and $GABA_{B2}$ constructs and ICC showed that Shrm4 and $GABA_{B1}$ colocalizes (arrows; Figure 19C). By contrast, in cells transfected with Shrm4-V5, $GABA_{B1}$-Δ859-961 and $GABA_{B2}$, the colocalization is lost showing that the C-terminal tail of $GABA_{B1}$ is necessary to bind Shrm4 (Figure 19C).

This interaction is specific for $GABA_{B1}$ subunits and not for $GABA_{B2}$ subunit as observed by coimmunoprecipitation assay using HEK293 cells (Figure 19B).

Finally, we investigated Shrm4/$GABA_B$ receptors ($GABA_BRs$) interaction in neurons. We performed CoIPs on rat brain extracts using a polyclonal antibody against Shrm4 for immunoprecipitation, demonstrating that Shrm4 and $GABA_BRs$ are associated (Figure 18D).

GST pull-down experiments were performed on (1) DIV18 hippocampal cultured neurons and (2) brain extracts: the PDZ domain of Shrm4 fused to GST, as expected, pulled down both the $GABA_{B1a}$ and $GABA_{B1b}$ subunit isoforms (Figure 18E).

Moreover immunofluorescence labelling of DIV18 rat hippocampal neurons showed that Shrm4 and $GABA_BRs$ colocalizes to some extent in dendrites and spines (Figure 18F).

All together, these data demonstrate that Shrm4 and $GABA_BRs$ interact in neurons and that the interaction is mediated by the PDZ domain of Shrm4 and the amino acids 859-870 of the $GABA_B$ receptor C-terminal tail.

4.4 Shrm4 regulates $GABA_B$ receptors intracellular distribution

Previous studies clearly demonstrated that the cytosolic C-terminal domain of $GABA_{B1}$ is important for receptor trafficking to the cell surface (Margeta-Mitrovic et al., 2000; Calver et al., 2001; Pagano et al., 2001). Because Shrm4 interacts with the C-terminal domain of $GABA_{B1}$, we asked whether Shrm4 could regulate $GABA_BRs$ trafficking in neurons. To test this hypothesis, we silenced Shrm4 using shRNA lentiviral delivery and performed surface biotinylation assay on cultured hippocampal neurons. Shrm4 knockdown induces a significant reduction in $GABA_BRs$ surface expression (Signal intensity normalized on scrambled: shRNA = 0,83±0,02; t test *$p < 0,05$) without affecting $GABA_A$ receptors α1 subunit ($GABA_A$ α1) surface expression (Signal intensity normalized on scrambled: shRNA= 0,97±0,02) (Figure 20A). Ionotropic $GABA_A$ receptors that mediate fast synaptic inhibition in neurons were used as control (Jacob et al., 2008; Heisler et al., 2011).

These results prompted us to analyse $GABA_{B1}$ surface immunostaining on cultured hippocampal neurons. Indeed, the surface $GABA_BRs$ along dendrites was reduced in shRNA

expressing neurons compared to scrambled shRNA-expressing neurons (surface $GABA_BRs$ intensity normalized on scrambled: shRNA = 0,77±0,04; t test *p < 0,05; surface $GABA_A$ α1 intensity normalized on scrambled was unchanged: shRNA = 0,96±0,06). Interestingly, the intensity of intracellular $GABA_BRs$ was significantly increased in Shrm4 knockdown neurons, suggesting that $GABA_BRs$ are accumulated in intracellular compartments (Intracellular $GABA_BRs$ intensity normalized on scrambled: shRNA = 2,23±0,07; t test **p < 0,01; intracellular $GABA_A$ α1 intensity normalized on scrambled was unchanged: 0,87±0,14) (Figure 20B).

In particular, in the absence of Shrm4, $GABA_BRs$ are concentrated into the Golgi apparatus as demonstrated by the colocalization between $GABA_BRs$ and the Golgi membrane resident protein Giantin ($GABA_BRs$ intensity in Giantin positive ROI normalized on scrambled: shRNA = 1,32±0,13; t test *p < 0,05; $GABA_A$ α1 intensity in Giantin positive ROI normalized on scrambled was unchanged: shRNA = 0,98±0,1) (Figure 20C).

In addition, when Shrm4 and $GABA_BRs$ are expressed alone in HEK293 cells, they both accumulate into the Golgi apparatus. By contrast, when the two proteins are coexpressed, their retention into the Golgi apparatus is significantly lower and their localization more diffuse (Figure 21).

These findings indicate that Shrm4 regulates specifically $GABA_BRs$ intracellular trafficking in neurons by a Golgi apparatus dependent mechanism.

4.5 Shrm4 mediates $GABA_{B1}$ association with the dynein/dynactin complex

$GABA_BRs$ accumulation into the Golgi apparatus and surface reduction could arise either from an increase in the rate of internalization of the surface receptor or from a defect in its transport from the Golgi apparatus along dendrites. To clarify this point, internalisation of $GABA_BRs$ in live hippocampal neurons was analysed as previously described in Hannan et. al, 2012. Hippocampal cultured neurons were transfected at DIV7 with cDNAs encoding for $GABA_{B1a}$ containing a bungarotoxin (BTX) binding site, $GABA_{B2}$ and either Shrm4-shRNA or scrambled. In particular, the $GABA_{B1a}$ isoform was used as it is more stable on the cell surface of hippocampal neurons than $GABA_{B1b}$ isoform and was therefore more suitable for the internalisation assay. We observed no changes in the internalization rate of $GABA_{B1a}$ in silenced Shrm4 neurons with respect to control neurons (Figure 22). These observations

indicate that Shrm4 silencing is affecting the intracellular transport of $GABA_BRs$ without altering the internalization rate of the receptor.

We next tested our second hypothesis in which Shrm4 regulates $GABA_BRs$ transport along dendrites, eventually allowing its insertion into the plasma membrane.

In neurons, active cargo transport into dendrites and axons is driven by the microtubules-based motor proteins kinesins and dynein. Kinesins move along microtubules to their plus end, and are responsible for receptor subunits and synaptic vesicle transport in axons while the dynein/dynactin complex moves along microtubules toward the minus end and sorts postsynaptic proteins, mitochondria and Golgi outposts to dendrites (Goldstein et al., 2000; Vale et al., 2003; Zheng et al., 2008; Kapitein et al., 2010; Van Spronsen et al., 2013).

A Recent work demonstrated that Kinesin-1 is responsible for $GABA_{B1a}$ subunit transport along the axonal ER and the ERGIC (Valdes et al., 2012), while the mechanism for $GABA_BRs$ trafficking along dendrites is largely unknown.

We assessed the existence of a complex containing Shrm4, $GABA_BRs$ and a microtubule-dependent motor protein, responsible for the intracellular transport. Interestingly in HEK293 cells, we observed that the dynein intermediate chain (DIC) and both $GABA_{B1a}$-myc and $GABA_{B1b}$-myc were coimmunoprecipitated by Shrm4-V5 (Figure 23A), while in HEK293 co-transfected with Shrm4-V5 and KIF5-GFP, the two proteins did not coimmunoprecipitate (Figure 23B). Similarly, coimmunoprecipitation experiments on adult rat brain extracts using polyclonal Shrm4 antibody showed that Shrm4, $GABA_BRs$ and DIC are associated (Figure 23C). We next investigate whether Shrm4 levels modulate the dynein/dynactin-$GABA_BRs$ association. We developed a model using Adeno-associated virus serotype 5 (AAV5) expressing scrambled (AAV5-scrambled) and shRNA (AAV5-shRNA) that selectively and locally silenced Shrm4 levels in the rat brain hippocampus (Figure 23D). AAV5-shRNA infection dramatically reduced Shrm4 protein levels compared to AAV5-scrambled injection (Figure 23E). We then carried out anti-DIC immunoprecipitations from scrambled and shRNA infected brain lysates. We observed co-immunoprecipitation of $GABA_BRs$ with anti-DIC in control condition while this association is significantly decreased in the abscence of Shrm4 (Mean percentage of $GABA_{B1}$ co-precipitation normalized on immunoprecipitated DIC; AAV5-shRNA = 53,7±4%, *$p < 0,05$, t test) suggesting that the dynein-$GABA_BRs$ association is dependent of Shrm4 endogenous level (Figure 23F).

Taken together, these data support a model in which Shrm4 regulates the binding between dynein/dynactin and $GABA_BRs$ in the rat brain hippocampus.

4.6 Shrm4 through the dynein/dynactin complex drives $GABA_BRs$ into dendrites

As the dynein/dynactin complex is involved in the transport of postsynaptic proteins and Golgi outposts and that we previously demonstrated that Shrm4 regulates the association of $GABA_BRs$ with this microtubules-based motor, we decided to investigate a possible involvement of Shrm4 in a dynein-dependent trafficking of $GABA_BRs$ along dendrites. We asked whether the modulation of Shrm4 levels or dynein activity could alter $GABA_BRs$ transport along dendrites and axon.

We first analysed the endogenous distribution of $GABA_BRs$ both in dendrites and axons of hippocampal neurons expressing GFP (control), Shrm4-shRNA or a dominant-negative dynactin construct (p150-cc1) that inhibited dynein activity (Kwinter et al., 2009; Spronsen et al., 2013). We first verified that the different vectors used had no effect on the endogenous distribution of $GABA_BRs$ (Figure 24A). We then measured both the average dendrite intensity I_d and average axonal intensity I_a and calculated the polarity index (PI) by using $PI = (I_d-I_a)/(I_d+I_a)$. For uniformly distributed proteins $I_d = I_a$ and $PI = 0$ whereas $PI > 0$ or $PI < 0$ indicates polarization toward dendrites or axons, respectively (Kapitein et al., 2010; Spronsen et al., 2013). We observed that dendritic $GABA_BRs$ fluorescence intensity in shRNA and GFP-p150-cc1 expressing neurons was dramatically reduced compared to GFP control (Mean intensity normalized on GFP control; shRNA = 0,58±0,03, ***p < 0,001; GFP-p150-cc1 = 0,42±0,06, ***p < 0,001- one way ANOVA) without any effect on axons mean intensity (Figure 25A). To further explore $GABA_BRs$ distribution in shRNA or GFP-p150-cc1 expressing neurons, we then calculated the PI. $GABA_BRs$ in control condition reveal a positive PI of 0,58±0,06 indicating that $GABA_BRs$ are more abundant in dendrites. PIs of shRNA and GFP-p150-cc1 expressing neurons are still positive but significantly lower indicating that the polarization toward dendrites and axons is not changed but the amount of endogenous $GABA_BRs$ into dendrites is decreased (PI shRNA = 0,37±0,02, *p < 0,05; GFP-p150-cc1 = 0,31±0,02, **p < 0,01- one way ANOVA) (Figure 25A).

In addition, by overexpressing HA-tagged p50/dynamitin in cultured hippocampal neurons to inhibit dynein function (Burkhardt et al., 1997; Kapitein et al., 2010), the PI of $GABA_BRs$ dramatically decreases (PI = 0,08±0,1, t test **p < 0,01 versus GFP control) and confirmed the effect observed in GFP-p150-cc1 expressing neurons (Figure 24B).

Furthermore, to assess whether the decrease in the amount of $GABA_B$ receptors into dendrites was the consequence of a decrease in the transport rate, we performed FRAP experiments on

hippocampal cultured neurons co-expressing $GABA_{B1}$-RFP together with Shrm4-shRNA or GFP-p150-cc1. In both situations, fluorescence recovery of $GABA_{B1}$-RFP was significantly delayed compared to GFP control expressing neurons. Indeed, only a defect in the half-time fluorescence recovery but not in the mobile fraction was observed in Shrm4 silenced and GFP-p150-cc1 expressing neurons, suggesting that transport rate of receptors into dendrites is affected (Figure 24C).

As $GABA_{B1a}$ and $GABA_{B1b}$ subunit isoforms can be both found into dendrites (Vigot et al., 2006; Daniel Ulrich and Bernhard Bettler, 2007), we then asked if Shrm4 knockdown or dynein inhibition can modify the intracellular transport of a specific $GABA_{B1}$ subunit isoform or if this regulation mechanism is shared between $GABA_{B1}$ subunits. We used cultured hippocampal neurons cotransfected at DIV8 with GFP (control), shRNA or GFP-p150-cc1 together with $GABA_{B1a}$-myc or $GABA_{B1b}$-myc and analysed immunostaining at DIV16 using a monoclonal antibody against myc to detect $GABA_{B1}$ subunits. We then calculated the PI for each condition and observed consistent similar effects previously noted regarding the endogenous distribution of $GABA_B$Rs in these conditions ($GABA_{B1a}$; PI shRNA = 0,23±0,006, *p < 0,05; GFP-p150-cc1 = 0,16±0,007, **p < 0,01- $GABA_{B1b}$; PI shRNA = 0,40±0,03, *p < 0,05; GFP-p150-cc1 = 0,31±0,034, **p < 0,01- One way ANOVA) (Figure 25B). Altogether, these results demonstrate that Shrm4 through the dynein/dynactin complex drives $GABA_B$Rs toward dendrites in hippocampal neurons.

4.7 *In vitro* and *in vivo* Shrm4 knockdown reduces $GABA_B$Rs-mediated K+ current

Postsynaptic $GABA_B$Rs activate G protein-activated inwardly rectifying potassium channels (GIRKs ; also known as Kir3 channels), generating slow inhibitory postsynaptic potentials (IPSCs) and membrane hyperpolarization (Lüscher et al., 1997 ; David et al., 2006). Having demonstrated that Shrm4 through the dynein/dynactin complex regulates receptors transport toward dendrites, we subsequently examined outward K^+ currents induced by application of the $GABA_B$Rs agonist baclofen to DIV14 hippocampal neurons transfected at DIV7 with Shrm4-shRNA or scrambled. We observed a significant decrease in the peak K^+ density (current density ; pA/pF) in both baclofen concentrations 10 μM (shRNA = -3,17±1,20 pA/pF, t test *p < 0,05; Scrambled = -6,53±1,12 pA/pF) and 100 μM (shRNA = -7,55±2,42 pA/pF, t test *p < 0,05; Scrambled = -13,42±1,45 pA/pF) in Shrm4 shRNA expressing neurons. In agreement with our previous results, we observed that Shrm4 knockdown induces

a reduction in the number of postsynaptic $GABA_BRs$-activated by baclofen (Figure 26A). Moreover, no significant changes were observed in the amplitude, decay time, area and frequence of miniature inhibitory postsynaptic currents (mIPSCs) showing that our results remained specific to $GABA_BR$-mediated responses (Figure 26B).

Furhermore, to assess whether Shrm4 knockdown affect physiological $GABA_BRs$-mediated responses, we unilaterally injected either AAV5-scrambled (left hemisphere) and AAV5-shRNA (right hemisphere) into the dorsal CA1 hippocampus, region where application of baclofen clearly evokes $GABA_B$ receptor-mediated responses in dendrites (Newberry and Nicoll, 1984, 1985 ; Lüscher et al., 1997). Fifteen days after injection, time necessary to reach the maximum expression, we prepared acute hippocampal slices from each hemisphere. We first analysed if Shrm4 silencing induced changes in the synaptic strenght, recording field excitatory post synaptic potentials (fEPSPs) in apical dendritic layer of the hippocampal CA1 region and inducing long term potentiation (LTP) after high frequency stimulation (HFS) of Schaffer collaterals (SC). Interestingly, we observed no differences in LTP induction and stability (Figure 27). These observations clearly indicate that the virus injection procedure does not affect physiological responses.

Afterward, we recorded outward currents evoked by baclofen application in CA1 pyramidal neurons. Similarly to *in vitro* experiments on shRNA-expressing neurons, we observed a significant decrease of the current K^+ peak respect to the AA5-scrambled injected hemisphere (Current density (pA/pF); AAV5-shRNA = 0,66±0,09 pA/pF, t test *$p < 0.05$; AAV5-scrambled = 0,95±0,1 pA/pF) (Figure 26C). Taken together, these data support that Shrm4 silencing decreases the peak of $GABA_B$ receptors response both *in vitro* and *in vivo* as expected from the reduced number of receptors observed in dendrites of cultured hippocampal neurons.

4.8 *In vivo* Shrm4 silencing causes increase in anxiety and propensity to seizures

It is now well established that $GABA_BRs$ are involved in anxiety (Cryan and Kaupmann 2005; Pilc and Nowak 2005) and epilepsy (Gambardella et al., 2003; Bettler et al., 2004).

We therefore found a particular interest in analysing behavioural characteristics on animals bilaterally injected with AAV5-scrambled versus AAV5-shRNA. Because we did not observed any changes in LTP induction and stability, we excluded spatial and memory behavioural tasks (Figure 27). We carried out elevated plus maze that is widely used to test

anxiety behavior (Rodgers et al., 1997; Holmes et al., 2001; Jacobson et al., 2007) and Pentylenetetrazol (PTZ)-induced seizures for sensibility to seizures and convulsions (Kong WL et al., 2013) (Figure 28A). We found that AAV5-shRNA injected rats displayed increased anxiety-like behavior (Figure 28B) and increased susceptibility to PTZ-induced seizures (Figure 28D). In details, in the elevated plus maze, we observed that AAV5-shRNA injected rats made significantly less open-arm entries (AAV5-shRNA, N = 1,6±0,3, t test *p < 0,05; AAV5-scrambled, N = 2,7±0,8) and spent less time in the open arms (AAV5-shRNA = 24±8 seconds, t test *p < 0,05; AAV5-scrambled = 72±19 seconds) than AAV5-scrambled injected rats. A slight, but not significant decrease in the number of total entries was found in AAV5-shRNA injected animals. To verify the integrity of motor function, we monitored the spontaneous motor activity (Figure 28C) and no difference between the two groups, even if AAV5-shRNA injected rats seemed less active than AAV5-scrambled injected animals (1261±324.4 for AAV5-shRNA and 1930 ± 417.1 for AAV5-scrambled injected animals horizontal counts) was observed.

Furthermore, we also examined the effect of intraperitoneal injection of PTZ (45 mg/kg), a GABA antagonist (Kong WL et al., 2013). Compared to AAV5-scrambled injected animals, there was a decrease in time latency to the 1st seizure and a significant increase of seizures duration (AAV5-shRNA = 167±38 minutes, t test *p < 0,05; AAV5-scrambled = 35±6 minutes). An increased number of AAV5-shRNA injected rats displayed seizures (stage 3-5) and death (figure 28D).

These results suggest that inducing *in vivo* silencing of Shrm4 in the rat CA1 hippocampus induces anxiety-related phenotypes and an increase in susceptibility to PTZ-induced epileptic seizures. These phenotypes strongly correlate with *in vitro* and *in vivo* defects on $GABA_BRs$ trafficking and transmission observed in the absence of Shrm4 in hippocampal neurons.

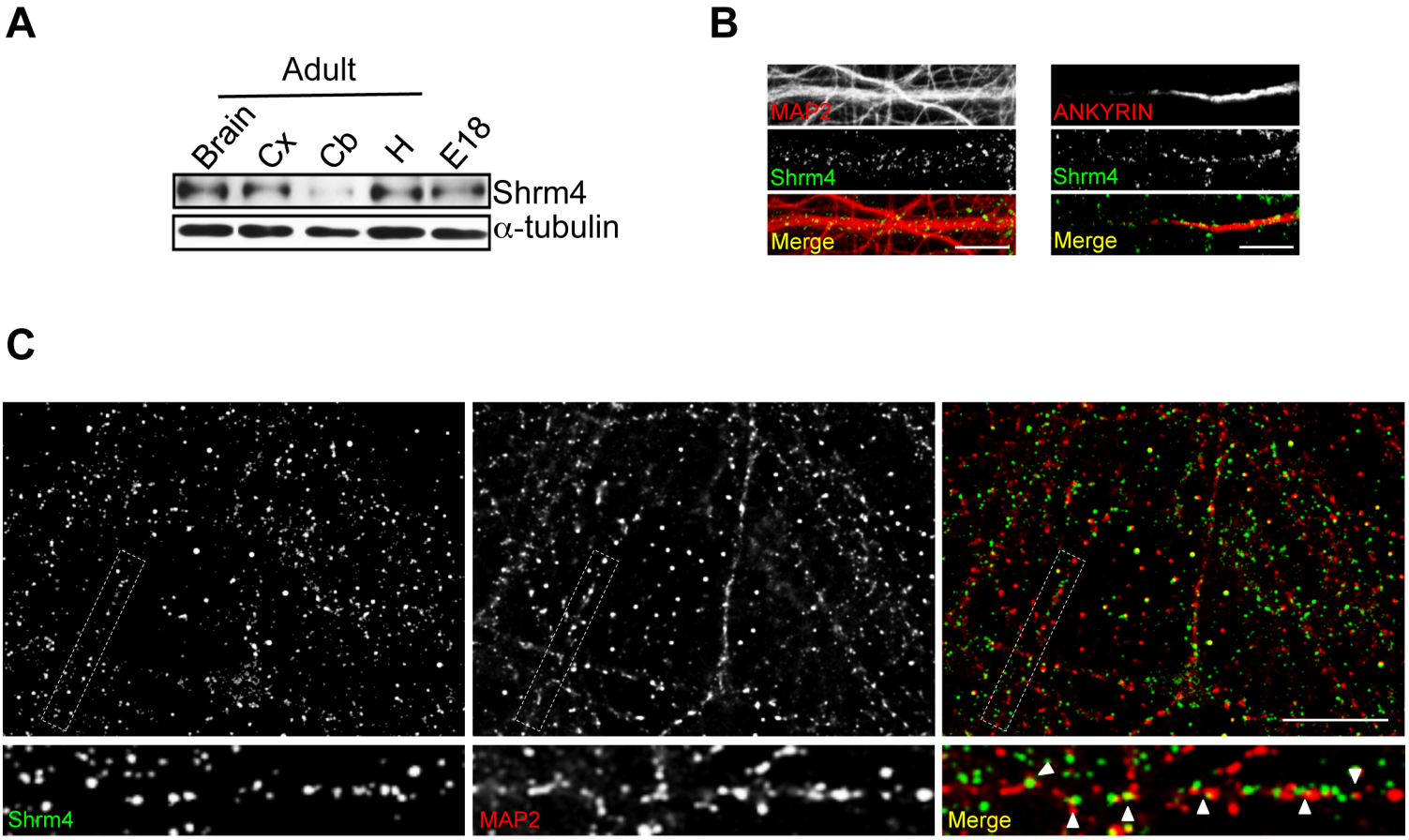
A
Adult
Brain
Cx
Cb
H
E18
Shrm4
α-tubulin
B
MAP2
Shrm4
Merge
ANKYRIN
Shrm4
Merge
C
Shrm4
MAP2
Merge
D
A
sv
sv
MT
dendritic spine
thin dendrite
dendrite
synaptic bouton
B
m
MT
C
m
Relative Labelling Index (RLI)
6
5
4
3
2
1
0
* p <0.0001
SYNAPTIC BOUTON
POST-SYNAPTIC TERMINAL
THIN DENDRITES
OTHER NON DETERMINED STRUCTURES
EMPTY SPACE
Shrm4
Control

Figure 15

Figure 15: Shrm4 distribution in rat brain. (A) Representative western blot of Shrm4 and tubulin expression in embryonic and adult rat brain regions using anti-Shrm4 and anti-α tubulin. Cx: cortex; Cb: cerebellum; H: hippocampus. E18: rat embryonic day 18. (B) Representative images of DIV18 neurons stained for endogenous Shrm4 and costained with MAP2 and Brevican to localize dendrites and axons, respectively. Scale bar, 10 μm. (C) Direct stochastic optical reconstruction microscopy (dSTORM). Representative images of DIV18 hippocampal neurons stained for endogenous Shrm4 and co-stained for MAP2. Scale bar, 5 μm. (D) Thin sections of EPON embedded rat cultured neurons immunolabeled with a primary antibody against Shrm4 and then with a secondary antibody conjugated to 1.4 nm Nanogold® particles enhanced with GoldEnhanceTM. Electron micrographs showing gold particles in dendrites (a-b) and synaptic boutons (c) of DIV20 rat cortical neurons. Scale bar, 200 nm.

TABLE 1: Distribution of gold nanoparticles in cultured rat cortical neurons immunolabeled with (Shrm4) or without (Control) primary antibodies against Shrm4

Compartments	Observed Gold, no	Observed Points (P)	LD Values ($no/P*a_p$)	Expected Gold, ne	RLI Values (no/ne)	X^2 Values
Shrm4						
Synaptic bouton	15	5	3	2.66	5.64	57.30*
Post-synaptic terminal	1	1	1	0.53	1.88	0.41
Thin dendrites	102	86	1.19	45.72	2.23	69.27*
Other non determined structures	4	70	0.06	37.22	0.11	29.65§
Empty space	4	75	0.05	39.87	0.10	32.27§
Total	126	237	0.53	126	1	188.91$
Control						
Synaptic bouton	1	1	1	0.60	1.67	0.27
Post-synaptic terminal	0	1	0	0.60	0	0.60
Thin dendrites	17	22	0.77	13.14	1.29	1.13
Other non determined structures	18	29	0.62	17.32	1.04	0.03
Empty space	10	24	0.42	14.34	0.70	1.31
Total	46	77	0.60	46	1	3.34

Table 1: Distribution of gold nanoparticules in cultured rat cortical neurons immunolabeled with (anti-Shrm4) or without (CONTROL) primary antibody.

Test of randomness was applied to evaluate the distribution of gold particles in cortical neurons incubated with (anti-Shrm4) or without (CONTROL) the specific primary antibody against Shrm4 (see Materials and Methods).

Applying a test point lattice (on which each test point occupied an area $a_p = 1\ \mu m^2$ on the section) on the micrographs, and counting the number of intersections between the grid and each compartment identified in the images (synaptic boutons, post-synaptic terminals, thin dendrites, other non determined structures and empty space) were estimated the Labelling Densities (LD, gold*μm^{-2}) and Relative Labelling Index (RLI) for every compartment and the results were tested for randomness (χ^2 analysis).

* Number of gold particles significantly higher than the expected value ($p < 0.0001$).

§ Number of gold particles significantly lower than the expected value ($p < 0.0001$).

$ Distribution of gold particles significantly deviates from random ($p < 0.0001$).

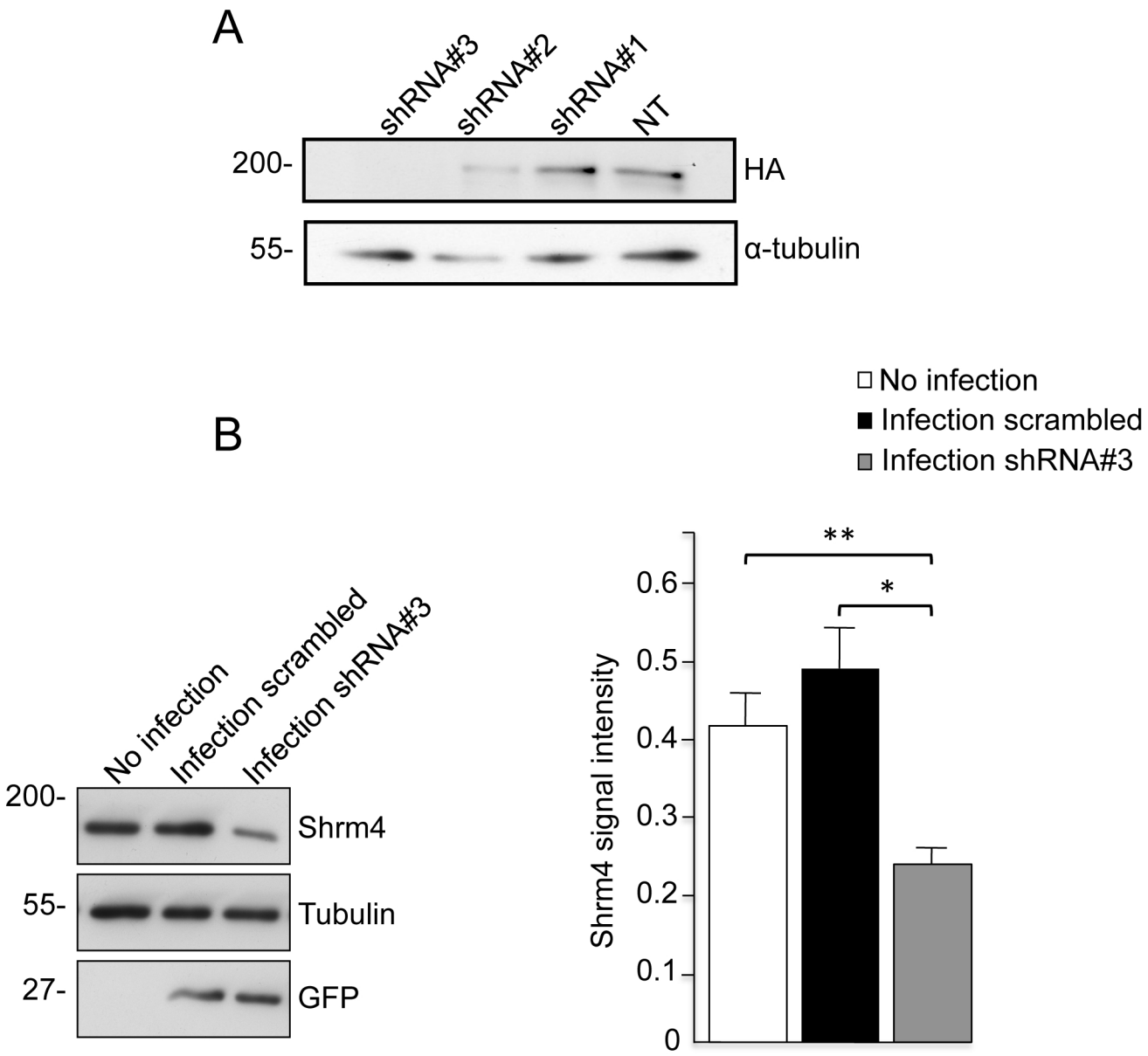
A
shRNA#3
shRNA#2
shRNA#1
NT
200-
HA
55-
α-tubulin
B
No infection
Infection scrambled
Infection shRNA#3
No infection
Infection scrambled
Infection shRNA#3
200-
Shrm4
55-
Tubulin
27-
GFP
Shrm4 signal intensity
0.6
0.5
0.4
0.3
0.2
0.1
0
**
*

Figure 16

Figure 16: ShRNA#3-mediated knockdown significantly reduces Shrm4 endogenous level in hippocampal neurons. (A) Representative western blot of Shrm4 and tubulin protein level in HEK293 cells co-transfected with the human Shrm4-HA cDNA together with three different shRNA sequences (ShRNA#1, 2 and 3). ShRNA#3 efficiently reduced Shrm4-HA expression. (B) (Left) Representative western blot of Shrm4, Tubulin and GFP expression after lentiviral infection of DIV8 cultured hippocampal neurons with scrambled or Shrm4 shRNA. Antibodies anti-Shrm4, anti-α tubulin and anti-GFP were used for western blot. GFP expression was used as control for infection. (Right) Histograms show mean (±SEM) signal intensity of endogenous Shrm4. Lentivirus infection significantly decreases Shrm4 endogenous level compared to non-infected (**p < 0,01) and scrambled-infected neurons (*p < 0,05) (Bonferroni test One way-ANOVA).

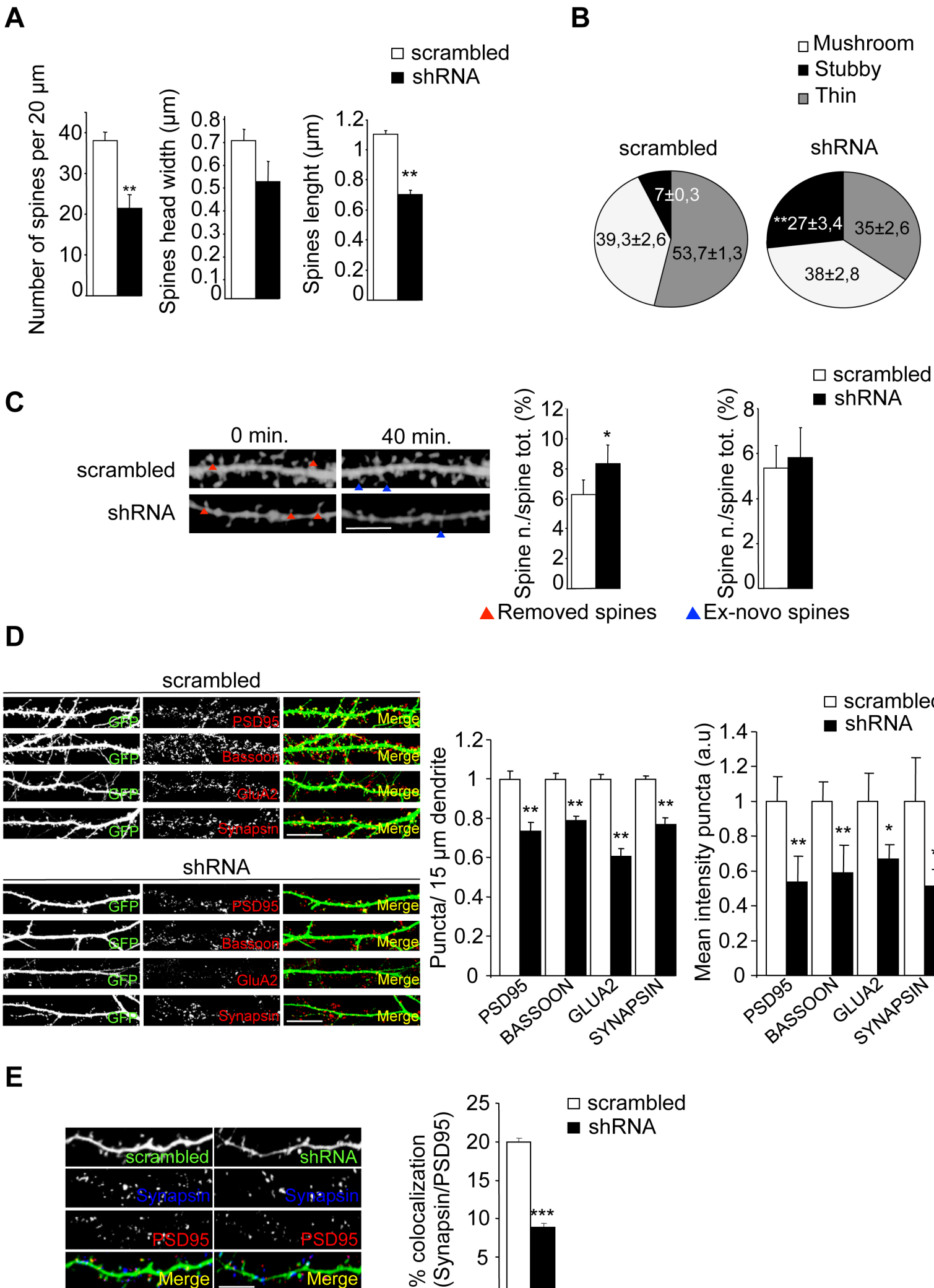
A
scrambled
shRNA
Number of spines per 20 µm
Spines head width (µm)
Spines lenght (µm)
B
Mushroom
Stubby
Thin
scrambled
shRNA
7±0,3
39,3±2,6
53,7±1,3
**27±3,4
35±2,6
38±2,8
C
0 min.
40 min.
scrambled
shRNA
Spine n./spine tot. (%)
Removed spines
Ex-novo spines
D
scrambled
shRNA
GFP
PSD95
Bassoon
GluA2
Synapsin
Merge
Puncta/ 15 µm dendrite
Mean intensity puncta (a.u)
PSD95
BASSOON
GLUA2
SYNAPSIN
E
% colocalization (Synapsin/PSD95)

Figure 17

Figure 17: Shrm4 knockdown induces an impairment in the morphological and molecular structure of dendritic spines. Primary rat hippocampal neurons were transfected at DIV8 with scrambled or Shrm4-shRNA (A-E). (A) The histograms compare mean (±SEM) spines density (Number of spines/20 μm), head width and length (twenty neurons examined for each construct). Spines density (**p < 0,01, t test) and length (**p < 0,01, t test) were significantly decreased in shRNA transfected neurons compared to scrambled controls while no changes were observed in spines head width. (B) The pie charts compare the mean percentage (±SEM) of Mushroom, Stubby and Thin spines. The percentage of stubby spines in shRNA expressing neurons was significantly increased (**p < 0,01, t test). (C) Time-lapse imaging comparing spine dynamics. The histograms show that the percentage (±SEM) (spines number/Total spines) of removed spines (red arrows) was significantly increased (*p < 0,05, t test) in shRNA expressing neurons while no changes in *ex-novo* spines (blue arrows) were observed. Scale bar, 10 μm (D) (Left) Immunostaining for PSD95, BASSOON, GluA2 and SYNAPSIN of DIV19 fixed neurons. (Right) Histograms show normalized mean (±SEM) number of puncta per 15 μm dendrite and intensity for each synaptic marker. A significant decrease in normalized mean number of puncta for PSD95 (**p < 0,01, t test), BASSOON (**p < 0,01, t test), GluA2 (**p < 0,01, t test) and SYNAPSIN (**p < 0,01, t test) was observed in shRNA expressing neurons. Similar results were obtained for normalized mean intensity of PSD95 (**p < 0,01, t test), BASSOON (**p < 0,01, t test), GluA2 (*p < 0,05, t test) and SYNAPSIN (*p < 0,05, t test). Scale bar, 20 μm (E) Co-immunostaining for SYNAPSIN and PSD95 of DIV20 fixed neurons. The histogram shows the mean (±SEM) percentage of puncta where SYNAPSIN and PSD95 colocalize. A significant decrease (***p < 0,001, t test) in the mean percentage was observed in shRNA expressing neurons. Scale bar, 10 μm

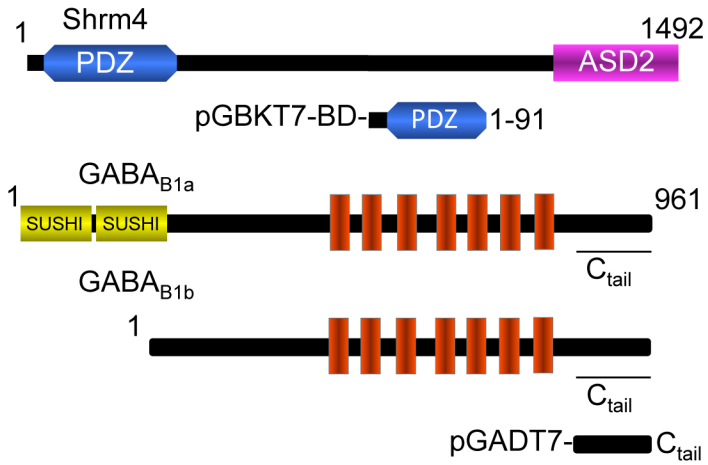

B

Shrm4	GABA$_{B1}$-C$_{terminus}$
Full-length (1-1492)	3+
ΔPDZ (91-1492)	-
Δ91-1492 (PDZ)	3+
ΔASD2 (1-1213)	3+

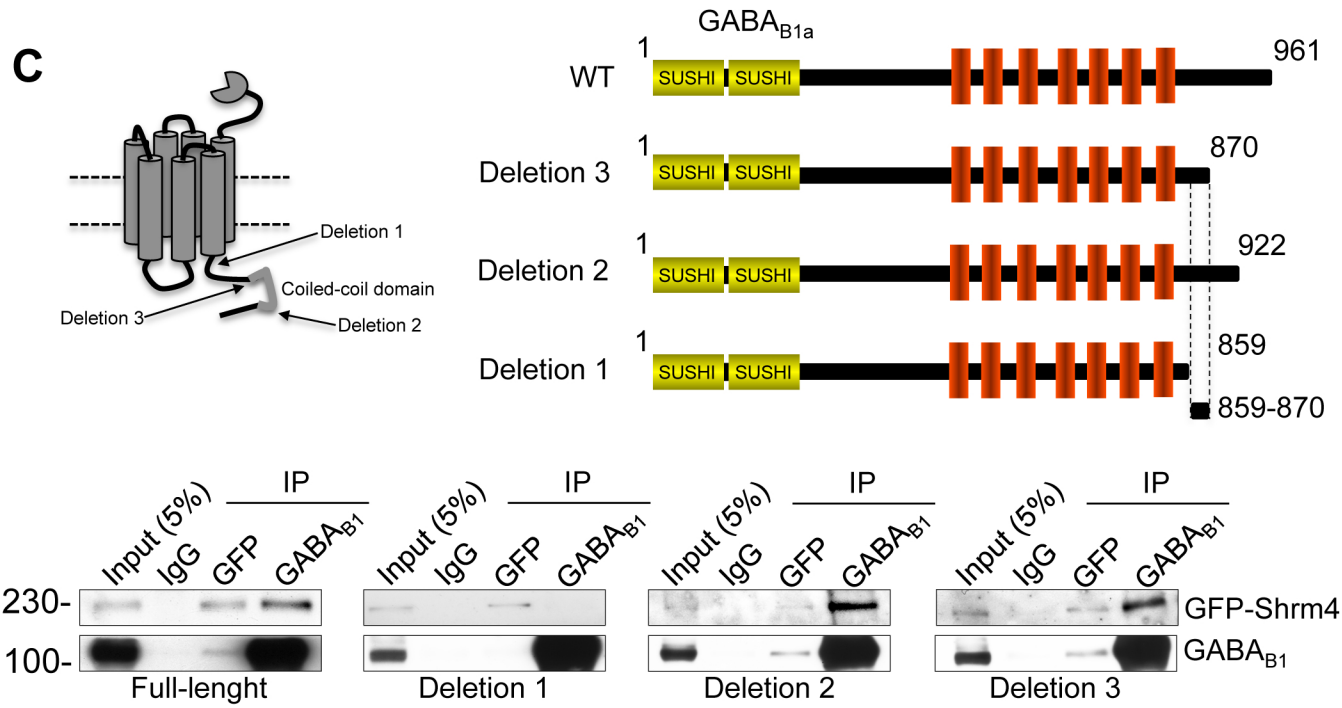

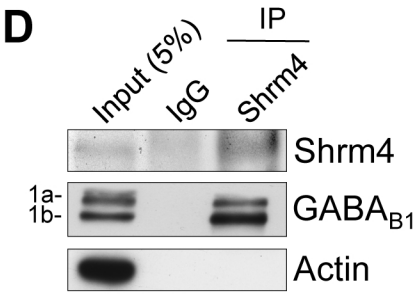

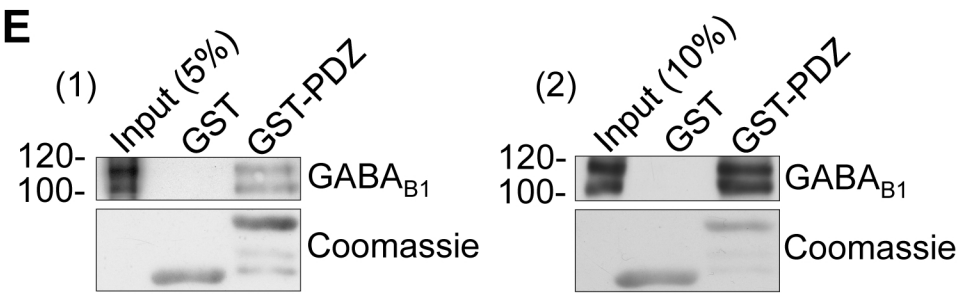

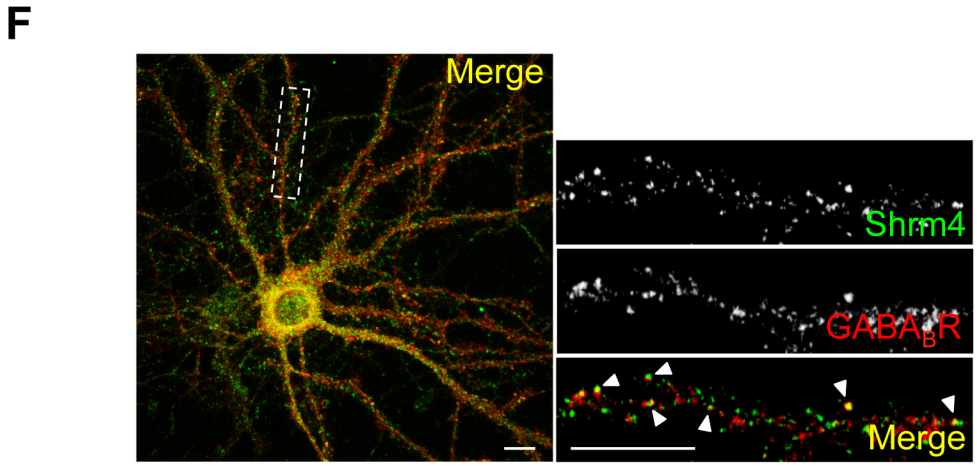

Figure 18

Figure 18: Direct interaction of Shrm4 with $GABA_BR$ subunit isoforms 1. (A) Scheme of Shrm4 structure showing the C-terminal ASD2 domain (pink) and N-terminal PDZ domain (blue). The vector pGBKT7-BD containing the PDZ domain sequence (aa 1-91) was used as bait to screen a human adult brain cDNA library. Above all the cDNA clones isolated, six of them coded for the C-terminal tail of $GABA_B$ receptor subunit isoforms 1 ($GABA_{B1}$). This stretch of 100 amino acids is shared by the two splice variants of this subunit: 1a ($GABA_{B1a}$) and 1b ($GABA_{B1b}$). (B) Yeast two hybrid test with, as bait, the full-length Shrm4 (1-1492) or different truncated forms (ΔPDZ (91-1492); Δ91-1492 (PDZ); (ΔASD2 (1-1213)). Full-length Shrm4, N-terminal PDZ and ΔASD2 constructs interacted with the C-terminal tail of $GABA_{B1}$ (3+). (C) The sequence aa 859-870 of the C-terminal tail of $GABA_{B1}$ is necessary for the interaction with the PDZ domain of Shrm4. HEK293 cells were cotransfected with Shrm4-GFP cDNA together with $GABA_{B1a}$ constructs bearing different amino acids deletion in their C-terminus (Deletion1: Δ859-961; Deletion2: Δ922-961; Deletion3: Δ870-961; See supplementary figure S2). Full-length $GABA_{B1a}$, Deletion 2 and Deletion 3 coimmunoprecipitated with Shrm4-GFP. Both anti-GFP and anti-$GABA_{B1}$ antibodies were used for immunoprecipitations. (D) Shrm4 and $GABA_{B1}$ interaction in the brain. Coimmunoprecipitation experiments on brain extracts using polyclonal Shrm4 antibody show that Shrm4 and $GABA_{B1}$ are associated. (E) GST pull-down experiments on DIV18 cultured hippocampal neurons (1) and brain (2) extracts. The PDZ domain of Shrm4 (GST-PDZ; aa 1-91) pulled down both $GABA_{B1}$ subunit isoforms. (F) Immunofluorescence labelling of DIV18 cultured hippocampal neurons shows that endogenous Shrm4 and $GABA_BRs$ colocalize in dendrites and spines. Scale bar, 10 μm

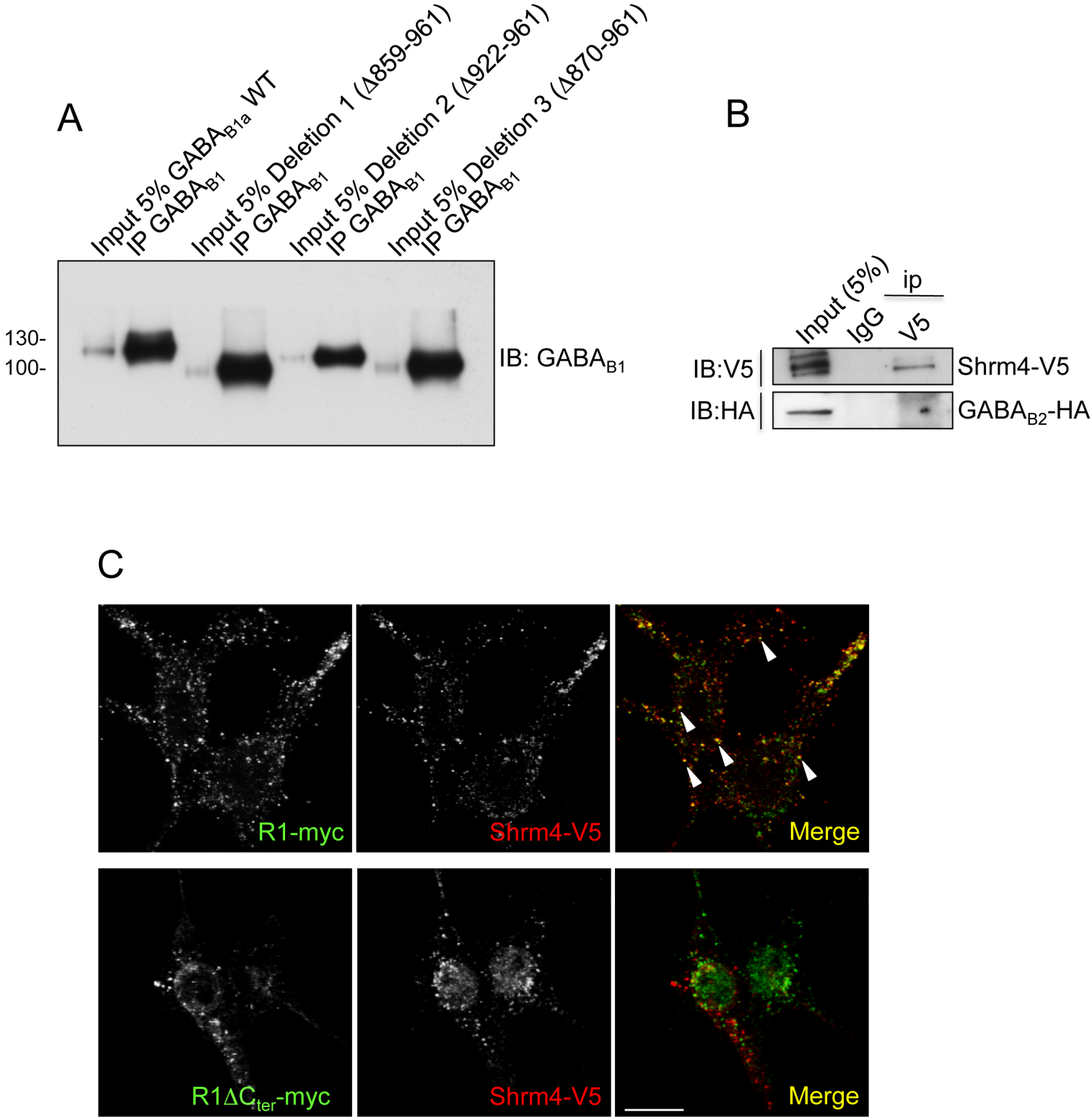
A
Input 5% GABA$_{B1a}$ WT
IP GABA$_{B1}$
Input 5% Deletion 1 (Δ859-961)
IP GABA$_{B1}$
Input 5% Deletion 2 (Δ922-961)
IP GABA$_{B1}$
Input 5% Deletion 3 (Δ870-961)
IP GABA$_{B1}$
130-
100-
IB: GABA$_{B1}$
B
Input (5%)
ip
IgG
V5
IB:V5
Shrm4-V5
IB:HA
GABA$_{B2}$-HA
C
R1-myc
Shrm4-V5
Merge
R1ΔC$_{ter}$-myc
Shrm4-V5
Merge

Figure 19

Figure 19: The interaction Shrm4/$GABA_BRs$ requires the C-terminal tail and remains specific to $GABA_{B1}$. (A) Representative western blot of the different amino acids deletion in $GABA_{B1a}$ C-terminal: Deletion1: Δ859-961; Deletion2: Δ922-961; Deletion3: Δ870-961. To test each cDNA constructs, HEK cells were transfected with each deletion constructs and immunoprecipitations using monoclonal anti-$GABA_{B1}$ were performed. (B) Representative western blot of coimmunoprecipitation experiments on HEK cells co-transfected with Shrm4-V5 and $GABA_{B2}$-HA. Shrm4 and $GABA_{B2}$ alone are not associated. (C) Immunofluorescence experiments of HEK cells co-transfected with Shrm4-V5 together with $GABA_{B1}$-myc full-length or $GABA_{B1}$-ΔC_{ter}-myc, show that Shrm4 and $GABA_{B1}$ colocalize (white arrows). By contrast, Shrm4 and $GABA_{B1}$-ΔC_{ter} did not. Monoclonal antibodies against -V5 and -Myc were used for immunolabelling. Scale bar, 10 μm

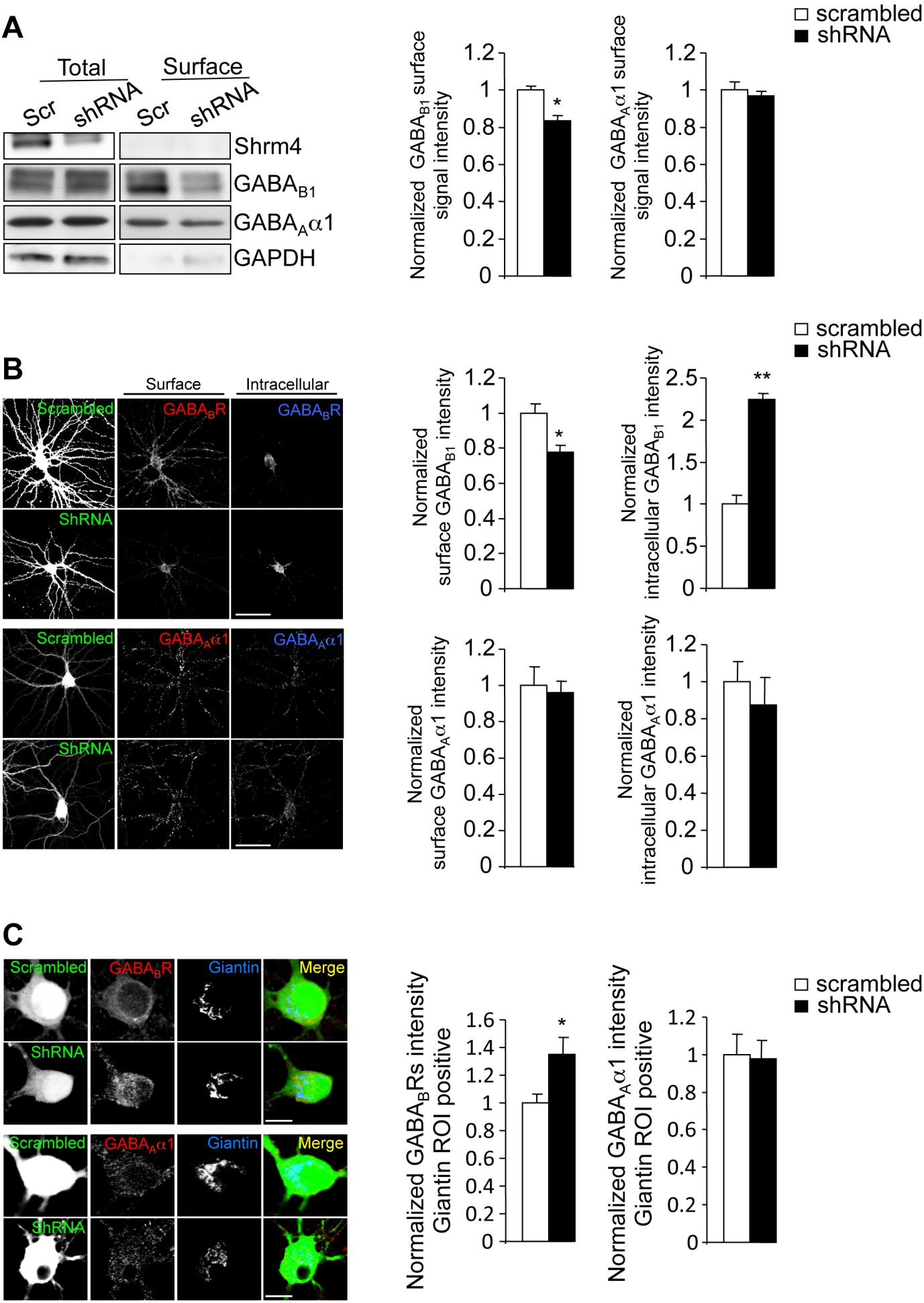
A
Total
Surface
Scr
shRNA
Scr
shRNA
Shrm4
GABA$_{B1}$
GABA$_A\alpha$1
GAPDH
scrambled
shRNA
Normalized GABA$_{B1}$ surface signal intensity
Normalized GABA$_A\alpha$1 surface signal intensity
B
Surface
Intracellular
Scrambled
GABA$_B$R
ShRNA
GABA$_A\alpha$1
Normalized surface GABA$_{B1}$ intensity
Normalized intracellular GABA$_{B1}$ intensity
Normalized surface GABA$_A\alpha$1 intensity
Normalized intracellular GABA$_A\alpha$1 intensity
C
Giantin
Merge
Normalized GABA$_B$Rs intensity Giantin ROI positive
Normalized GABA$_A\alpha$1 intensity Giantin ROI positive

Figure 20

Figure 20: Shrm4 silencing induces decreased $GABA_BRs$ surface expression with accumulation into the Golgi apparatus. (A) Analysis of $GABA_BRs$ biotinylation from DIV18 cultured hippocampal neurons infected with scrambled or Shrm4-shRNA at DIV8. Representative western blot (left) and histograms (right) showing that Shrm4 silencing induces a significant decrease in mean (±SEM) normalized $GABA_{B1}$ surface signal intensity (*p < 0,05; t test) compared to scrambled controls. No changes were observed in the mean (±SEM) normalized $GABA_A\alpha1$ surface signal intensity in Shrm4-shRNA versus scrambled infections. (B) Surface and intracellular $GABA_BRs$ immunostaining of DIV18 cultured hippocampal neurons transfected with scrambled or Shrm4-shRNA at DIV8 (See staining protocol; Materials and Methods). The mean (±SEM) normalized surface $GABA_{B1}$ intensity was significantly decreased (*p < 0,05; t test) in shRNA-expressing neurons while a significant increase (**p < 0,01; t test) in the mean (±SEM) normalized intracellular $GABA_{B1}$ intensity was observed. No changes were observed in either intracellular or extracellular mean (±SEM) normalized $GABA_A\alpha1$ signal intensity in Shrm4-shRNA compared to scrambled transfected neurons. Scale bar, 20 μm. (C) Immunofluorescence staining for anti-$GABA_BRs$ and anti-Giantin from DIV18 cultured hippocampal neurons transfected with scrambled or Shrm4-shRNA at DIV8. A significant increase (*p < 0,05; t test) in the mean (±SEM) normalized $GABA_BRs$ intensity in region of interest (ROI) positive for Giantin was observed in Shrm4 silenced neurons while no changes were observed for $GABA_A\alpha1$.

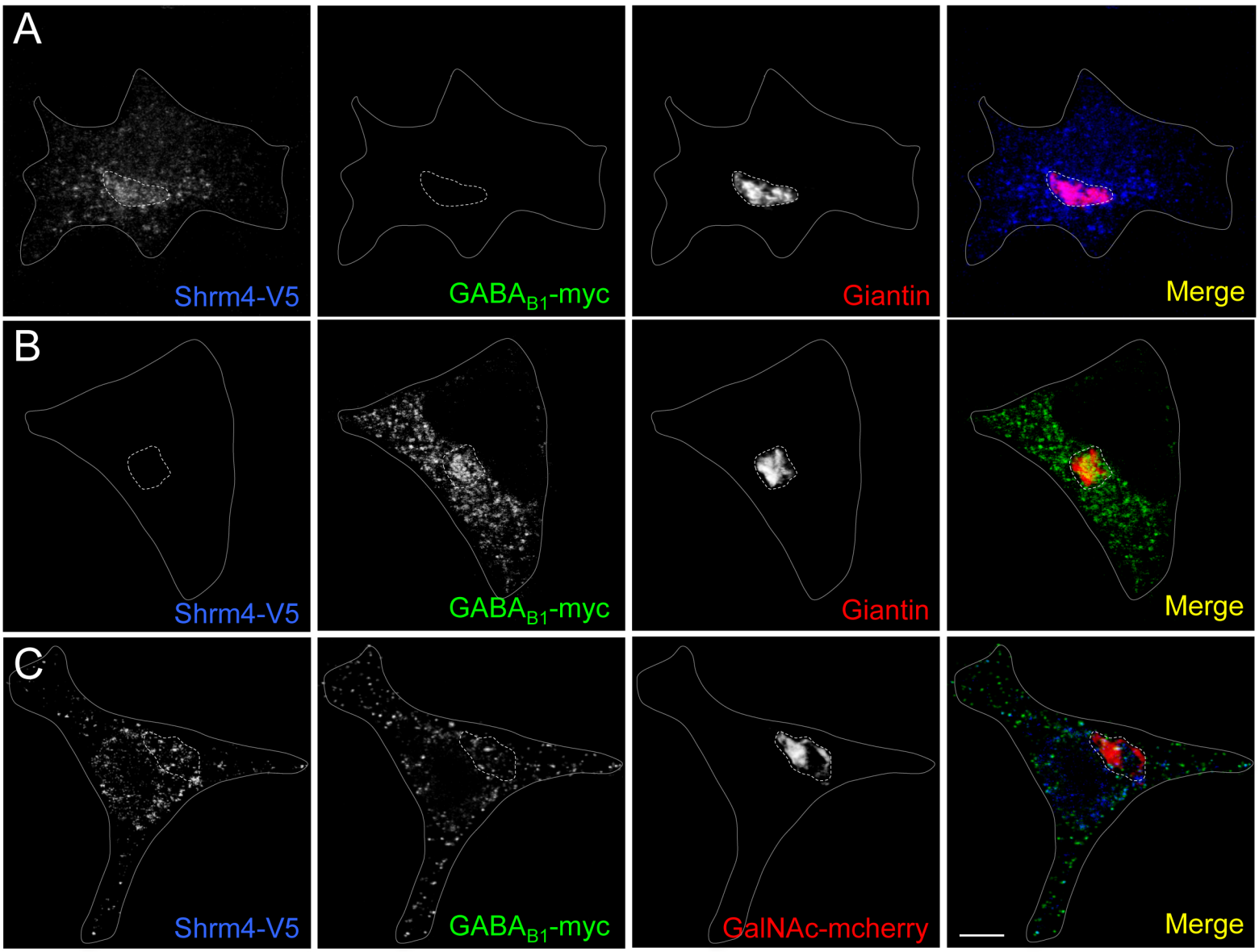
A
Shrm4-V5
GABA$_{B1}$-myc
Giantin
Merge
B
Shrm4-V5
GABA$_{B1}$-myc
Giantin
Merge
C
Shrm4-V5
GABA$_{B1}$-myc
GalNAc-mcherry
Merge

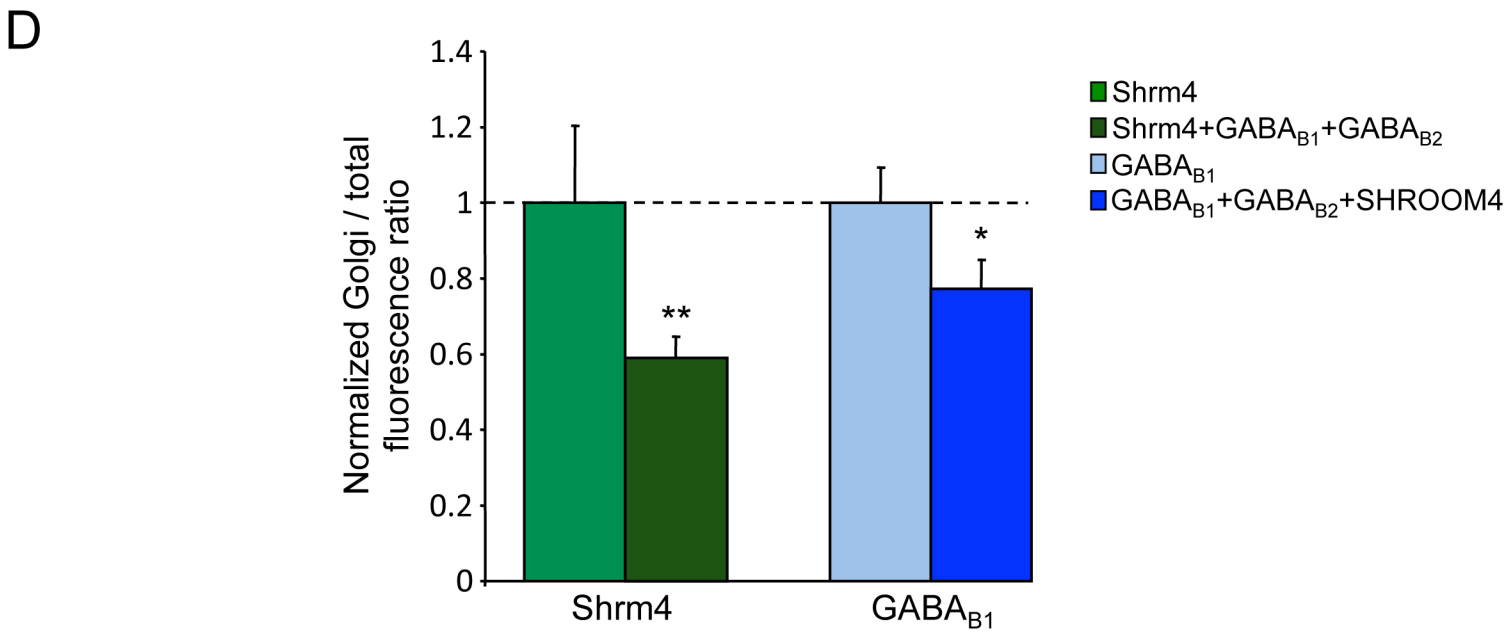
D
Normalized Golgi / total fluorescence ratio
1.4
1.2
1
0.8
0.6
0.4
0.2
0
**
*
Shrm4
GABA$_{B1}$
Shrm4
Shrm4+GABA$_{B1}$+GABA$_{B2}$
GABA$_{B1}$
GABA$_{B1}$+GABA$_{B2}$+SHROOM4

Figure 21

Figure 21: Co-expression of Shrm4 and $GABA_BRs$ decreases their Golgi apparatus retention in a heterologous expression system. (A-C) Representative immunostaining and (D) histogram of Shrm4-V5 and/or $GABA_{B1}$-myc mean (±SEM) normalized fluorescence intensity ratio (Intensity of protein into Golgi apparatus positive ROI/Total intensity) from HEK cells.

(A) Shrm4-V5 and (B) $GABA_BRs$-myc were transfected in HEK293 cells, stained by using monoclonal anti-V5 (A) or anti-myc (B) and costained using a polyclonal anti-giantin to localize the Golgi apparatus. When overexpressed alone, both proteins accumulate into the Golgi apparatus. (C and D) By contrast, when the two proteins are expressed together and by using GalNAc-mcherry to localize the Golgi, their retention into the Golgi apparatus is significantly lower and their localization more diffuse (Shrm4: **p < 0,01, t test and $GABA_BRs$: **p < 0,01, t test). Scale bar, 10 μm.

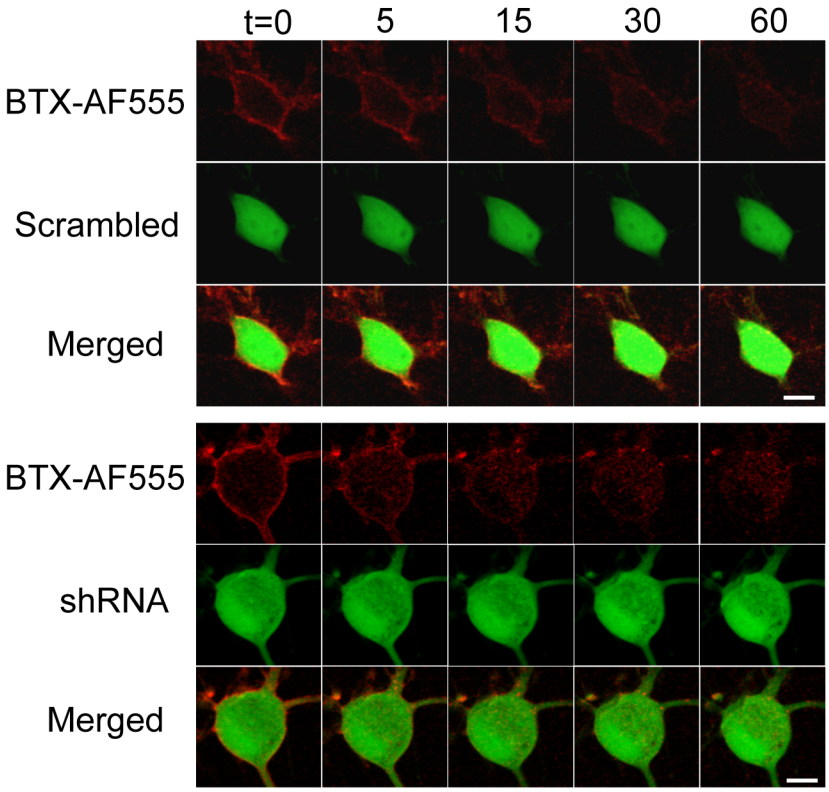
t=0
5
15
30
60
BTX-AF555
Scrambled
Merged
BTX-AF555
shRNA
Merged

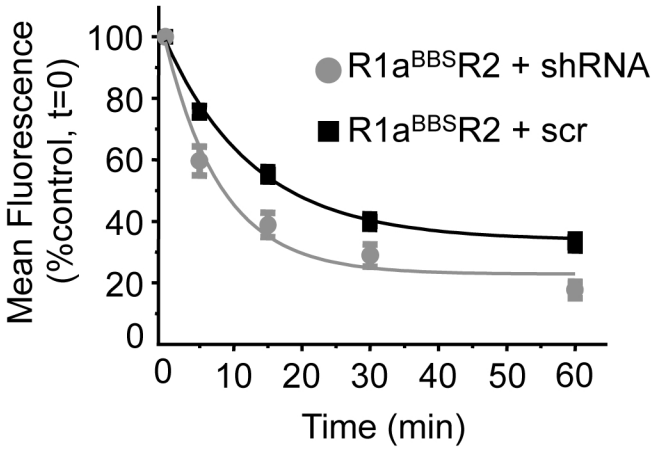
Mean Fluorescence
(%control, t=0)
100
80
60
40
20
0
0
10
20
30
40
50
60
Time (min)
R1a^BBSR2 + shRNA
R1a^BBSR2 + scr

Figure 22

Figure 22: Internalisation of $GABA_B$ receptors in live hippocampal neurons. Hippocampal neurons were transfected at DIV7 with cDNAs encoding for R1a containing a bungarotoxin (BTX) binding site (R1aBBS), R2 and Shrm4-shRNA or scrambled. At DIV 14-21, neurons were pre-incubated in 1 mM d-tubocurarine for 5 min at room temperature followed by incubation in 4 μg/ml BTX coupled to Alexa-fluor 555 for 10 min at room temperature to label cell surface $GABA_B$ receptors (See Materials and Methods). No changes were found in the rate $GABA_{B1a}$ internalization in shRNA and scrambled transfected neurons.

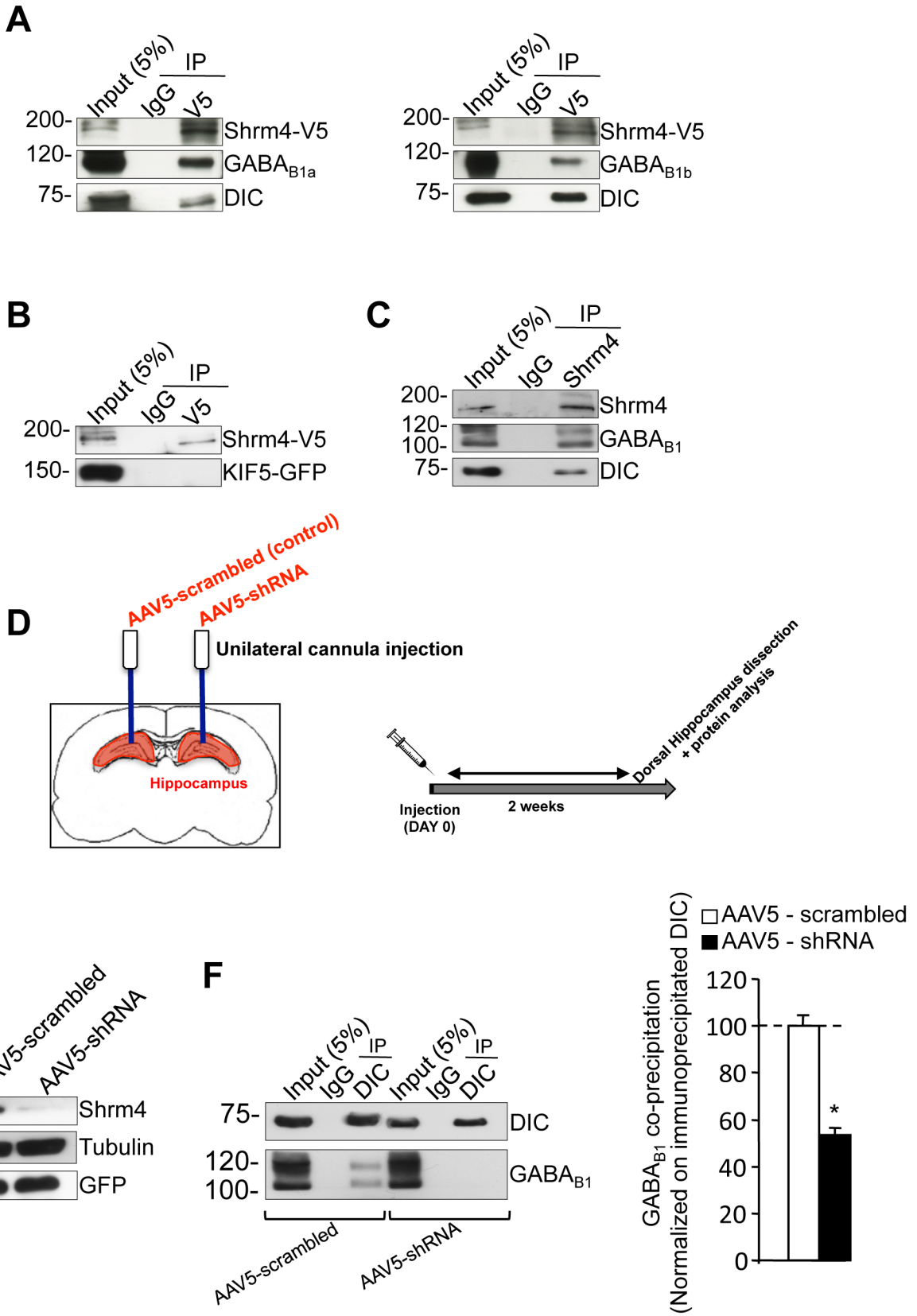
A
Input (5%)
IP
IgG
V5
200-
120-
75-
Shrm4-V5
GABA$_{B1a}$
DIC
Input (5%)
IP
IgG
V5
200-
120-
75-
Shrm4-V5
GABA$_{B1b}$
DIC
B
Input (5%)
IP
IgG
V5
200-
150-
Shrm4-V5
KIF5-GFP
C
Input (5%)
IP
IgG
Shrm4
200-
120-
100-
75-
Shrm4
GABA$_{B1}$
DIC
D
AAV5-scrambled (control)
AAV5-shRNA
Unilateral cannula injection
Hippocampus
Injection
(DAY 0)
2 weeks
Dorsal Hippocampus dissection
+ protein analysis
E
AAV5-scrambled
AAV5-shRNA
200-
55-
30-
Shrm4
Tubulin
GFP
F
Input (5%)
IP
IgG
DIC
Input (5%)
IP
IgG
DIC
75-
120-
100-
DIC
GABA$_{B1}$
AAV5-scrambled
AAV5-shRNA
AAV5 - scrambled
AAV5 - shRNA
GABA$_{B1}$ co-precipitation
(Normalized on immunoprecipitated DIC)
120
100
80
60
40
20
0
*

Figure 23

Figure 23: Shrm4 regulates $GABA_BRs$-Dynein/Dynactin association. (A-C) Coimmunoprecipitation with Shrm4, $GABA_BRs$ and Dynein/Dynactin. (A) HEK cells were transfected with (Left) Shrm4-V5 and $GABA_{B1a}$-myc or (Right) Shrm4-V5 with $GABA_{B1b}$-myc. In HEK cells, (Left) $GABA_{B1a}$ or (Right) $GABA_{B1b}$ with the endogenous Dynein Intermediate Chain (DIC) coimmunoprecipitated with Shrm4-V5. Monoclonal antibodies anti-V5, anti-myc and anti-DIC were used for western blot. (B) HEK cells were transfected with Shrm4-V5 and KIF5-GFP. KIF5-GFP did not coimmunoprecipitated with Shrm4-V5. A polyclonal anti-GFP was used for western blot. (C) Coimmunoprecipitation experiments on brain extracts using polyclonal Shrm4 antibody show that Shrm4, $GABA_{B1}$ and DIC are associated. (D-F) Dynein/Dynactin-$GABA_BRs$ association is modulated by Shrm4 amount. (D) Scheme representing unilateral local injection of AAV5-scrambled (Left hemisphere) and AAV5-shRNA (Right hemisphere) in the rat brain hippocampus. (E) Representative western blot of Shrm4, Tubulin and GFP from hippocampal brain extracts. Fifteen days after injections, hippocampus from injected rat brain were dissected and analysed by western blot. Rat hippocampus extracts infected by AAV5-shRNA show strong decrease in Shrm4 expression levels. (F) From hippocampus extracts used in (E), monoclonal anti-DIC immunoprecipitations from scrambled and shRNA infected lysates were performed. We observed co-immunoprecipitation of $GABA_BRs$ with DIC in control condition while this association is significantly decreased ($*p < 0,05$, t test) in shRNA infected hippocampal lysates. Values of co-precipitated $GABA_{B1}$ were normalized on DIC immunoprecipitated levels and the normalized mean (±SEM) percentage of $GABA_{B1}$ co-precipitated was calculated.

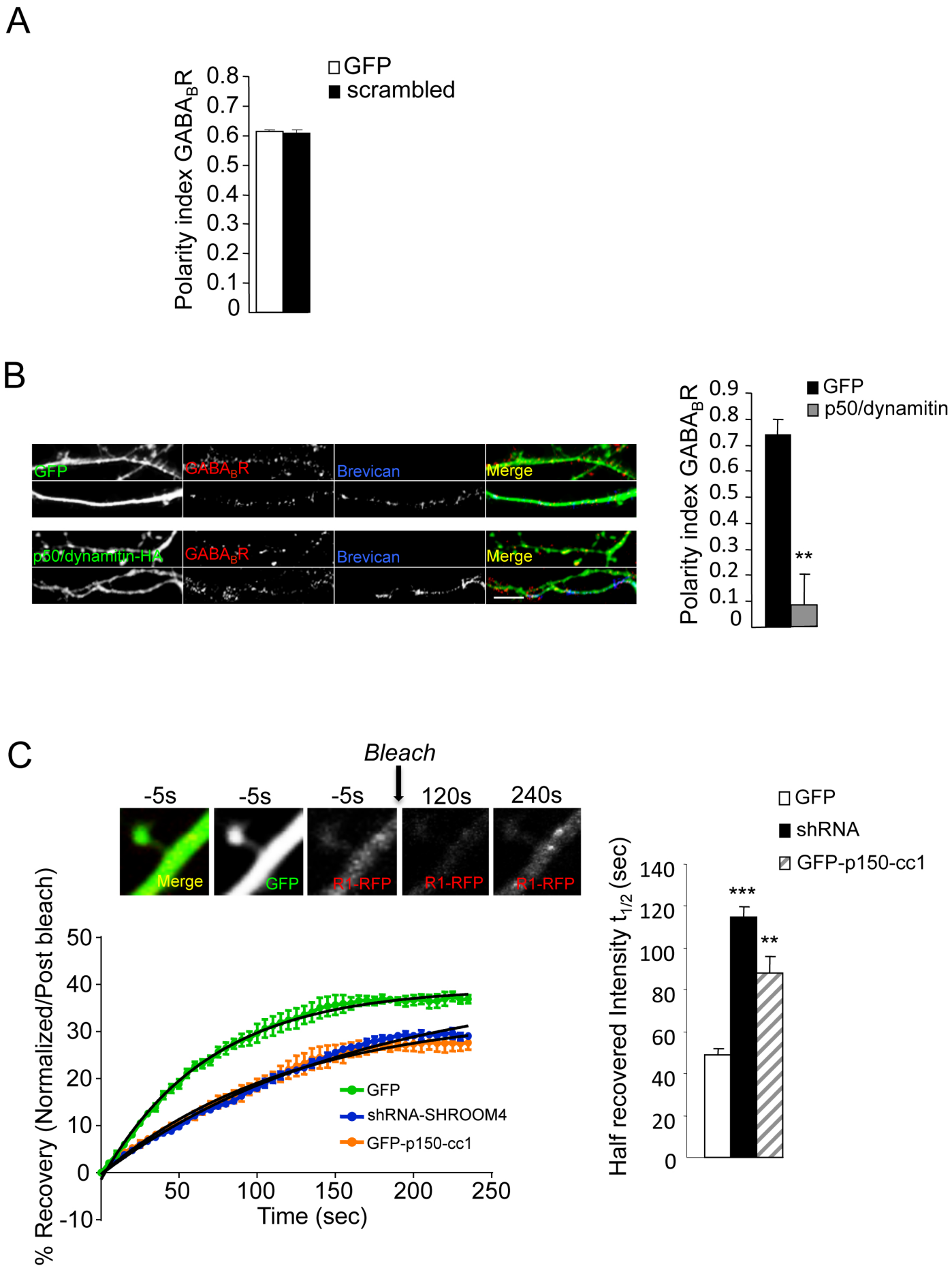
A
GFP
scrambled
Polarity index GABA$_B$R
0.8
0.7
0.6
0.5
0.4
0.3
0.2
0.1
0
B
GFP
GABA$_B$R
Brevican
Merge
p50/dynamitin-HA
GABA$_B$R
Brevican
Merge
GFP
p50/dynamitin
Polarity index GABA$_B$R
0.9
0.8
0.7
0.6
0.5
0.4
0.3
0.2
0.1
0
**
C
Bleach
-5s
-5s
-5s
120s
240s
Merge
GFP
R1-RFP
R1-RFP
R1-RFP
% Recovery (Normalized/Post bleach)
50
40
30
20
10
0
-10
50
100
150
200
250
Time (sec)
GFP
shRNA-SHROOM4
GFP-p150-cc1
GFP
shRNA
GFP-p150-cc1
Half recovered Intensity $t_{1/2}$ (sec)
140
120
100
80
60
40
20
0
***
**

Figure 24

Figure 24: Shrm4 and Dynein/Dynactin regulate $GABA_BRs$ transport into dendrites. (A) Either GFP and scrambled controls had no effect on the endogenous distribution of $GABA_BRs$. Histogram of DIV14 hippocampal neurons transfected with GFP or scrambled controls at DIV8. Neurons were stained for endogenous $GABA_BRs$ and costained with Brevican to localize axons (data not shown). Quantification of endogenous $GABA_BRs$ intensity into dendrites and axons were analysed (data not shown) and the PI was calculated. No changes in the PI of $GABA_BRs$ were observed in both conditions. (B) Representative images and histogram of DIV14 hippocampal neurons transfected with GFP (control) or HA-tagged p50/dynamitin used to inhibit dynein function (Kapitein et al., 2010) at DIV8. Neurons were stained for endogenous $GABA_BRs$ and costained with Brevican to localize axons. Quantification of endogenous $GABA_BRs$ intensity into dendrites and axons were analysed (data not shown) and the PI was calculated. The mean (±SEM) PI of HA-tagged p50/dynamitin expressing neurons were significantly decreased compared to GFP expressing neurons (PI HA-tagged p50/dynamitin = 0,09±0,1, **p < 0,01, t test). Scale bar, 20 μm. (C) FRAP experiments on hippocampal cultured neurons co-expressing $GABA_{B1}$-RFP together with Shrm4-shRNA or GFP-p150-cc1 (Protocol from Fossati et al., 2013). The mean (±SEM) half time fluorescence recovery normalized on GFP control (seconds) was significantly decreased in shRNA and GFP-p150-cc1 expressing neuron. Mean half time fluorescence recovery; shRNA = 114,69±5,23, *** p < 0,001; GFP-p150-cc1 = 88,18±7,55, ** p < 0,01, t test.

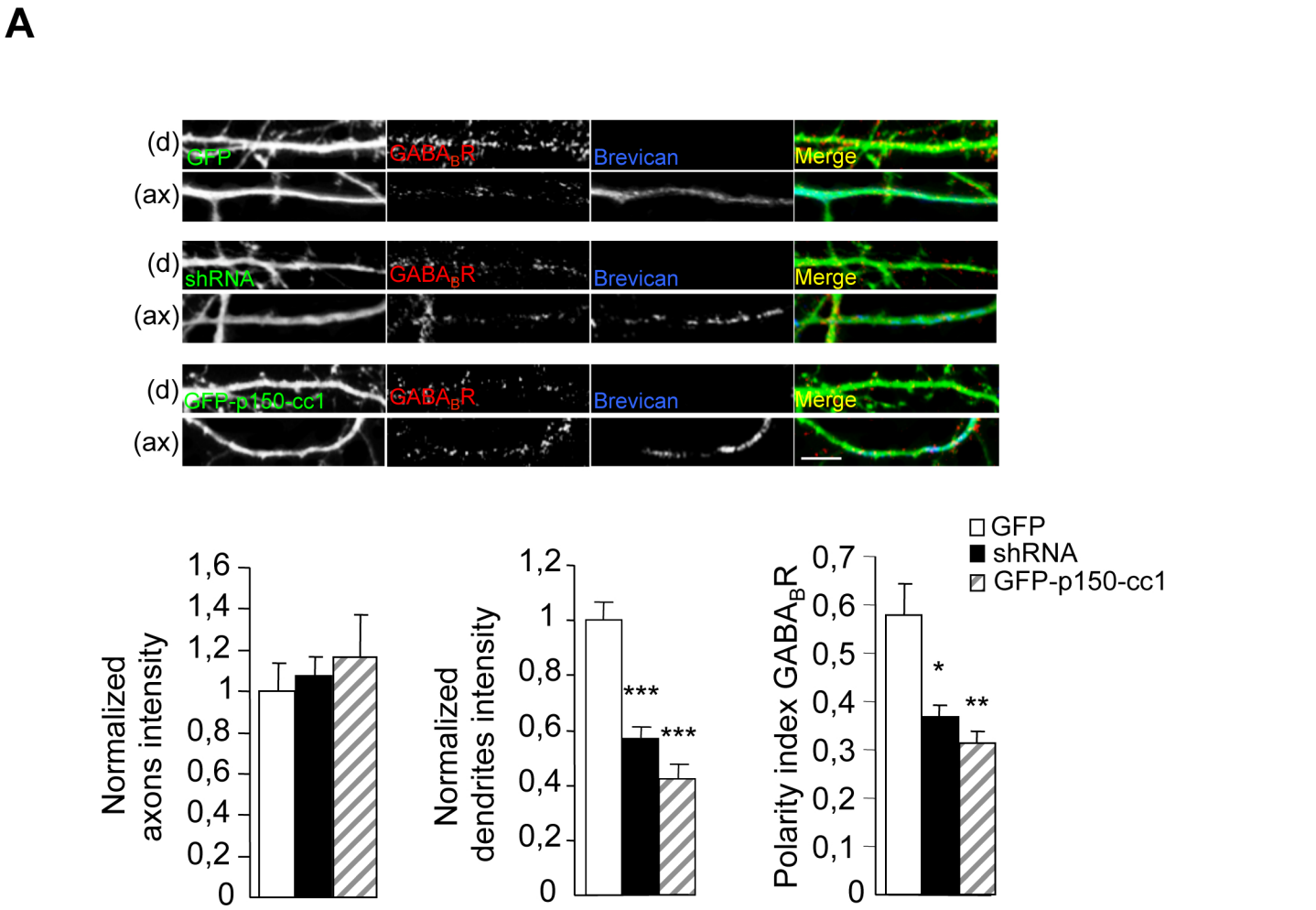
A
(d)
(ax)
GFP
shRNA
GFP-p150-cc1
GABA$_B$R
Brevican
Merge
Normalized axons intensity
Normalized dendrites intensity
Polarity index GABA$_B$R
GFP
shRNA
GFP-p150-cc1
B
R1A-myc
R1B-myc
Polarity index GABA$_{B1a}$
Polarity index GABA$_{B1b}$

Figure 25

Figure 25: Shrm4 and Dynein/Dynactin drive $GABA_BRs$ into dendrites. (A) Representative images and histograms of DIV14 hippocampal neurons cotransfected with GFP (control), Shrm4-shRNA or GFP-p150-cc1 at DIV8. Neurons were stained for endogenous $GABA_BRs$ and costained with Brevican to localize axons. Quantification of endogenous $GABA_BRs$ intensity into dendrites and axons were analysed and the PI was calculated. The mean (±SEM) normalized intensity into dendrites was significantly decreased in shRNA (***p < 0,001) and GFP-p150-cc1 (***p < 0,001) expressing neurons (One way-ANOVA). Furthermore, the mean (±SEM) PI of shRNA (*p < 0,05) and GFP-p150-cc1 (**p < 0,01) expressing neurons were significantly decreased (One way-ANOVA). Scale bar, 20 μm. (B) Representative images and histograms of DIV14 hippocampal neurons cotransfected with GFP (control), Shrm4-shRNA or GFP-p150-cc1 together with $GABA_{B1a}$-myc or $GABA_{B1b}$-myc at DIV8. Neurons were stained using anti-myc to detect $GABA_{B1}$ subunit isoforms and costained with Brevican to localize axons. The Mean (±SEM) PI for both $GABA_{B1}$ subunit isoforms were calculated in GFP (control), shRNA and GFP-p150-cc1 expressing neurons. The PI of both $GABA_{B1a}$ and $GABA_{B1b}$ was significantly decreased in shRNA (*p < 0,05) and GFP-150-cc1 (**p < 0,01) (One way-ANOVA). Scale bar, 20 μm.

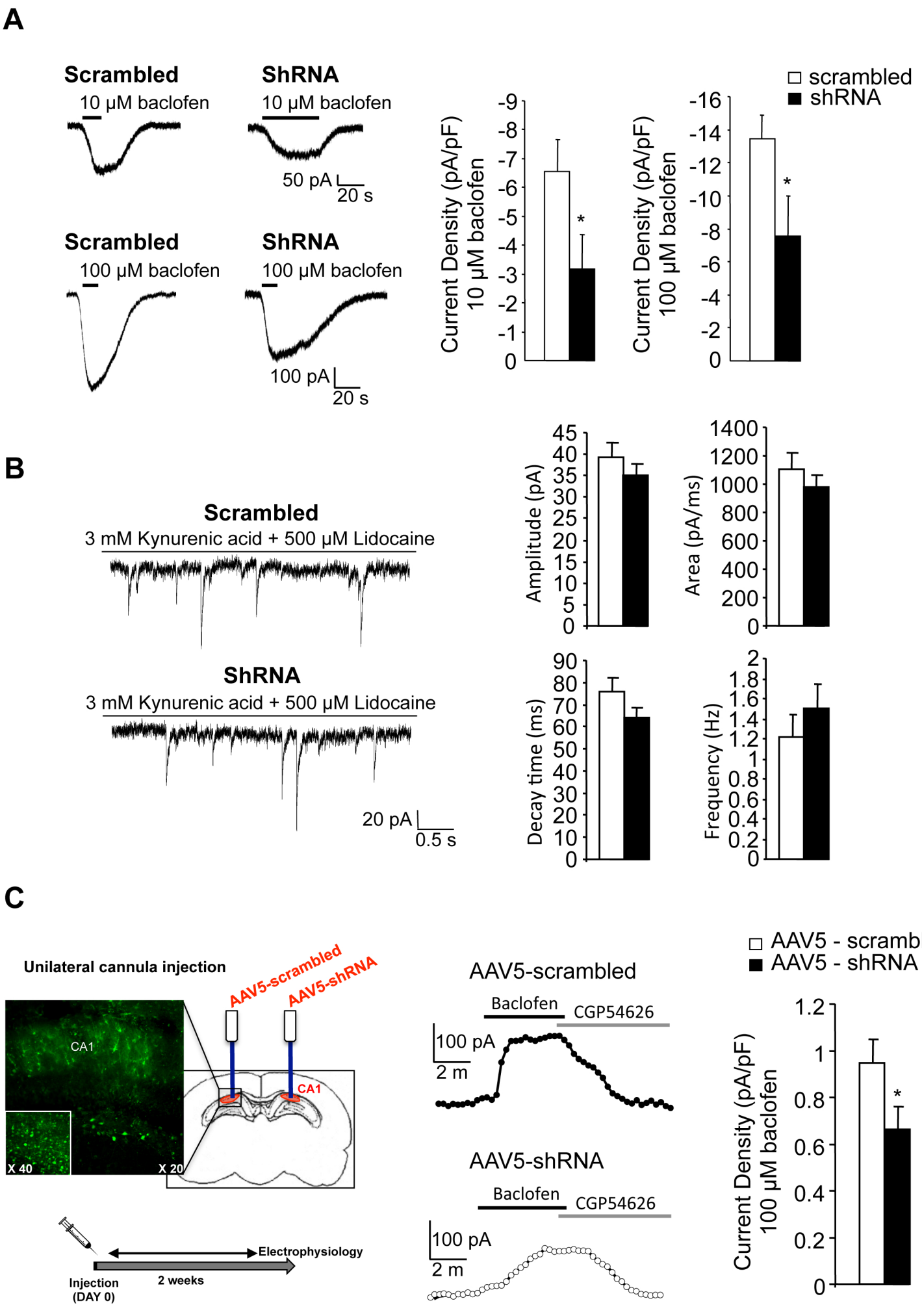
A
Scrambled
10 μM baclofen
ShRNA
10 μM baclofen
50 pA
20 s
Scrambled
100 μM baclofen
ShRNA
100 μM baclofen
100 pA
20 s
scrambled
shRNA
Current Density (pA/pF)
10 μM baclofen
Current Density (pA/pF)
100 μM baclofen
B
Scrambled
3 mM Kynurenic acid + 500 μM Lidocaine
ShRNA
3 mM Kynurenic acid + 500 μM Lidocaine
20 pA
0.5 s
Amplitude (pA)
Area (pA/ms)
Decay time (ms)
Frequency (Hz)
C
Unilateral cannula injection
AAV5-scrambled
AAV5-shRNA
CA1
X 40
X 20
Injection
(DAY 0)
2 weeks
Electrophysiology
AAV5-scrambled
Baclofen
CGP54626
100 pA
2 m
AAV5-shRNA
Baclofen
CGP54626
100 pA
2 m
AAV5 - scrambled
AAV5 - shRNA
Current Density (pA/pF)
100 μM baclofen

Figure 26

Figure 26: Shrm4 knockdown reduces $GABA_BRs$-mediated peak K^+ current amplitude wihtout affecting $GABA_ARs$–mediated inhibitory transmission. (A) Whole-cell GIRK currents and current densities recorded in response to 10 and 100 μM baclofen application from hippocampal neurons at 14 DIV transfected either with scrambled or Shrm4-shRNA at DIV7. Shrm4 knockdown induces a significant decrease in the peak K^+ current in both baclofen concentrations. Recordings were made in the presence of bicuculline, CNQX and APV. n = 6 for scrambled, n = 7 for ShRNA (*p < 0.05 t-test). (B) GABAergic transmission of DIV14 hippocampal neurons transfected at DIV8 with scrambled or Shrm4-shRNA. Miniature inhibitory postsynaptic currents (mIPSCs) were measured in the presence of Kynurenic acid (3 mM) and lidocaine (500 μM). No significant changes were observed in the amplitude, decay time, area and frequence of mIPSCs. n =11 for scrambled, n = 15 for ShRNA (C) Scheme of injections procedure and representative histogram of changes in current densities (pA/pF) of CA1 pyramidal neurons following application of baclofen (100 μM) and selective $GABA_BRs$ antagonist CGP54626 (5 μM) on acute hippocampal slices. The mean (±SEM) amplitude of the outward K^+ current induced by baclofen application was significantly decrease (*p < 0.05 t-test) in acute hippocampal slices injected with AAV5-shRNA compared to AAV5-scrambled.

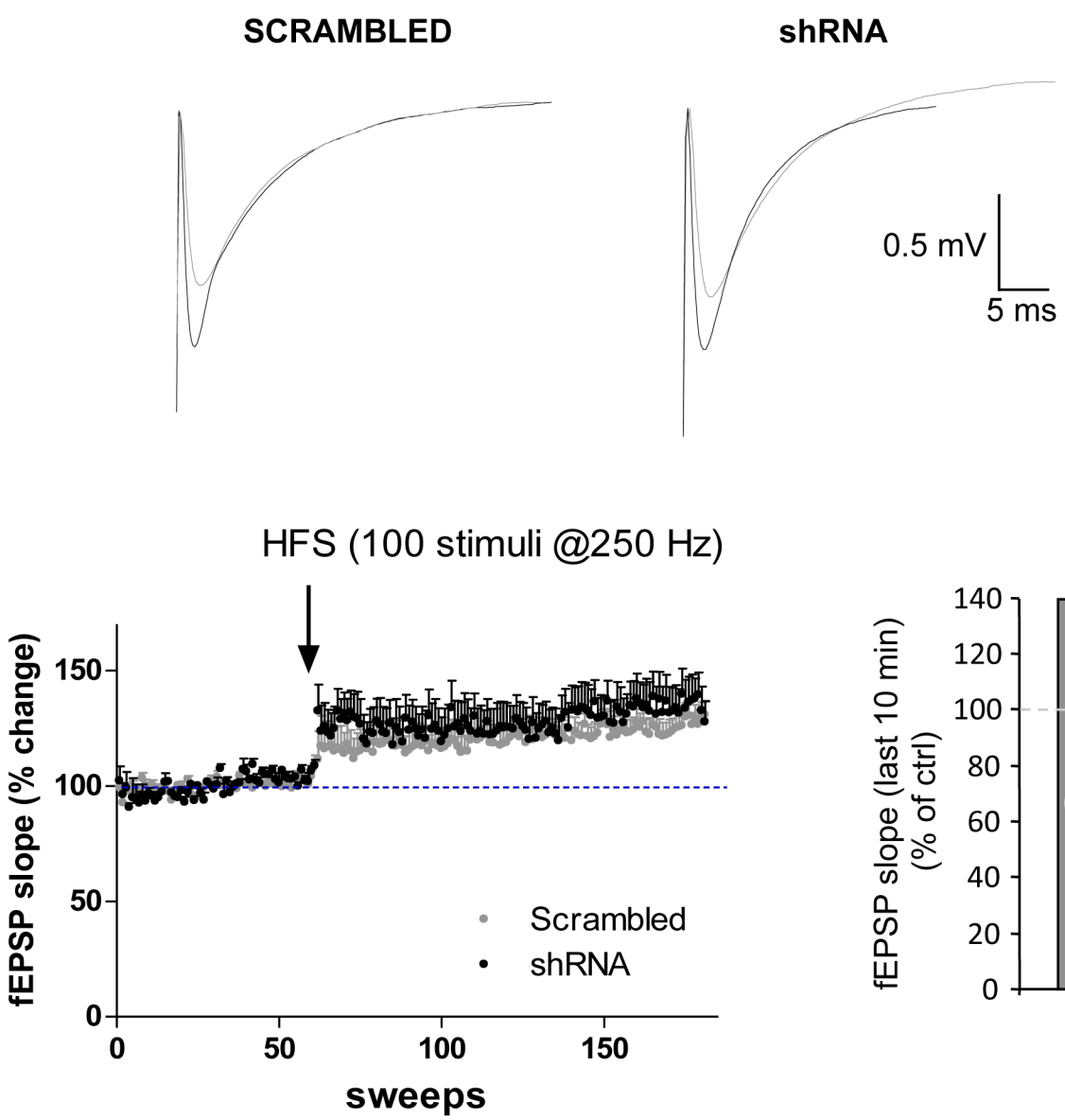
SCRAMBLED
shRNA
0.5 mV
5 ms
HFS (100 stimuli @250 Hz)
fEPSP slope (% change)
150
100
50
0
0
50
100
150
sweeps
Scrambled
shRNA
fEPSP slope (last 10 min)
(% of ctrl)
140
120
100
80
60
40
20
0
6
6

Figure 27

Figure 27: Shrm4 is not required for long term potentiation (LTP). Representative traces and histogram of changes in field excitatory post synaptic potentials (fEPSPs) from hippocampal acute slices of AAV5-shRNA and AAV5-scrambled injected rats (n = 6 animals for each conditions). Recording of fEPSPs were carried out on the apical dendritic layer of the hippocampal CA1 region and long term potentiation (LTP) was induced by high frequency stimulation (HFS) (100 stimuli at 250 Hz) of Schaffer collaterals (SC) (See Materials and Methods). We observed no differences in LTP induction and stability between the two groups.

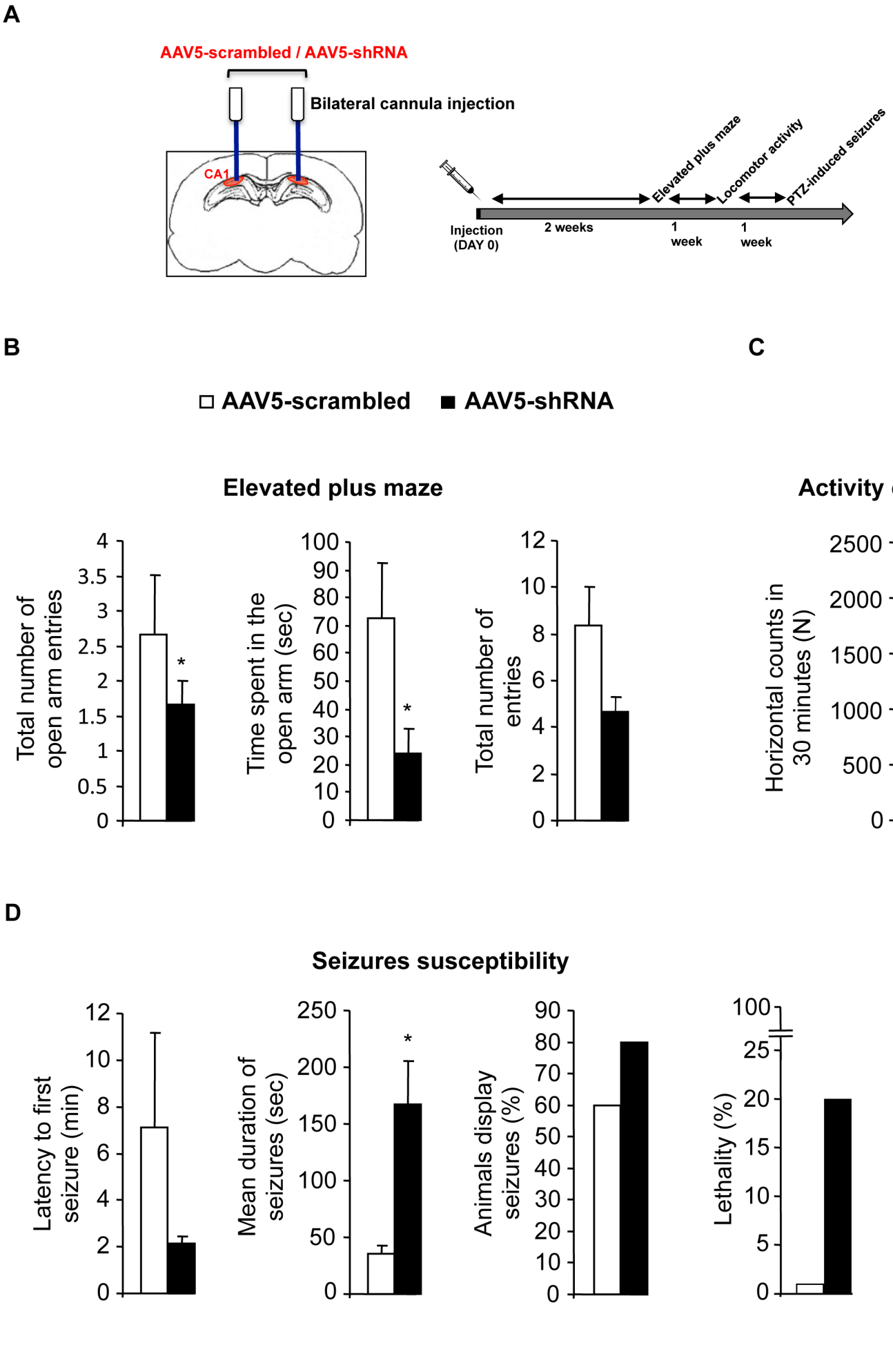
A
AAV5-scrambled / AAV5-shRNA
Bilateral cannula injection
CA1
Injection
(DAY 0)
2 weeks
Elevated plus maze
1
week
Locomotor activity
1
week
PTZ-induced seizures
B
C
AAV5-scrambled
AAV5-shRNA
Elevated plus maze
Activity cage
Total number of open arm entries
Time spent in the open arm (sec)
Total number of entries
Horizontal counts in 30 minutes (N)
D
Seizures susceptibility
Latency to first seizure (min)
Mean duration of seizures (sec)
Animals display seizures (%)
Lethality (%)

Figure 28

Figure 28: *In vivo* Shrm4 silencing causes increase in anxiety and propensity to seizures. (A-D) Experimental design for *in vivo* knockdown of Shrm4 expression in the CA1 dorsal hippocampus. Animals were bilaterally injected with either AAV5-scrambled (n= 6) or AAV5-shRNA (n= 6). Two weeks later, all animals were tested for elevated plus maze, locomotor activity and PTZ-induced seizures. One week passed between the different tests. (B and C) *In vivo* knockdown of Shrm4 induces significant increase in the mean (±SEM) total number of open arm entries (*$p < 0.05$ t-test) and mean (±SEM) time spent in the open arm (*$p < 0.05$ t-test). No changes were observed in the mean (±SEM) total number of entries and mean (±SEM) horizontal counts in 30 minutes. (D) The Mean (±SEM) duration of seizures (sec) was significantly increased in AAV5-shRNA injected animals (*$p < 0.05$ t-test). The percentage of lethality and animals that displayed seizures were also increased.

6. DISCUSSION

In this study, we unravelled the mechanism by which $GABA_BR$ is trafficked to dendrites in mature hippocampal neurons. We propose a model by which Shrm4, a protein involved in X-LID, serves as adaptor to link $GABA_BR$ to the dynein/dynactin motor protein complex. According to this model, Shrm4 loss of function compromises the delivery of $GABA_BRs$ to the postsynapse and ultimately impairs inhibitory transmission. *In vivo* Shrm4 silencing increases neuronal network excitability and anxiety-related behaviour.

Furthermore, Shrm4 loss of function in immature neurons, before synaptogenesis, affects dendritic spine density and stability and the number of synaptic contacts.

6.1 Shrm4 and the dynein/dynactin motor protein complex mediate $GABA_BRs$ transport to dendrites

In cultured hippocampal neurons Shrm4 localizes at synapses and in particular on dendrites along MAP2-positive microtubule filaments, as revealed by dSTORM imaging and ultrastructural immunolocalization.

To gain insights into Shrm4 function in neuronal dendrites, we decided to look for Shrm4 interacting proteins.

We identified the $GABA_B$ receptor subunit isoforms 1 ($GABA_{B1}$), receptors that mediate the slow inhibitory transmission in the mammalian brain, as a direct interactor of Shrm4. By yeast two-hybrid screening, we showed that Shrm4 PDZ domain binds amino acids 859-870 of $GABA_{B1}$ intracellular C-terminal tail, a region that is known to be required for the trafficking of the receptor to the cell surface in dendrites (Margeta-Mitrovic et al., 2000; Calver et al., 2001; Pagano et al., 2001). GST pull-down and coimmunoprecipitation in hippocampal cultured neurons and brain homogenates confirmed this interaction. Furthermore, immunofluorescence labelling of hippocampal neurons showed that some puncta of Shrm4, that distribute along dendrites, also colocalize with $GABA_BR$.

Interestingly, Shrm4 silencing in hippocampal neurons strongly reduces $GABA_BRs$ amount along dendrites and on the plasma membrane, as demonstrated by fluorescent staining and biotinylation assay. This effect is specific for $GABA_BRs$ as no changes were observed in the distribution of the $\alpha 1$ subunit of $GABA_A$ receptor, which mediates fast inhibitory transmission in the brain (Heisler et al., 2011; Nakajima et al.,

2012). At the same time, Shrm4 silencing induces the intracellular accumulation of $GABA_BRs$ in the Golgi apparatus as demonstrated by the colocalization of the receptors with giantin, a Golgi membrane-resident protein.

To recapitulate, Shrm4 distributes along dendritic microtubules, directly binds the C-terminal tail of $GABA_{B1}$ and its silencing strongly affects $GABA_BRs$ intracellular distribution. Notably, the intracellular C-terminal tail of $GABA_BRs$ is known to be required for the trafficking of the receptor to the cell surface in dendrites (Margeta-Mitrovic et al., 2000; Calver et al., 2001; Pagano et al., 2001). These data suggest that Shrm4 is involved in $GABA_BR$ trafficking along dendrites.

To examine whether the distribution defects could be due to an increased internalization of the $GABA_BRs$ from the plasma membrane to the Golgi apparatus following a retrograde transport, we performed an internalisation assay. No changes in the internalisation rate of $GABA_BRs$ between control and silenced neurons were observed, thus leading us to exclude this possibility.

We therefore hypothesized that Shrm4 silencing could prevent the anterograde trafficking of $GABA_BRs$ from the Golgi apparatus to the plasma membrane. Indeed, it has been reported that the inhibition of Golgi export by the expression of a constitutively active form of ADP-rybosilation factor 1 (ARF1) causes an intracellular accumulation of $GABA_BRs$ that are unable to reach the surface (Valdés et al., 2012). In addition, FRAP experiments on neurons expressing $GABA_{B1}$-mRFP showed a reduction in the transport rate of $GABA_BRs$ receptors into dendrites in Shrm4 knockdown and validate our hypothesis.

The trafficking of proteins from the Golgi apparatus to the surface involves microtubule–based motors proteins such as kinesin and/or the dynein/dynactin complex. $GABA_{B1a}$ subunits are trafficked along the axon through the Kinesin-1 (Valdés et al., 2012). By contrast the mechanism and molecules that mediate postsynaptic $GABA_BRs$ transport along dendrites remain elusive.

As the Dynein/Dynactin motor protein complex steers neuronal transport toward the microtubule minus end (Pilling et al., 2006) and has been involved in the sorting of various cargos toward dendrites including the AMPA receptor GluA2 subunit (Kapitein et al., 2010a), Golgi outposts (Hirokawa et al., 1998; Zheng et al., 2008) and more recently mitochondria (Van Spronsen et al., 2013), we first investigated

whether the Dynein/Dynactin motor complex was involved in $GABA_BRs$ trafficking along dendrites.

Indeed, dynein inhibition induced by expression of p50/dynamitin or the first coiled-coil domain of $p150^{Glued}$ (GFP-p150-cc1) (Burkhardt et al., 1997; Kwinter et al., 2009) in hippocampal neurons affected the polarized transport of $GABA_BRs$. $GABA_BRs$ dendritic sorting is reduced, while axonal sorting is unaffected. A similar result was obtained by silencing Shrm4, thus demonstrating the requirement of both the dynein/dynactin motor complex and Shrm4 to target $GABA_BRs$ specifically to dendrites.

Moreover, we showed by coimmunoprecipitation experiments that the dynein/dynactin motor, Shrm4 and $GABA_BRs$ form a complex in the brain. Which is the function of Shrm4 in this complex? We speculated that Shrm4 could be an adaptor protein (Kunde et al., 2011; Van Spronsen et al., 2013; Franker et a., 2013) that mediates the specific and selective binding between the dynein/dynactin motor protein complex and $GABA_BRs$. According with this hypothesis, *in vivo* silencing of Shrm4 reduces the association between $GABA_BRs$ and the dynein/dynactin motor protein.

Shrm4 binds both $GABA_{B1a}$ and $GABA_{B1b}$ subunit isoforms and, according to our model, both subunits should be linked to the dynein/dynactin complex and preferentially sorted to dendrites. Indeed, Shrm4 silencing reduced the dendritic targeting of both subunits.

However, $GABA_{B1a}$, unlike $GABA_{B1b}$ subunits, is preferentially sorted to axons in physiological conditions, suggesting that $GABA_{B1a}$ subunits sorting toward the axon is predominant over Shrm4-dependent sorting towards dendrites. It has been demonstrated that $GABA_{B1a}$ subunits could be sorted to the axon through their sushi domains in pre-Golgi compartments, more precisely in the endoplasmic reticulum (ER) or ER-Golgi intermediate compartment (ERGIC) (Valdés et al., 2012).

Our data suggest that Shrm4-mediated $GABA_BRs$ selective sorting occurs in the Golgi apparatus. We therefore hypothesize that $GABA_{B1a}$ subunits selective sorting occurs in pre-Golgi compartments before Shrm4 selection and that Shrm4 mediates $GABA_{B1b}$ subunits trafficking and the transport of the portion of $GABA_{B1a}$ that physiologically escapes from the ER and ERGIC sorting (Biermann et al., 2010).

In summary, this study demonstrates that Shrm4 mediates the targeting of $GABA_B$ receptor to dendrites. In particular, we propose a model by which Shrm4, by binding the C-terminal tail of both $GABA_{B1a}$ and $GABA_{B1b}$ subunits and Dynein, function as an adaptor protein. However, how $GABA_B$Rs are transported along dendrites: in dense core vesicles or in Golgi outposts, remain to be addressed and will be the focus of future studies.

6.2 *In vivo* Shrm4 silencing increases neuronal network excitability and anxiety-related behaviour

To address whether Shrm4 silencing functionally affects inhibitory transmission, we measured $GABA_B$R-mediated K^+ currents in hippocampal neurons transfected with Shrm4 shRNA. The $GABA_B$R agonist baclofen evoked smaller K^+ current response in shRNA expressing-neurons with respect of control neurons, indicating that the alteration of $GABA_B$Rs transport along dendrites depletes the postsynaptic $GABA_B$Rs pool, thus affecting synaptic transmission. By contrast, miniature inhibitory postsynaptic currents (mIPSCs) mediated by $GABA_A$Rs were unaffected in Shrm4 knockdown, showing that Shrm4 specifically regulates $GABA_B$R-mediated responses.

We next validated our results *in vivo*, by AAV-mediated silencing of Shrm4 in the CA1 dorsal hippocampus of adult male rats (5-7 weeks). As expected, the baclofen-induced K^+ current measured in CA1 neurons 2 weeks after virus injection was reduced in silenced neurons compared with controls. By contrast, LTP induction and stability were unaffected in shRNA expressing animals. These results are consistent with previous findings from $GABA_{B1b}^{-/-}$ knockout mice, in which LTP induction was maintained, and indicate that postsynaptic $GABA_B$Rs are not essential for LTP induction (Vigot et al., 2006).

Depletion of postsynaptic $GABA_B$Rs has been correlated with epilepsy. Indeed, $GABA_{B1}^{-/-}$ knockout mice experience spontaneous epileptic seizures (Schuler et al., 2001). Moreover, the *weaver* mouse, which has a mutated GIRK2 channel, and the $Girk2^{-/-}$ null mouse are both characterized by significant loss of $GABA_B$R-mediated inhibition and increased susceptibility to seizures (Signorini et al., 1997; Slesinger et

al., 1997). Consistent with these results, we showed that Shrm4-shRNA injected animals were more susceptible to convulsive seizures than control animals after intraperitoneal injection of pentylenetetrazol (PTZ) (Kliouéva et al., 2001). Our data demonstrate that *in vivo* Shrm4 silencing affects the excitability of the neuronal network.

The involvement of $GABA_BRs$ in anxiety-related disorders has been widely debated in the last decade. While $GABA_{B1}^{-/-}$ knockout mice show increased anxiety (Cryan et al., 2004; Mombereau et al., 2004), mice that specifically lack either the 1a or 1b isoform do not show anxiety (Jacobson et al., 2007), possibly suggesting compensation between the two isoforms. Interestingly, animals in which Shrm4 has been locally silenced displayed increased anxiety with respect of control animals, according to the elevated plus-maze test results. As Shrm4 silencing impaired the postsynaptic trafficking of both subunit isoforms of $GABA_BRs$, we hypothesize that the anxiety-related behaviour is the result of a significant decrease in postsynaptic $GABA_BRs$, specifically. However, other Shrm4 silencing-dependent mechanisms cannot be excluded.

A well-known hallmark of X-LID is the defects in dendritic spine density and shape (Purpura, 1974).
Therefore we investigated whether Shrm4 loss of function could affect dendritic spine dynamics in cultured hippocampal neurons, by silencing Shrm4 before synaptogenesis (DIV7-8). We observed a reduction in spine density and length. Moreover spines appear less stable as the number of removed spines exceeded that of new spines in time-lapse imaging. Dendritic spine molecular composition is also affected as pre- and postsynaptic marker expression is reduced, as well as the extent of colocalization between Synapsin and PSD-95 that reveals the number of synaptic contacts.
The present study did not unravel the mechanism by which Shrm4 silencing affects dendritic spine and synaptic contacts formation. However, it has been reported that Shrm4 binds F-actin and influences actin remodelling in non-neuronal cells (Yoder et al., 2007). As F-actin remodelling is crucial for synaptogenesis and spine plasticity (Kim IH et al., 2013), a possibility is that Shrm4 regulates spine cytoskeleton.
On the other hand, the cause of dendritic spine defects could indirectly derive from $GABA_BR$ trafficking impairment. In fact, $GABA_BR$ has recently been involved in

neuronal migration and neurite growth as demonstrated by *in utero* knockdown of $GABA_{B2}$ in rat embryos (Bony et al., 2013). Moreover $GABA_BRs$ are located in close proximity to glutamate receptors (Kulik et al., 2003) and directly inhibit NMDAR signalling (Chalifoux et al., 2010), which is a well-known regulator of spine morphology and density (Ultanir et al., 2007). A decrease of $GABA_BR$ amount could affect NMDAR signalling and therefore synaptogenesis.

REFERENCES

Bartoi, T., Rigbolt, K.T., Du, D., Kohr, G., Blagoev, B., and Kornau, H.C. (2010). GABAB receptor constituents revealed by tandem affinity purification from transgenic mice. The Journal of biological chemistry 285, 20625-20633.

Bassani, S., Zapata, J., Gerosa, L., Moretto, E., Murru, L., and Passafaro, M. (2013). The neurobiology of X-linked intellectual disability. The Neuroscientist : a review journal bringing neurobiology, neurology and psychiatry 19, 541-552.

Benarroch, E.E. (2012). GABAB receptors: structure, functions, and clinical implications. Neurology 78, 578-584.

Bettler, B., Kaupmann, K., Mosbacher, J., and Gassmann, M. (2004). Molecular structure and physiological functions of GABA(B) receptors. Physiological reviews 84, 835-867.

Biermann, B., Ivankova-Susankova, K., Bradaia, A., Abdel Aziz, S., Besseyrias, V., Kapfhammer, J.P., Missler, M., Gassmann, M., and Bettler, B. (2010). The Sushi domains of GABAB receptors function as axonal targeting signals. The Journal of neuroscience : the official journal of the Society for Neuroscience 30, 1385-1394.

Boda, B., Mas, C., and Muller, D. (2002). Activity-dependent regulation of genes implicated in X-linked non-specific mental retardation. Neuroscience 114, 13-17.

Bony, G., Szczurkowska, J., Tamagno, I., Shelly, M., Contestabile, A., and Cancedda, L. (2013). Non-hyperpolarizing GABAB receptor activation regulates neuronal migration and neurite growth and specification by cAMP/LKB1. Nature communications 4, 1800.

Bowery, N.G., Bettler, B., Froestl, W., Gallagher, J.P., Marshall, F., Raiteri, M., Bonner, T.I., and Enna, S.J. (2002). International Union of Pharmacology. XXXIII. Mammalian gamma-aminobutyric acid(B) receptors: structure and function. Pharmacological reviews 54, 247-264.

Braida, D., Zani, A., Capurro, V., Rossoni, G., Pegorini, S., Gori, E., and Sala, M. (2008). Diazepam protects against the enhanced toxicity of cocaine adulterated with atropine. Journal of pharmacological sciences 107, 408-418.

Brewer, G.J., Torricelli, J.R., Evege, E.K., and Price, P.J. (1993). Optimized survival of hippocampal neurons in B27-supplemented Neurobasal, a new serum-free medium combination. Journal of neuroscience research 35, 567-576.

Burkhardt, J.K., Echeverri, C.J., Nilsson, T., and Vallee, R.B. (1997). Overexpression of the dynamitin (p50) subunit of the dynactin complex disrupts dynein-dependent maintenance of membrane organelle distribution. The Journal of cell biology 139, 469-484.

Calver, A.R., Robbins, M.J., Cosio, C., Rice, S.Q., Babbs, A.J., Hirst, W.D., Boyfield, I., Wood, M.D., Russell, R.B., Price, G.W., et al. (2001). The C-terminal domains of the GABA(b) receptor subunits mediate intracellular trafficking but are not required for receptor signaling. The Journal of neuroscience : the official journal of the Society for Neuroscience 21, 1203-1210.

Chalifoux, J.R., and Carter, A.G. (2010). GABAB receptors modulate NMDA receptor calcium signals in dendritic spines. Neuron 66, 101-113.

Chalifoux, J.R., and Carter, A.G. (2011). GABAB receptor modulation of voltage-sensitive calcium channels in spines and dendrites. The Journal of neuroscience : the official journal of the Society for Neuroscience 31, 4221-4232.

Chalifoux, J.R., and Carter, A.G. (2011). GABAB receptor modulation of synaptic function. Current opinion in neurobiology 21, 339-344.

Cingolani, L.A., Thalhammer, A., Yu, L.M., Catalano, M., Ramos, T., Colicos, M.A., and Goda, Y. (2008). Activity-dependent regulation of synaptic AMPA receptor composition and abundance by beta3 integrins. Neuron 58, 749-762.

Colin, E., Zala, D., Liot, G., Rangone, H., Borrell-Pages, M., Li, X.J., Saudou, F., and Humbert, S. (2008). Huntingtin phosphorylation acts as a molecular switch for anterograde/retrograde transport in neurons. The EMBO journal 27, 2124-2134.

Couve, A., Filippov, A.K., Connolly, C.N., Bettler, B., Brown, D.A., and Moss, S.J. (1998). Intracellular retention of recombinant GABAB receptors. The Journal of biological chemistry 273, 26361-26367.

Couve, A., Moss, S.J., and Pangalos, M.N. (2000). GABAB receptors: a new paradigm in G protein signaling. Molecular and cellular neurosciences 16, 296-312.

Cryan, J.F., and Kaupmann, K. (2005). Don't worry 'B' happy!: a role for GABA(B) receptors in anxiety and depression. Trends in pharmacological sciences 26, 36-43.

Cryan, J.F., Kelly, P.H., Chaperon, F., Gentsch, C., Mombereau, C., Lingenhoehl, K., Froestl, W., Bettler, B., Kaupmann, K., and Spooren, W.P. (2004). Behavioral characterization of the novel GABAB receptor-positive modulator GS39783 (N,N'-dicyclopentyl-2-methylsulfanyl-5-nitro-pyrimidine-4,6-diamine): anxiolytic-like activity without side effects associated with baclofen or benzodiazepines. The Journal of pharmacology and experimental therapeutics 310, 952-963.

David, M., Richer, M., Mamarbachi, A.M., Villeneuve, L.R., Dupre, D.J., and Hebert, T.E. (2006). Interactions between GABA-B1 receptors and Kir 3 inwardly rectifying potassium channels. Cellular signalling 18, 2172-2181.

Davies, C.H., Starkey, S.J., Pozza, M.F., and Collingridge, G.L. (1991). GABA autoreceptors regulate the induction of LTP. Nature 349, 609-611.

Dempsey, G.T., Vaughan, J.C., Chen, K.H., Bates, M., and Zhuang, X. (2011). Evaluation of fluorophores for optimal performance in localization-based super-resolution imaging. Nature methods 8, 1027-1036.

Deng, H., Zheng, W., and Song, Z. (2013). Genetics, Molecular Biology, and Phenotypes of X-Linked Epilepsy. Molecular neurobiology.

Dietz, M.L., Bernaciak, T.M., Vendetti, F., Kielec, J.M., and Hildebrand, J.D. (2006). Differential actin-dependent localization modulates the evolutionarily conserved activity of Shroom family proteins. The Journal of biological chemistry 281, 20542-20554.

Driskell, O.J., Mironov, A., Allan, V.J., and Woodman, P.G. (2007). Dynein is required for receptor sorting and the morphogenesis of early endosomes. Nature cell biology 9, 113-120.

Dutar, P., and Nicoll, R.A. (1988). Pre- and postsynaptic GABAB receptors in the hippocampus have different pharmacological properties. Neuron 1, 585-591.

Dutar, P., and Nicoll, R.A. (1988). A physiological role for GABAB receptors in the central nervous system. Nature 332, 156-158.

Edelstein, A., Amodaj, N., Hoover, K., Vale, R., and Stuurman, N. (2010). Computer control of microscopes using microManager. Current protocols in molecular biology / edited by Frederick M Ausubel [et al] Chapter 14, Unit14 20.

Egan, M.J., Tan, K., and Reck-Peterson, S.L. (2012). Lis1 is an initiation factor for dynein-driven organelle transport. The Journal of cell biology 197, 971-982.

Ellison, J.W., Rosenfeld, J.A., and Shaffer, L.G. (2013). Genetic basis of intellectual disability. Annual review of medicine 64, 441-450.

Emson, P.C. (2007). GABA(B) receptors: structure and function. Progress in brain research 160, 43-57.

Fairbank, P.D., Lee, C., Ellis, A., Hildebrand, J.D., Gross, J.M., and Wallingford, J.B. (2006). Shroom2 (APXL) regulates melanosome biogenesis and localization in the retinal pigment epithelium. Development 133, 4109-4118.

Fatemi, S.H., Folsom, T.D., Reutiman, T.J., and Thuras, P.D. (2009). Expression of GABA(B) receptors is altered in brains of subjects with autism. Cerebellum 8, 64-69.

Fejtova, A., Davydova, D., Bischof, F., Lazarevic, V., Altrock, W.D., Romorini, S., Schone, C., Zuschratter, W., Kreutz, M.R., Garner, C.C., et al. (2009). Dynein light chain regulates axonal trafficking and synaptic levels of Bassoon. The Journal of cell biology 185, 341-355.

Franker, M.A., and Hoogenraad, C.C. (2013). Microtubule-based transport - basic mechanisms, traffic rules and role in neurological pathogenesis. Journal of cell science 126, 2319-2329.

Gahwiler, B.H., and Brown, D.A. (1985). GABAB-receptor-activated K+ current in voltage-clamped CA3 pyramidal cells in hippocampal cultures. Proceedings of the National Academy of Sciences of the United States of America 82, 1558-1562.

Galanopoulou, A.S., and Moshe, S.L. (2009). The epileptic hypothesis: developmentally related arguments based on animal models. Epilepsia 50 Suppl 7, 37-42.

Gambardella, A., Manna, I., Labate, A., Chifari, R., La Russa, A., Serra, P., Cittadella, R., Bonavita, S., Andreoli, V., LePiane, E., et al. (2003). GABA(B) receptor 1 polymorphism (G1465A) is associated with temporal lobe epilepsy. Neurology 60, 560-563.

Gandal, M.J., Sisti, J., Klook, K., Ortinski, P.I., Leitman, V., Liang, Y., Thieu, T., Anderson, R., Pierce, R.C., Jonak, G., et al. (2012). GABAB-mediated rescue of altered excitatory-inhibitory balance, gamma synchrony and behavioral deficits following constitutive NMDAR-hypofunction. Translational psychiatry 2, e142.

Gassmann, M., and Bettler, B. (2012). Regulation of neuronal GABA(B) receptor functions by subunit composition. Nature reviews Neuroscience 13, 380-394.

Gassmann, M., and Bettler, B. (2012). Regulation of neuronal GABA(B) receptor functions by subunit composition. Nature reviews Neuroscience 13, 380-394.

Gauthier, L.R., Charrin, B.C., Borrell-Pages, M., Dompierre, J.P., Rangone, H., Cordelieres, F.P., De Mey, J., MacDonald, M.E., Lessmann, V., Humbert, S., and Saudou, F. (2004). Huntingtin controls neurotrophic support and survival of neurons by enhancing BDNF vesicular transport along microtubules. Cell 118, 127-138.

Gertler, F.B., Niebuhr, K., Reinhard, M., Wehland, J., and Soriano, P. (1996). Mena, a relative of VASP and Drosophila Enabled, is implicated in the control of microfilament dynamics. Cell 87, 227-239.

Girod, A., Storrie, B., Simpson, J.C., Johannes, L., Goud, B., Roberts, L.M., Lord, J.M., Nilsson, T., and Pepperkok, R. (1999). Evidence for a COP-I-independent transport route from the Golgi complex to the endoplasmic reticulum. Nature cell biology 1, 423-430.

Goldstein, L.S., and Yang, Z. (2000). Microtubule-based transport systems in neurons: the roles of kinesins and dyneins. Annual review of neuroscience 23, 39-71.

Hagens, O., Dubos, A., Abidi, F., Barbi, G., Van Zutven, L., Hoeltzenbein, M., Tommerup, N., Moraine, C., Fryns, J.P., Chelly, J., et al. (2006). Disruptions of the novel KIAA1202 gene are associated with X-linked mental retardation. Human genetics 118, 578-590.

Haigo, S.L., Hildebrand, J.D., Harland, R.M., and Wallingford, J.B. (2003). Shroom induces apical constriction and is required for hingepoint formation during neural tube closure. Current biology : CB 13, 2125-2137.

Hampson, D.R., Adusei, D.C., and Pacey, L.K. (2011). The neurochemical basis for the treatment of autism spectrum disorders and Fragile X Syndrome. Biochemical pharmacology 81, 1078-1086.

Hannan, S., Wilkins, M.E., Dehghani-Tafti, E., Thomas, P., Baddeley, S.M., and Smart, T.G. (2011). GABAB receptor internalisation is regulated by the R2 subunit. The Journal of biological chemistry.

Hannan, S., Wilkins, M.E., and Smart, T.G. (2012). Sushi domains confer distinct trafficking profiles on GABAB receptors. Proceedings of the National Academy of Sciences of the United States of America 109, 12171-12176.

Heilemann, M., van de Linde, S., Schuttpelz, M., Kasper, R., Seefeldt, B., Mukherjee, A., Tinnefeld, P., and Sauer, M. (2008). Subdiffraction-resolution fluorescence imaging with conventional fluorescent probes. Angewandte Chemie 47, 6172-6176.

Heisler, F.F., Loebrich, S., Pechmann, Y., Maier, N., Zivkovic, A.R., Tokito, M., Hausrat, T.J., Schweizer, M., Bahring, R., Holzbaur, E.L., et al. (2011). Muskelin regulates actin filament- and microtubule-based GABA(A) receptor transport in neurons. Neuron 70, 66-81.

Hildebrand, J.D. (2005). Shroom regulates epithelial cell shape via the apical positioning of an actomyosin network. Journal of cell science 118, 5191-5203.

Hildebrand, J.D., and Soriano, P. (1999). Shroom, a PDZ domain-containing actin-binding protein, is required for neural tube morphogenesis in mice. Cell 99, 485-497.

Hirokawa, N., Niwa, S., and Tanaka, Y. (2010). Molecular motors in neurons: transport mechanisms and roles in brain function, development, and disease. Neuron 68, 610-638.

Hirokawa, N., and Noda, Y. (2008). Intracellular transport and kinesin superfamily proteins, KIFs: structure, function, and dynamics. Physiological reviews 88, 1089-1118.

Hirokawa, N., Noda, Y., and Okada, Y. (1998). Kinesin and dynein superfamily proteins in organelle transport and cell division. Current opinion in cell biology 10, 60-73.

Holmes, A. (2001). Targeted gene mutation approaches to the study of anxiety-like behavior in mice. Neuroscience and biobehavioral reviews 25, 261-273.

Horton, A.C., and Ehlers, M.D. (2003). Neuronal polarity and trafficking. Neuron 40, 277-295.

Humeau, Y., Gambino, F., Chelly, J., and Vitale, N. (2009). X-linked mental retardation: focus on synaptic function and plasticity. Journal of neurochemistry 109, 1-14.

Jacob, T.C., Moss, S.J., and Jurd, R. (2008). GABA(A) receptor trafficking and its role in the dynamic modulation of neuronal inhibition. Nature reviews Neuroscience 9, 331-343.

Jacobson, L.H., Bettler, B., Kaupmann, K., and Cryan, J.F. (2007). Behavioral evaluation of mice deficient in GABA(B(1)) receptor isoforms in tests of unconditioned anxiety. Psychopharmacology 190, 541-553.

Jarolimek, W., Bijak, M., and Misgeld, U. (1994). Differences in the Cs block of baclofen and 4-aminopyridine induced potassium currents of guinea pig CA3 neurons in vitro. Synapse 18, 169-177.

Johansson, M., Rocha, N., Zwart, W., Jordens, I., Janssen, L., Kuijl, C., Olkkonen, V.M., and Neefjes, J. (2007). Activation of endosomal dynein motors by stepwise assembly of Rab7-RILP-p150Glued, ORP1L, and the receptor betalll spectrin. The Journal of cell biology 176, 459-471.

Kapitein, L.C., Schlager, M.A., Kuijpers, M., Wulf, P.S., van Spronsen, M., MacKintosh, F.C., and Hoogenraad, C.C. (2010). Mixed microtubules steer dynein-driven cargo transport into dendrites. Current biology : CB 20, 290-299.

Karki, S., and Holzbaur, E.L. (1999). Cytoplasmic dynein and dynactin in cell division and intracellular transport. Current opinion in cell biology 11, 45-53.

Kim, I.H., Racz, B., Wang, H., Burianek, L., Weinberg, R., Yasuda, R., Wetsel, W.C., and Soderling, S.H. (2013). Disruption of Arp2/3 results in asymmetric structural plasticity of dendritic spines and progressive synaptic and behavioral abnormalities. The Journal of neuroscience : the official journal of the Society for Neuroscience 33, 6081-6092.

Kimura, T., Watanabe, H., Iwamatsu, A., and Kaibuchi, K. (2005). Tubulin and CRMP-2 complex is transported via Kinesin-1. Journal of neurochemistry 93, 1371-1382.

Klioueva, I.A., van Luijtelaar, E.L., Chepurnova, N.E., and Chepurnov, S.A. (2001). PTZ-induced seizures in rats: effects of age and strain. Physiology & behavior 72, 421-426.

Kong, W.L., Min, J.W., Liu, Y.L., Li, J.X., He, X.H., and Peng, B.W. (2013). Role of TRPV1 in susceptibility to PTZ-induced seizure following repeated hyperthermia challenges in neonatal mice. Epilepsy & behavior : E&B.

Kulik, A., Vida, I., Fukazawa, Y., Guetg, N., Kasugai, Y., Marker, C.L., Rigato, F., Bettler, B., Wickman, K., Frotscher, M., and Shigemoto, R. (2006). Compartment-dependent colocalization of Kir3.2-containing K+ channels and GABAB receptors in hippocampal pyramidal cells. The Journal of neuroscience : the official journal of the Society for Neuroscience 26, 4289-4297.

Kulik, A., Vida, I., Lujan, R., Haas, C.A., Lopez-Bendito, G., Shigemoto, R., and Frotscher, M. (2003). Subcellular localization of metabotropic GABA(B) receptor

subunits GABA(B1a/b) and GABA(B2) in the rat hippocampus. The Journal of neuroscience : the official journal of the Society for Neuroscience 23, 11026-11035.

Kumar, K., Sharma, S., Kumar, P., and Deshmukh, R. (2013). Therapeutic potential of GABA(B) receptor ligands in drug addiction, anxiety, depression and other CNS disorders. Pharmacology, biochemistry, and behavior 110, 174-184.

Kunde, S.A., Musante, L., Grimme, A., Fischer, U., Muller, E., Wanker, E.E., and Kalscheuer, V.M. (2011). The X-chromosome-linked intellectual disability protein PQBP1 is a component of neuronal RNA granules and regulates the appearance of stress granules. Human molecular genetics 20, 4916-4931.

Kuramoto, N., Wilkins, M.E., Fairfax, B.P., Revilla-Sanchez, R., Terunuma, M., Tamaki, K., Iemata, M., Warren, N., Couve, A., Calver, A., et al. (2007). Phospho-dependent functional modulation of GABA(B) receptors by the metabolic sensor AMP-dependent protein kinase. Neuron 53, 233-247.

Kwinter, D.M., Lo, K., Mafi, P., and Silverman, M.A. (2009). Dynactin regulates bidirectional transport of dense-core vesicles in the axon and dendrites of cultured hippocampal neurons. Neuroscience 162, 1001-1010.

Kwinter, D.M., Lo, K., Mafi, P., and Silverman, M.A. (2009). Dynactin regulates bidirectional transport of dense-core vesicles in the axon and dendrites of cultured hippocampal neurons. Neuroscience 162, 1001-1010.

Lee, C., Le, M.P., and Wallingford, J.B. (2009). The shroom family proteins play broad roles in the morphogenesis of thickened epithelial sheets. Developmental dynamics : an official publication of the American Association of Anatomists 238, 1480-1491.

Leonard, H., and Wen, X. (2002). The epidemiology of mental retardation: challenges and opportunities in the new millennium. Mental retardation and developmental disabilities research reviews 8, 117-134.

Leung, L.S., and Peloquin, P. (2006). GABA(B) receptors inhibit backpropagating dendritic spikes in hippocampal CA1 pyramidal cells in vivo. Hippocampus 16, 388-407.

Luscher, C., Jan, L.Y., Stoffel, M., Malenka, R.C., and Nicoll, R.A. (1997). G protein-coupled inwardly rectifying K+ channels (GIRKs) mediate postsynaptic but not presynaptic transmitter actions in hippocampal neurons. Neuron 19, 687-695.

Maas, C., Belgardt, D., Lee, H.K., Heisler, F.F., Lappe-Siefke, C., Magiera, M.M., van Dijk, J., Hausrat, T.J., Janke, C., and Kneussel, M. (2009). Synaptic activation modifies microtubules underlying transport of postsynaptic cargo. Proceedings of the National Academy of Sciences of the United States of America 106, 8731-8736.

Margeta-Mitrovic, M., Jan, Y.N., and Jan, L.Y. (2000). A trafficking checkpoint controls GABA(B) receptor heterodimerization. Neuron 27, 97-106.

Marshall, F.H., White, J., Main, M., Green, A., and Wise, A. (1999). GABA(B) receptors function as heterodimers. Biochemical Society transactions 27, 530-535.

Mayhew, T.M., Lucocq, J.M., and Griffiths, G. (2002). Relative labelling index: a novel stereological approach to test for non-random immunogold labelling of organelles and membranes on transmission electron microscopy thin sections. Journal of microscopy 205, 153-164.

Mohan, S., Rizaldy, R., Das, D., Bauer, R.J., Heroux, A., Trakselis, M.A., Hildebrand, J.D., and VanDemark, A.P. (2012). Structure of Shroom domain 2 reveals a three-segmented coiled-coil required for dimerization, Rock binding, and apical constriction. Molecular biology of the cell 23, 2131-2142.

Mombereau, C., Kaupmann, K., Froestl, W., Sansig, G., van der Putten, H., and Cryan, J.F. (2004). Genetic and pharmacological evidence of a role for GABA(B) receptors in the modulation of anxiety- and antidepressant-like behavior. Neuropsychopharmacology : official publication of the American College of Neuropsychopharmacology 29, 1050-1062.

Mombereau, C., Kaupmann, K., Gassmann, M., Bettler, B., van der Putten, H., and Cryan, J.F. (2005). Altered anxiety and depression-related behaviour in mice lacking GABAB(2) receptor subunits. Neuroreport 16, 307-310.

Moore, J.K., Stuchell-Brereton, M.D., and Cooper, J.A. (2009). Function of dynein in budding yeast: mitotic spindle positioning in a polarized cell. Cell motility and the cytoskeleton 66, 546-555.

Nakajima, K., Yin, X., Takei, Y., Seog, D.H., Homma, N., and Hirokawa, N. (2012). Molecular motor KIF5A is essential for GABA(A) receptor transport, and KIF5A deletion causes epilepsy. Neuron 76, 945-961.

Newberry, N.R., and Nicoll, R.A. (1984). Direct hyperpolarizing action of baclofen on hippocampal pyramidal cells. Nature 308, 450-452.

Newberry, N.R., and Nicoll, R.A. (1985). Comparison of the action of baclofen with gamma-aminobutyric acid on rat hippocampal pyramidal cells in vitro. The Journal of physiology 360, 161-185.

Nightingale, S. (2012). Autism spectrum disorders. Nature reviews Drug discovery 11, 745-746.

Nishimura, T., and Takeichi, M. (2008). Shroom3-mediated recruitment of Rho kinases to the apical cell junctions regulates epithelial and neuroepithelial planar remodeling. Development 135, 1493-1502.

Oblak, A.L., Gibbs, T.T., and Blatt, G.J. (2010). Decreased GABA(B) receptors in the cingulate cortex and fusiform gyrus in autism. Journal of neurochemistry 114, 1414-1423.

Pagano, A., Rovelli, G., Mosbacher, J., Lohmann, T., Duthey, B., Stauffer, D., Ristig, D., Schuler, V., Meigel, I., Lampert, C., et al. (2001). C-terminal interaction is essential for surface trafficking but not for heteromeric assembly of GABA(b) receptors. The Journal of neuroscience : the official journal of the Society for Neuroscience 21, 1189-1202.

Paxinos, G., Watson, C., Pennisi, M., and Topple, A. (1985). Bregma, lambda and the interaural midpoint in stereotaxic surgery with rats of different sex, strain and weight. Journal of neuroscience methods 13, 139-143.

Pfister, K.K., Fisher, E.M., Gibbons, I.R., Hays, T.S., Holzbaur, E.L., McIntosh, J.R., Porter, M.E., Schroer, T.A., Vaughan, K.T., Witman, G.B., et al. (2005). Cytoplasmic dynein nomenclature. The Journal of cell biology 171, 411-413.

Pilc, A., and Nowak, G. (2005). GABAergic hypotheses of anxiety and depression: focus on GABA-B receptors. Drugs of today 41, 755-766.

Pilc, A., and Nowak, G. (2005). GABAergic hypotheses of anxiety and depression: focus on GABA-B receptors. Drugs of today 41, 755-766.

Pilling, A.D., Horiuchi, D., Lively, C.M., and Saxton, W.M. (2006). Kinesin-1 and Dynein are the primary motors for fast transport of mitochondria in Drosophila motor axons. Molecular biology of the cell 17, 2057-2068.

Pitler, T.A., and Alger, B.E. (1994). Differences between presynaptic and postsynaptic GABAB mechanisms in rat hippocampal pyramidal cells. Journal of neurophysiology 72, 2317-2327.

Piton, A., Redin, C., and Mandel, J.L. (2013). XLID-causing mutations and associated genes challenged in light of data from large-scale human exome sequencing. American journal of human genetics 93, 368-383.

Plageman, T.F., Jr., Chung, M.I., Lou, M., Smith, A.N., Hildebrand, J.D., Wallingford, J.B., and Lang, R.A. (2010). Pax6-dependent Shroom3 expression regulates apical constriction during lens placode invagination. Development 137, 405-415.

Presley, J.F., Cole, N.B., Schroer, T.A., Hirschberg, K., Zaal, K.J., and Lippincott-Schwartz, J. (1997). ER-to-Golgi transport visualized in living cells. Nature 389, 81-85.

Purpura, D.P. (1974). Dendritic spine "dysgenesis" and mental retardation. Science 186, 1126-1128.

Ramirez, O.A., Vidal, R.L., Tello, J.A., Vargas, K.J., Kindler, S., Hartel, S., and Couve, A. (2009). Dendritic assembly of heteromeric gamma-aminobutyric acid type B receptor subunits in hippocampal neurons. The Journal of biological chemistry 284, 13077-13085.

Rex, C.S., Gavin, C.F., Rubio, M.D., Kramar, E.A., Chen, L.Y., Jia, Y., Huganir, R.L., Muzyczka, N., Gall, C.M., Miller, C.A., et al. (2010). Myosin IIb regulates actin dynamics during synaptic plasticity and memory formation. Neuron 67, 603-617.

Roberts, A.J., Kon, T., Knight, P.J., Sutoh, K., and Burgess, S.A. (2013). Functions and mechanics of dynein motor proteins. Nature reviews Molecular cell biology 14, 713-726.

Rodgers, R.J., Cao, B.J., Dalvi, A., and Holmes, A. (1997). Animal models of anxiety: an ethological perspective. Brazilian journal of medical and biological research = Revista brasileira de pesquisas medicas e biologicas / Sociedade Brasileira de Biofisica [et al] 30, 289-304.

Rondard, P., Goudet, C., Kniazeff, J., Pin, J.P., and Prezeau, L. (2011). The complexity of their activation mechanism opens new possibilities for the modulation of mGlu and GABAB class C G protein-coupled receptors. Neuropharmacology 60, 82-92.

Roos, J., and Kelly, R.B. (2000). Preassembly and transport of nerve terminals: a new concept of axonal transport. Nature neuroscience 3, 415-417.

Rost, B.R., Nicholson, P., Ahnert-Hilger, G., Rummel, A., Rosenmund, C., Breustedt, J., and Schmitz, D. (2011). Activation of metabotropic GABA receptors increases the energy barrier for vesicle fusion. Journal of cell science 124, 3066-3073.

Rowlett, J.K., Platt, D.M., Lelas, S., Atack, J.R., and Dawson, G.R. (2005). Different GABAA receptor subtypes mediate the anxiolytic, abuse-related, and motor effects of benzodiazepine-like drugs in primates. Proceedings of the National Academy of Sciences of the United States of America 102, 915-920.

Sakaba, T., and Neher, E. (2003). Direct modulation of synaptic vesicle priming by GABA(B) receptor activation at a glutamatergic synapse. Nature 424, 775-778.

Satoh, D., Sato, D., Tsuyama, T., Saito, M., Ohkura, H., Rolls, M.M., Ishikawa, F., and Uemura, T. (2008). Spatial control of branching within dendritic arbors by dynein-dependent transport of Rab5-endosomes. Nature cell biology 10, 1164-1171.

Schiaffino, M.V., Bassi, M.T., Galli, L., Renieri, A., Bruttini, M., De Nigris, F., Bergen, A.A., Charles, S.J., Yates, J.R., Meindl, A., and et al. (1995). Analysis of the OA1 gene reveals mutations in only one-third of patients with X-linked ocular albinism. Human molecular genetics 4, 2319-2325.

Schuler, V., Luscher, C., Blanchet, C., Klix, N., Sansig, G., Klebs, K., Schmutz, M., Heid, J., Gentry, C., Urban, L., et al. (2001). Epilepsy, hyperalgesia, impaired memory, and loss of pre- and postsynaptic GABA(B) responses in mice lacking GABA(B(1)). Neuron 31, 47-58.

Schwenk, J., Metz, M., Zolles, G., Turecek, R., Fritzius, T., Bildl, W., Tarusawa, E., Kulik, A., Unger, A., Ivankova, K., et al. (2010). Native GABA(B) receptors are heteromultimers with a family of auxiliary subunits. Nature 465, 231-235.

Setou, M., Nakagawa, T., Seog, D.H., and Hirokawa, N. (2000). Kinesin superfamily motor protein KIF17 and mLin-10 in NMDA receptor-containing vesicle transport. Science 288, 1796-1802.

Setou, M., Seog, D.H., Tanaka, Y., Kanai, Y., Takei, Y., Kawagishi, M., and Hirokawa, N. (2002). Glutamate-receptor-interacting protein GRIP1 directly steers kinesin to dendrites. Nature 417, 83-87.

Signorini, S., Liao, Y.J., Duncan, S.A., Jan, L.Y., and Stoffel, M. (1997). Normal cerebellar development but susceptibility to seizures in mice lacking G protein-coupled, inwardly rectifying K+ channel GIRK2. Proceedings of the National Academy of Sciences of the United States of America 94, 923-927.

Slesinger, P.A., Stoffel, M., Jan, Y.N., and Jan, L.Y. (1997). Defective gamma-aminobutyric acid type B receptor-activated inwardly rectifying K+ currents in cerebellar granule cells isolated from weaver and Girk2 null mutant mice. Proceedings of the National Academy of Sciences of the United States of America 94, 12210-12217.

Sodickson, D.L., and Bean, B.P. (1996). GABAB receptor-activated inwardly rectifying potassium current in dissociated hippocampal CA3 neurons. The Journal of neuroscience : the official journal of the Society for Neuroscience 16, 6374-6385.

Songyang, Z., Fanning, A.S., Fu, C., Xu, J., Marfatia, S.M., Chishti, A.H., Crompton, A., Chan, A.C., Anderson, J.M., and Cantley, L.C. (1997). Recognition of unique carboxyl-terminal motifs by distinct PDZ domains. Science 275, 73-77.

Staub, O., Verrey, F., Kleyman, T.R., Benos, D.J., Rossier, B.C., and Kraehenbuhl, J.P. (1992). Primary structure of an apical protein from Xenopus laevis that participates in amiloride-sensitive sodium channel activity. The Journal of cell biology 119, 1497-1506.

Straessle, A., Loup, F., Arabadzisz, D., Ohning, G.V., and Fritschy, J.M. (2003). Rapid and long-term alterations of hippocampal GABAB receptors in a mouse model of temporal lobe epilepsy. The European journal of neuroscience 18, 2213-2226.

Tamas, G., Lorincz, A., Simon, A., and Szabadics, J. (2003). Identified sources and targets of slow inhibition in the neocortex. Science 299, 1902-1905.

Taylor, J., Chung, K.H., Figueroa, C., Zurawski, J., Dickson, H.M., Brace, E.J., Avery, A.W., Turner, D.L., and Vojtek, A.B. (2008). The scaffold protein POSH regulates axon outgrowth. Molecular biology of the cell 19, 5181-5192.

Thompson, R.E., Larson, D.R., and Webb, W.W. (2002). Precise nanometer localization analysis for individual fluorescent probes. Biophysical journal 82, 2775-2783.

Thompson, S.M. (1994). Modulation of inhibitory synaptic transmission in the hippocampus. Progress in neurobiology 42, 575-609.

Twelvetrees, A.E., Yuen, E.Y., Arancibia-Carcamo, I.L., MacAskill, A.F., Rostaing, P., Lumb, M.J., Humbert, S., Triller, A., Saudou, F., Yan, Z., and Kittler, J.T. (2010). Delivery of GABAARs to synapses is mediated by HAP1-KIF5 and disrupted by mutant huntingtin. Neuron 65, 53-65.

Ulrich, D., and Bettler, B. (2007). GABA(B) receptors: synaptic functions and mechanisms of diversity. Current opinion in neurobiology 17, 298-303.

Ultanir, S.K., Kim, J.E., Hall, B.J., Deerinck, T., Ellisman, M., and Ghosh, A. (2007). Regulation of spine morphology and spine density by NMDA receptor signaling in vivo. Proceedings of the National Academy of Sciences of the United States of America 104, 19553-19558.

Valdes, V., Valenzuela, J.I., Salas, D.A., Jaureguiberry-Bravo, M., Otero, C., Thiede, C., Schmidt, C.F., and Couve, A. (2012). Endoplasmic reticulum sorting and kinesin-1 command the targeting of axonal GABAB receptors. PloS one 7, e44168.

Vale, R.D. (2003). The molecular motor toolbox for intracellular transport. Cell 112, 467-480.

van Spronsen, M., Mikhaylova, M., Lipka, J., Schlager, M.A., van den Heuvel, D.J., Kuijpers, M., Wulf, P.S., Keijzer, N., Demmers, J., Kapitein, L.C., et al. (2013). TRAK/Milton motor-adaptor proteins steer mitochondrial trafficking to axons and dendrites. Neuron 77, 485-502.

Vaughan, K.T., and Vallee, R.B. (1995). Cytoplasmic dynein binds dynactin through a direct interaction between the intermediate chains and p150Glued. The Journal of cell biology 131, 1507-1516.

Vigot, R., Barbieri, S., Brauner-Osborne, H., Turecek, R., Shigemoto, R., Zhang, Y.P., Lujan, R., Jacobson, L.H., Biermann, B., Fritschy, J.M., et al. (2006). Differential compartmentalization and distinct functions of GABAB receptor variants. Neuron 50, 589-601.

Wells, C.A., Betke, K.M., Lindsley, C.W., and Hamm, H.E. (2012). Label-free detection of G protein-SNARE interactions and screening for small molecule modulators. ACS chemical neuroscience 3, 69-78.

Yoder, M., and Hildebrand, J.D. (2007). Shroom4 (Kiaa1202) is an actin-associated protein implicated in cytoskeletal organization. Cell motility and the cytoskeleton 64, 49-63.

Yoon, S.S., Lee, B.H., Kim, H.S., Choi, K.H., Yun, J., Jang, E.Y., Shim, I., Kim, J.A., Kim, M.R., and Yang, C.H. (2007). Potential roles of GABA receptors in morphine self-administration in rats. Neuroscience letters 428, 33-37.

Yuen, E.Y., Jiang, Q., Feng, J., and Yan, Z. (2005). Microtubule regulation of N-methyl-D-aspartate receptor channels in neurons. The Journal of biological chemistry 280, 29420-29427.

Zheng, Y., Wildonger, J., Ye, B., Zhang, Y., Kita, A., Younger, S.H., Zimmerman, S., Jan, L.Y., and Jan, Y.N. (2008). Dynein is required for polarized dendritic transport and uniform microtubule orientation in axons. Nature cell biology 10, 1172-1180.

Zupanc, M.L. (2009). Clinical evaluation and diagnosis of severe epilepsy syndromes of early childhood. Journal of child neurology 24, 6S-14S.

ACKNOWLEDGMENTS

Je tiens tout d'abord à remercier ma directrice de thèse, Maria Passafaro pour sa patience, ses conseils et toute sa confiance qui m'ont permis d'avancer durant cette étape importante de ma vie.

Un MERCI particulier à un ami: Eddi, pour son aide scientifique et morale.

Un grand merci à tous les membres de mon labo: particulièrement à Silvia mais aussi à Luca, Ale et Laura.

Je tiens par la suite à remercier mes amis sans qui la vie au laboratoire aurait été bien triste. Merci à vous Francesca et Doudou mais aussi au laboratoire Sala et Borgese.

Je tiens à remercier ma famille qui même à distance aura toujours su me réconforter. Merci à bastoune, Marion, papa et maman et aux petits nouveaux Aitor et Laura.

Enfin, Je tiens à remercier ma femme, Alicia, sans qui, rien n'aurait été possible durant cette thèse. Merci pour ton soutient et surtout ta patience !!